UNITED STATES DEPARTMENT OF COMMERCE
JESSE H. JONES, Secretary
NATIONAL BUREAU OF STANDARDS
Lyman J. Briggs, Director

✦

Journal of Research

of the

National Bureau of Standards

✦

Volume 29, Number 1

July 1942

[Published with approval of the Director of the Budget]

UNITED STATES
GOVERNMENT PRINTING OFFICE
WASHINGTON : 1942

For sale by the Superintendent of Documents, Washington, D. C. - - - - - Price 30 cents
$3.50 per year on subscription

The prices of the separate Research Papers appearing in this JOURNAL are given on the front cover page. If 100 or more copies of any separate are ordered, a discount of 25 percent is allowed. Those who desire copies of separate Research Papers should send their orders and remittances without delay to the Superintendent of Documents, U. S. Government Printing Office, Washington, D. C. This will aid him to determine the number of copies to be printed for sale. Research Papers are not printed from electrotypes, and usually no more reprints can be had when the first and only printing is exhausted.

MATHEMATICAL TABLES

A list of the mathematical tables now obtainable from the National Bureau of Standards is printed on pages 3 and 4 of the JOURNAL cover. New tables will be announced from time to time as they become available.

U. S. DEPARTMENT OF COMMERCE NATIONAL BUREAU OF STANDARDS

RESEARCH PAPER RP1480

Part of Journal of Research of the National Bureau of Standards, Volume 29, July 1942

A NEW DETERMINATION OF THE CONSTANT OF GRAVITATION

By Paul R. Heyl and Peter Chrzanowski

ABSTRACT

A new determination of the constant of gravitation by means of the torsion balance has been made in the hope of improving the precision of the result published in 1930. A number of suggested improvements in the apparatus were tried, and two of these were adopted The result obtained shows so slight an improvement over the 1930 result that it appears that the limiting point of diminishing returns has been reached with this form of apparatus.

CONTENTS

	Page
I. Introduction	1
II. Suggested improvements in the torsion balance	2
1. Best filament material	3
2. Length of filament	3
3. Increase inmass of attracting bodies	3
4. Multiple filament	3
5. Bifilar suspension	4
6. Length of beam	4
7. Increasing the number of masses	5
8. Disk beam	5
III. Adopted improvements	5
IV. Mathematical theory	7
V. Description of apparatus	20
VI. Method of observing	22
1. Adjustments	22
(a) Adjustment of cylinders	22
(b) Adjustment of pendulum	23
2. Length measurements	24
3. Time measurements	24
(a) Standard of time	24
(b) Optical system	25
(c) The camera	25
VII. Results	30

I. INTRODUCTION

In 1930 [1] the senior author of the present paper published a redetermination of the constant of gravitation, the results of which, though of a precision higher than that of the previously accepted value, showed a curious relation among themselves for which no explanation was available. The work was done with the torsion balance, using small moving masses of gold, platinum, and glass. The results with each material were reasonably concordant among themselves, but there appeared to be considerable difference with the nature of the material. For instance, the mean values of the platinum and glass sets differed by an amount five times as great as the average departure from the mean in either set. Moreover, there was no overlap in the spreads of the two sets. While it seemed reasonable to attribute this

[1] Paul R. Heyl, *Redetermination of the constant of gravitation*, BS J. Research 5, 1243 (1930) RP256.

to experimental error of some nature, it was possible to interpret it as a departure from Newton's law of the constant proportionality of mass and weight. To test this point experiments were made with a Eötvös balance, using one ball of platinum and one of glass. The results were negative.

As stated in the 1930 paper, it was felt that the solution of this difficulty could best be attained by working with an apparatus sufficiently sensitive to give the next decimal place. The attempt to do this forms the subject matter of the present paper.

The general question of improvements in the torsion balance was considered, and a few suggestions that seemed promising were tried experimentally. Most of these, however, were failures, only two of them qualifying for adoption. For the benefit of future workers it has been thought well to discuss these failures in some detail.

II. SUGGESTED IMPROVEMENTS IN THE TORSION BALANCE

In the way in which the torsion balance was used, in the 1930 paper and in the present work, the time of swing was measured in two positions of the large attracting masses, called "near" and "far" (fig. 1). As compared with the free time of swing, with the large masses removed to a distance, the period in the near position will be shortened, and in the far position lengthened. The difference of these two times is a multiplying factor in the formula for the gravitational constant, and anything which will increase this difference without introducing other difficulties will be a move in the right direction. There are two ways in which this difference may be increased, by reducing the torsion of the suspending filament, and by increasing the moment of the force exerted by the large attracting masses upon the moving system. The latter may again be done in two ways, by increasing the force of attraction or by increasing the lever arm by which this force acts. We shall now consider a number of suggestions that come under these headings.

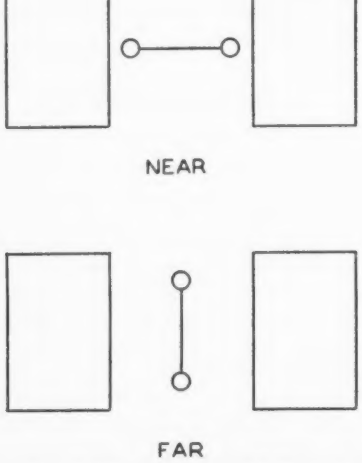

FIGURE 1.—*Relative position of balls and cylinders.*

1. BEST FILAMENT MATERIAL

Since the modulus of torsion of a wire is proportional to the fourth power of its diameter, it is desirable to use a wire of as small a diameter as will safely carry the load of the beam and balls. This requires a material of high tensile strength. In this respect tungsten has no superior. Its tensile strength in the form of lamp filament 0.001 inch in diameter is, when hard drawn, from 300 to 400 kg/mm^2, and when annealed about 200. Larger sizes of tungsten filament show a somewhat smaller tensile strength, as this property increases with swaging and drawing. In comparison, the maximum value for chrome-vanadium steel is 232, and for fused silica, 120. In addition, tungsten can readily be obtained in finer wires than steel, and, as was found in the 1930 work, is the equal of fused silica in returning to the zero point after a large deflection.

2. LENGTH OF FILAMENT

The longer the filament the less the torsion for the same twist; but in practice there is a limit to the length that can safely be used. The filament is contained in a long tube rising from the lid of the apparatus case, and a slight warping at the bottom of the tube may be multiplied at the top to an amount sufficient to disturb seriously the centering adjustment of the beam. In practice, we have found that 1 meter is a safe limit to the length of the filament.

3. INCREASE IN MASS OF ATTRACTING BODIES

An increased mass of either the large or the small bodies will augment the force of attraction between them and heighten the sensitivity of the apparatus. With the small masses a limit of size is soon reached, as a filament of large diameter is required to carry the increased load, and by the fourth-power law the torsion will rapidly outrun the attraction.

There is no theoretical objection to increasing the large masses if material of sufficient homogeneity can be obtained in large pieces. Uniformity of density is important, as otherwise the position of the center of attraction would be uncertain.

4. MULTIPLE FILAMENT

It is theoretically possible to turn the fourth-power law of torsion to advantage. Suppose that a given load can be carried safely by a filament of diameter D and torsion τ. Replace this filament by two filaments of diameter $D/2^{1/2}$ and torsion $\tau/4$. The joint tensile strength of the double filament will be the same as that of the larger single filament, but the joint torsion will be half the previous value; and for more than two filaments the torsion will be rapidly reduced.

With a multiple filament of this character the question of friction between the components must be considered. We thought it worthwhile to test this experimentally, but an unforeseen practical difficulty prevented our getting any evidence on this point. This was the difficulty of obtaining an equal division of the load among the component filaments. Several attempts were made, but in every case the multiple filament broke down after a few days in operation.

5. BIFILAR SUSPENSION

Theoretically there should be no difficulty in obtaining an equal division of load in the case of a bifilar suspension, and with a small separation between the two components the question of friction will not arise. However, in such a suspension the restoring force consists of both gravity and torsion, the gravity component varying as the square of the distance separating the component filaments, and this distance must therefore be kept small to avoid undue loss of sensitivity. But even if this distance be only a few tenths of a millimeter, the restoring force of gravity will be greater than that of torsion. This, however, appeared to be not without advantage. Experience with a single filament suspension indicated that the modulus of torsion, like most mechanical properties, varied slightly from time to time, probably from fatigue. Gravity, however, is constant under all known conditions, and in a suspension in which gravity is predominant in the restoring force, it seemed that greater uniformity in the observations might outweigh the disadvantage of a reduced time of swing.

A suspension was constructed with a separation of 0.5 mm between the filaments, maintained by the use of wire hooks at each end. At the top, each end of the filament was given a complete turn around the hook, and the loose ends were wrapped several times around the shank of the hook and fastened with hard wax. The hook at the lower end was passed through the loop of filament without wax or solder. Our experience with breakdowns in multiple filaments had impressed upon us the necessity of having the tension equal in both components, and this is difficult to obtain or to maintain when solder is used. It was thought that in a short time under load the tungsten wire would cut into the hook sufficiently to prevent slipping.

Measurements of time of swing with this suspension over a period of a month were disappointing. Fluctuations from day to day were observed, amounting to as much as 1 part in 3,000, probably due to slight shifts in the position of the filament on the lower hook. The time of swing varies inversely as the distance between the filaments, and when this distance is 0.5 mm a change in the time of 1 part in 3,000 would be produced by an alteration in the distance of 0.00017 mm. If the separation were increased, this fluctuation would be reduced, but at the expense of a corresponding reduction in time of swing and diminished sensitivity of the apparatus.

6. LENGTH OF BEAM

The beam used in the 1930 apparatus was about 20 cm long. Considerable time was spent in the recent work in the attempt to use a beam 80 cm long. The difficulty with a beam of this length is its tendency to bend slightly with the weight of the balls during a long series of measurements, and thus alter the distance between the centers of the balls. Beams of different materials and different shapes of cross section were tried without overcoming this difficulty. The addition of braces to the beam to prevent this bending greatly increases the labor of computing the attraction of the large masses for the beam. This attraction, though only about 1 percent of the attraction for the balls, takes much longer to calculate.

Theoretically, it is possible to eliminate the attraction for the beam. Let the time of swing be measured with heavy balls on the beam.

Replace these balls by lighter ones, and repeat the measurement of the time of swing. From two such measurements in both near and far positions it is possible to eliminate the attraction for the beam, other things remaining equal. But here comes in the difficulty. Other things (torsion, for instance) will not remain equal.

In order to change the balls it is necessary to relieve the filament temporarily of its load. The effect of this upon the torsion was experimentally investigated.

A series of 10 measurements of time of swing with a beam carrying platinum balls weighing 175 g each gave a mean value of 1892.62 $\pm$0.21 sec. The case was then opened and the beam let down on two supporting blocks. No change was made in the balls or in their position on the beam. The next day the beam was again raised and the case closed. The time of swing was then found to be 1886.69 sec. And since a change of balls could not be made without temporarily relieving the tension, the elimination of the attraction for the beam was found to be impracticable.

7. INCREASING THE NUMBER OF MASSES

By the use of a beam with four arms, carrying four balls, and providing four large masses, the total attraction can be doubled without increasing the load on any one arm of the beam. This arrangement, however, would be practicable only with rather long beams, which, as shown in the preceding section, are not practicable. A pair of large masses, when in the near position with respect to one pair of balls, will be in the far position with respect to the other pair, and these two effects will partly neutralize each other. This neutralization will be the more nearly complete as the arms of the beam are shortened. Carried to the limit, with arms so short that the large masses are close enough to touch each other, these masses would approximate a continuous ring, which would have no resultant attraction on the beam.

8. DISK BEAM

The idea of replacing the rod-shaped beam by a circular disk, carrying the balls at its circumference, is attractive from the point of view of the computer, since the torque of the large masses for such a disk is zero. The objection is the increase in weight. Such a disk, even though made of aluminum, would weigh more than the balls it carried, with the consequence of increased filament diameter and lessened sensitivity. Moreover, the moment of inertia of the disk would be great enough to be an important factor in the time of swing, and the differential effect of the large masses on the balls in the near and far positions would be correspondingly reduced.

III. ADOPTED IMPROVEMENTS

With the failure of the suggested improvements discussed in section II, it would appear that in dimensions, masses, and general arrangement the apparatus described in the 1930 paper is perhaps the best that is practicable. There were, however, two improvements which were found to be worthy of adoption. One of these was photographic recording, which will be described in detail in a later section. The other was a change in the position of the large attracting masses.

In the 1930 apparatus the large masses were steel cylinders weighing about 66 kg each, arranged with their axes vertical. This position gave rise to two difficulties. In measuring the distance between the cylinders it was necessary to grope for the minimum distance. This required so many measurements that the whole operation normally required about 2½ days.

In addition, the time of swing in the near position varied considerably with the amplitude, making necessary an extrapolation for the limiting value of the time as the amplitude approached zero. In the far position the time-amplitude curve was nearly a straight horizontal line. The reason for this is obvious. With vertical cylinders in the near position, the balls swing in a gravitational field of varying intensity, whereas in the far position the field is much more nearly uniform.

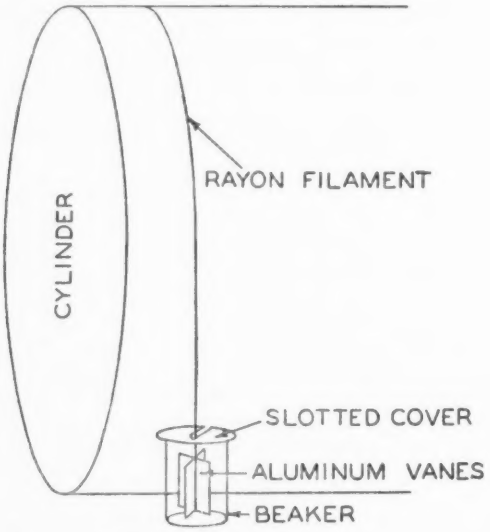

FIGURE 2.—*Rayon plumb bob.*

By laying the cylinders on their sides with their axes horizontal both these difficulties were avoided. In measuring the distance between the cylinders, delicate plumb bobs were hung touching the inner surface of each cylinder. This gave at once the minimum distance, which was measured by micrometer microscopes as described in the 1930 paper. These plumb bobs consisted of single filaments of rayon which were attached by a small fragment of adhesive tape to the upper surface of the cylinder near the ends, and hung down over the inner surfaces (fig. 2). The bob at the end of a filament was a small vane of sheet aluminum weighing about half a gram. To avoid disturbance from air currents this vane hung in a small empty beaker with a slotted cardboard cover. By this device the measurement of the distance between the cylinders could be made in about 3 hours.

After the measurements were made the beakers were removed, but the plumb bobs were left in place for use again after the time of swing had been measured. No correction was made for the attraction of

the vanes on the moving system, as the effect of two vanes was of the order of one hundred thousandth of the attraction of the cylinder, and our results did not reach that degree of precision.

With the axes of the cylinders horizontal the time of swing in the near position became nearly independent of the amplitude, thus removing the uncertainty of the extrapolation. Near the middle of a cylinder the equipotential surfaces are very nearly parallel to the cylinder, and if the amplitude of the swing of the ball is not more than a few degrees, the motion takes place in a practically uniform gravitational field.

While this position of the cylinders simplifies the physical measurements, it greatly increases the labor of calculating the attraction of the cylinders on the pendulum. However, one must always use the simplest physical procedure, involving the least probability of experimental error, without shrinking from the mathematical labor which it may entail.

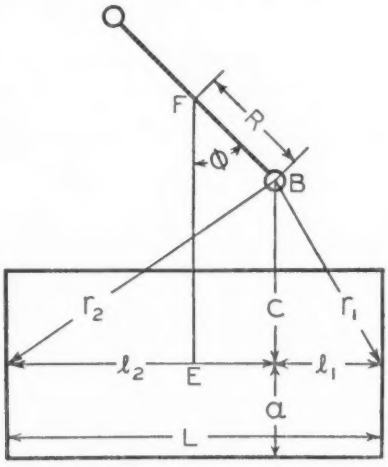

FIGURE 3.—*Geometrical constants in attraction formula.*

IV. MATHEMATICAL THEORY

In deriving the formulas for the torsion pendulum as used in the present work, it will be convenient to consider first the action between a single cylinder and one ball of the pendulum (fig. 3). We shall assume for the present that the center of the ball is at the same level as the axis of the cylinder.

The beam of the pendulum is supported by a filament at F. From F is drawn the line FE perpendicular to the axis of the cylinder. The beam makes a position angle ϕ with FE, the positive direction of ϕ being counterclockwise. B is the ball under consideration and R its radius of gyration.

From B draw a line of length C perpendicular to the axis of the cylinder and dividing it into two parts, l_1 and l_2. In the present work, l_1 will be considered positive and l_2 negative, although in the 1930 paper both were regarded as positive. The distances from the ball B to the ends of the axis of the cylinder are r_1 and r_2, respectively.

It must be carefully noted that ϕ is merely an angle defining the position of the ball under consideration with respect to the cylinder which is attracting it, and does not necessarily measure the angle of displacement from the position of equilibrium, where the torque due to the suspending filament is zero. This angle of displacement will be denoted by θ. Its positive direction is the same as that of ϕ.

Figure. 4 shows the relation between ϕ and θ in the four cases that occur in practice. The relation may be summarized as follows:

Near position, close ball	$\phi=\theta$
Near position, distant ball	$\phi=180°+\theta$
Far position, right ball	$\phi=90°+\theta$
Far position, left ball	$\phi=270°+\theta$

In all cases it is to be noted that $d\phi=d\theta$ and $d^2\phi=d^2\theta$.

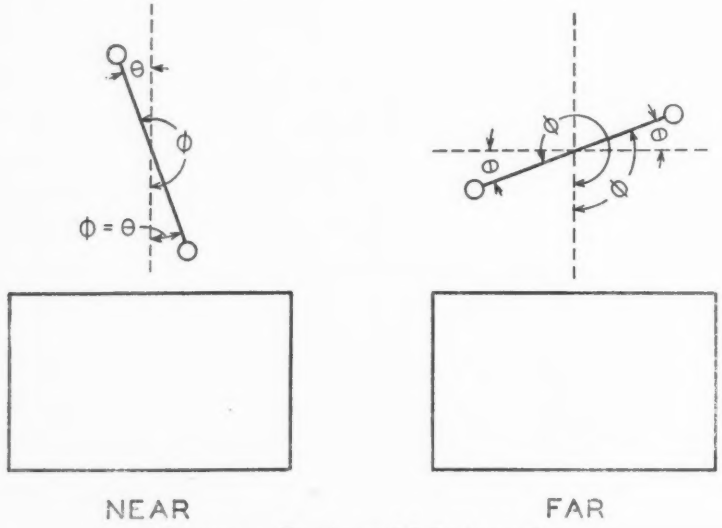

FIGURE 4.—*Position and deflection angles.*

The differential equation for the motion of the pendulum may be conveniently derived as an energy equation. Considering the complete system, beam, balls, and cylinders, for any position angle ϕ:

$$\left.\begin{array}{l}\text{Kinetic energy of the pendulum + potential energy due to filament}\\ \quad\text{+potential energy of attraction = constant.}\end{array}\right\}(1)$$

Let I = moment of inertia of the pendulum

τ = modulus of torsion of the filament (moment required to give the beam an angular displacement of 1 radian)

Then:

$$\text{Kinetic energy of pendulum}=\frac{I}{2}\left(\frac{d\theta}{dt}\right)^2$$

$$\text{Potential energy due to filament}=\frac{1}{2}\tau\theta^2,$$

and it remains to find an expression for the potential energy of attraction as a function of θ.

To find the potential energy of attraction we must take the sum of the attractions of the cylinders for the whole moving system, beam and balls. The attraction for the balls is comparatively simple, as we may suppose the mass of either ball concentrated at its center. For the beam the calculation is more laborious, as it is necessary to imagine the beam divided into a number of elementary segments so small that it is permissible to assume the attractive force concentrated at the center of a segment. We shall consider first the attraction of one cylinder on the pendulum.

Let V_0 be the potential of the cylinder at the center of any element of the pendulum (ball or beam segment) when the beam is in an equilibrium position (near or far) where $\theta=0$, and let V_θ be the potential when the beam is displaced from equilibrium by an angle θ. Then, by Taylor's theorem:

$$V_\theta - V_0 = \theta\frac{dV_0}{d\theta} + \frac{\theta^2}{2}\frac{d^2V_0}{d\theta^2}, \qquad (2)$$

neglecting terms in θ^3 and higher powers. This is a valid procedure, not because the pendulum actually swings through a small angle, but because its time of swing is reduced empirically to its value T_0 for an infinitesimal arc before being used in the calculations.

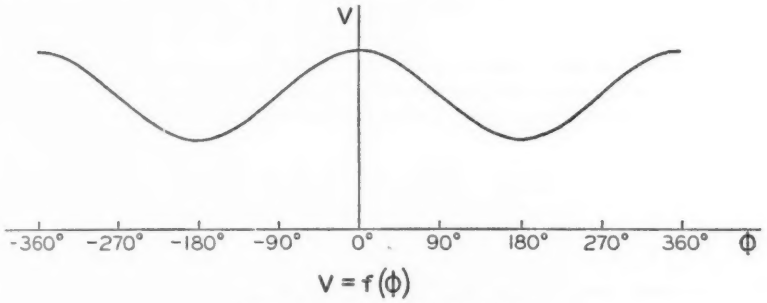

FIGURE 5.—*Curve of potential.*

If m=mass of an element of the pendulum, $-m(V_\theta - V_0)$ will be the potential energy of attraction of the cylinder for this element. Taking into account both cylinders and all elements of the pendulum:

$$\text{Potential energy of attraction} = -\Sigma\left(m\theta\frac{dV_0}{d\theta} + \frac{m}{2}\theta^2\frac{d^2V_0}{d\theta^2}\right). \qquad (3)$$

In the ideal case of perfect centering of the pendulum, and symmetry and parallelism of the cylinders, the terms in $dV_0/d\theta$ disappear in both near and far positions. In the near position, V_0 is a maximum for the position angle $\phi=0$, and $dV_0/d\phi=0$; and for the position angle $\phi=180°$, V_0 will be a minimum and $dV_0/d\phi$ will again be zero. And since, as we have seen (fig. 4), $d\phi=d\theta$, all terms in $dV_0/d\theta$ are individually zero in the near position.

In the far position (ideal case), for the equilibrium angles $\phi=90°$ and $\phi=270°$, $dV_0/d\phi$ will not be zero, but will have equal and opposite values in these two positions (fig. 5). In consequence, the terms in $dV/d\theta$ will mutually cancel out in the summation.

In the ideal case, therefore, we have in both near and far positions:

$$\text{Potential energy of attraction} = -\sum \frac{m}{2}\left(\theta^2 \frac{d^2V_0}{d\theta^2}\right) = -\frac{1}{2} KG\theta^2, \quad (4)$$

where G is the constant of gravitation and K is a calculable function of the masses and dimensions in the apparatus.

Equation 1 now becomes, in the ideal case:

$$\frac{I}{2}\left(\frac{d\theta}{dt}\right)^2 + \frac{1}{2}\tau\theta^2 - \frac{1}{2}KG\theta^2 = \text{constant}. \quad (5)$$

Differentiating and reducing:

$$\frac{d^2\theta}{dt^2} + \frac{\tau - KG}{I}\theta = 0,$$

whose solution is:

$$\theta = A \sin\left(\sqrt{\frac{\tau - KG}{I}}\right)t \quad (6)$$

with a periodic time:

$$T = 2\pi\sqrt{\frac{I}{\tau - KG}}. \quad (7)$$

Formula 7 applied to the near and far positions gives two equations for the unknown quantities τ and G. Assuming τ to remain constant in the two positions, and eliminating it, we obtain the following formula for G:

$$(KG)_F - (KG)_N = 4\pi^2\left(\frac{I}{T_N^2} - \frac{I}{T_F^2}\right). \quad (8)$$

So much for the ideal case; but any practical setup must be expected to fall short of perfection, and we must expect that the potential energy of attraction, as given by eq 3, will contain a term in θ. We must therefore rewrite eq 4 as follows:

$$\text{Potential energy of attraction} = -\frac{1}{2}KG\theta^2 + Q\theta, \quad (9)$$

in which Q, like K, is a calculable function of the masses and dimensions in the apparatus. Equation 1 now becomes, in the practical case:

$$\frac{I}{2}\left(\frac{d\theta}{dt}\right)^2 + \frac{1}{2}(\tau - KG)\theta^2 + Q\theta = \text{constant}. \quad (10)$$

Differentiating and reducing:

$$\frac{d^2\theta}{dt^2} + \frac{\tau - KG}{I}\theta + \frac{Q}{I} = 0, \quad (11)$$

whose solution is:

$$\theta = A \sin\left(\sqrt{\frac{\tau - KG}{I}}\right)t - \frac{Q}{\tau - KG}, \quad (12)$$

which has the same periodic time as in the ideal case (formula 6). It appears, then, that even in cases where a term in θ is present, we may follow the same procedure for the calculation of G as when it is absent.

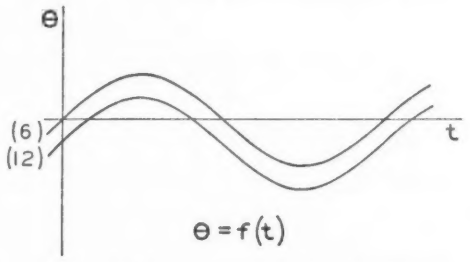

FIGURE 6.—*Ideal and practical time-of-swing curves.*

The relation between the ideal and the practical solutions is shown in figure 6. The ideal solution (6) is a sine curve which is symmetrical with respect to the axis of t; the practical solution (12) is a similar sine curve at a constant distance below the other. The curve has the same periodic time, but while the "half-periods" in the practical case are alternately long and short, in the ideal case they are equal.

In the present work the θ term is insignificant compared with the θ^2 term. A calculation made for one of the near positions showed that the ratio of the coefficients of the two terms was about 1 to 40,000.

In order to apply formula 8 to the calculation of G, it is necessary to compute the value of

$$KG=\sum\left(m\frac{d^2V_0}{d\theta^2}\right)$$

for both the near and the far positions. The 1930 paper gives a formula for V at any point exterior to a cylinder (eq 9, p. 1264–66), and by differentiation with respect to ϕ, we can obtain from this the value of

$$\frac{d^2V}{d\phi^2}\left(\equiv\frac{d^2V}{d\theta^2}\right)$$

at any desired point.

Using the notation given in figure 3 for the fundamental quantities, we obtain the following relations:

$$\left.\begin{aligned} C_\phi&=C_0+R(1-\cos\phi)\\ \frac{dC_\phi}{d\phi}&=R\sin\phi\\ \frac{d^2C_\phi}{d\phi^2}&=R\cos\phi \end{aligned}\right\} \tag{13}$$

At the four equilibrium values of ϕ these derivatives of C have the following values:

ϕ	$\frac{dC_\phi}{d\phi}$	$\frac{d^2C_\phi}{d\phi^2}$
0°	0	R
90°	R	0
180°	0	$-R$
270°	$-R$	0

(14)

We have also the following values of l_1 and l_2, and their derivatives as functions of ϕ, in which Δ_1 and Δ_2 denote errors in centering:

$$\left.\begin{aligned} l_1&=\frac{L}{2}\pm\Delta_1-R\sin\phi \qquad l_2=-\left(\frac{L}{2}\pm\Delta_2+R\sin\phi\right)\\ \frac{dl_1}{d\phi}&=\frac{dl_2}{d\phi}=-R\cos\phi\\ \frac{d^2l_1}{d\phi^2}&=\frac{d^2l_2}{d\phi^2}=R\sin\phi \end{aligned}\right\} \tag{15}$$

At the equilibrium values of ϕ these derivatives of ϕ have the following values:

ϕ	$\frac{dl}{d\phi}$	$\frac{d^2l}{d\phi^2}$
0°	$-R$	0
90°	0	R
180°	R	0
270°	0	$-R$

(16)

And since, for both subscripts, $r^2=C_\phi^2+l^2$, we obtain

$$\left.\begin{aligned} \frac{dr}{d\phi}&=\frac{C_\phi}{r}\frac{dC_\phi}{d\phi}+\frac{l}{r}\frac{dl}{d\phi}\\ \frac{d^2r}{d\phi^2}&=\left\{\begin{aligned} &+\frac{C_\phi}{r}\frac{d^2C_\phi}{d\phi^2}+\frac{1}{r}\left(\frac{dC_\phi}{d\phi}\right)^2-\frac{C_\phi}{r^2}\frac{dr}{d\phi}\frac{dC_\phi}{d\phi}\\ &+\frac{l}{r}\frac{d^2l}{d\phi^2}+\frac{1}{r}\left(\frac{dl}{d\phi}\right)^2-\frac{l}{r^2}\frac{dr}{d\phi}\frac{dl}{d\phi} \end{aligned}\right. \end{aligned}\right\} \tag{17}$$

At the equilibrium values of ϕ these derivatives of r have the following values:

ϕ	$\frac{dr}{d\phi}$	$\frac{d^2r}{d\phi^2}$
0°	$-R\frac{l}{r}$	$R\frac{C_\phi}{r}+\frac{R^2}{r}-R^2\frac{l^2}{r^3}$
90°	$R\frac{C_\phi}{r}$	$\frac{R^2}{r}-R^2\frac{C_\phi^2}{r^3}+R\frac{l}{r}$
180°	$R\frac{l}{r}$	$-R\frac{C_\phi}{r}+\frac{R^2}{r}-R^2\frac{l^2}{r^3}$
270°	$-R\frac{C_\phi}{r}$	$\frac{R^2}{r}-\frac{R^2C_\phi^2}{r^3}-R\frac{l}{r}$

(18)

The foregoing formulas will enable us to obtain $d^2V/d\phi^2$ from the formula for V in the 1930 paper. In performing this differentiation it is to be remembered that a change in the sign of l_2 has been made

for the present work. We thus obtain the following formula (19) for $d^2V/d\phi^2$. For convenience in printing, only the first term is given in full. In this it will be seen that to each term in l_2 and r_2 there corresponds a similar term in l_1 and r_1, but with opposite sign. The same holds true in all terms after the first, and in these terms, for brevity, the terms in l_1 and r_1 are omitted.

It will be convenient to classify all terms after the first according to the different derivatives which they contain. These are five in number:

$$\frac{d^2l}{d\phi^2}, \frac{d^2r}{d\phi^2}, \left(\frac{dr}{d\phi}\right)^2, \left(\frac{dl}{d\phi}\right)^2 \text{ and } \frac{dr}{d\phi}\frac{dl}{d\phi}.$$

And finally, all terms, including the first, are to be multiplied by $2\pi\rho a^2G$, where ρ is the density of the cylinder. (This factor is incorrectly given with a negative sign in the 1930 paper.)

$$\frac{1}{2\pi\rho a^2G}\frac{d^2V}{d\phi^2} \quad \ldots\ldots\ldots\ldots\ldots\ldots\ldots\ldots \quad (19)$$

FIRST TERM

$$\frac{dC_\phi}{d\phi}\left[-\frac{1}{{C_\phi}^3}\left(l_2\frac{dr_2}{d\phi}-l_1\frac{dr_1}{d\phi}-r_2\frac{dl_2}{d\phi}+r_1\frac{dl_1}{d\phi}\right)\right]+\frac{d^2r_2}{d\phi^2}\frac{l_2}{2{C_\phi}^2}-\frac{d^2r_1}{d\phi^2}\frac{l_1}{2{C_\phi}^2}-$$
$$\frac{d^2l_2}{d\phi^2}\frac{r_2}{2{C_\phi}^2}+\frac{d^2l_1}{d\phi^2}\frac{r_1}{2{C_\phi}^2}.$$

TERMS IN $\dfrac{d^2l}{d\phi^2}$

Term

2. $$\frac{a^2}{16}\frac{d^2l_2}{d\phi^2}\left(-\frac{1}{{r_2}^3}\right)$$

3. $$\frac{a^4}{128}\frac{d^2l_2}{d\phi^2}\left(+\frac{15{l_2}^2}{{r_2}^7}-\frac{3}{{r_2}^5}\right)$$

4. $$\frac{5a^6}{2048}\frac{d^2l_2}{d\phi^2}\left(-\frac{105{l_2}^4}{{r_2}^{11}}+\frac{70{l_2}^2}{{r_2}^9}-\frac{5}{{r_2}^7}\right)$$

5. $$\frac{7a^8}{32768}\frac{d^2l_2}{d\phi^2}\left(+\frac{3003{l_2}^6}{{r_2}^{15}}-\frac{3465{l_2}^4}{{r_2}^{13}}+\frac{945{l_2}^2}{{r_2}^{11}}-\frac{35}{{r_2}^9}\right)$$

6. $$\frac{21a^{10}}{262144}\frac{d^2l_2}{d\phi^2}\left(-\frac{21879{l_2}^8}{{r_2}^{19}}+\frac{36036{l_2}^6}{{r_2}^{17}}-\frac{18018{l_2}^4}{{r_2}^{15}}+\frac{2772{l_2}^2}{{r_2}^{13}}-\frac{63}{{r_2}^{11}}\right)$$

7. $$\frac{33a^{12}}{2097152}\frac{d^2l_2}{d\phi^2}\left(+\frac{323323{l_2}^{10}}{{r_2}^{23}}-\frac{692835{l_2}^8}{{r_2}^{21}}+\frac{510510{l_2}^6}{{r_2}^{19}}\right.$$
$$\left.-\frac{150150{l_2}^4}{{r_2}^{17}}+\frac{15015{l_2}^2}{{r_2}^{15}}-\frac{231}{{r_2}^{13}}\right)$$

8. $$\frac{429a^{14}}{67108864}\frac{d^2l_2}{d\phi^2}\left(-\frac{2414425{l_2}^{12}}{{r_2}^{27}}+\frac{6374082{l_2}^{10}}{{r_2}^{25}}-\frac{6235515{l_2}^8}{{r_2}^{23}}\right.$$
$$\left.+\frac{2771340{l_2}^6}{{r_2}^{21}}-\frac{546975{l_2}^4}{{r_2}^{19}}+\frac{38610{l_2}^2}{{r_2}^{17}}-\frac{429}{{r_2}^{15}}\right)$$

9. $$\frac{715a^{16}}{2147483648}\frac{d^2l_2}{d\phi^2}\left(+\frac{145422675l_2^{14}}{r_2^{31}}-\frac{45632635l_2^{12}}{r_2^{29}}+\frac{5577321751_2^{10}}{r_2^{27}}-\frac{334639305l_2^{8}}{r_2^{25}}+\frac{101846745l_2^{6}}{r_2^{23}}-\frac{14549535l_2^{4}}{r_2^{21}}+\frac{765765l_2^{2}}{r_2^{19}}-\frac{6435}{r_2^{17}}\right)$$

10. $$\frac{2431a^{18}}{17179869184}\frac{d^2l_2}{d\phi^2}\left(-\frac{1101980715l_2^{16}}{r_2^{35}}+\frac{4007202600l_2^{14}}{r_2^{33}}-\frac{5881539300l_2^{12}}{r_2^{31}}+\frac{4461857400l_2^{10}}{r_2^{29}}-\frac{1859107250l_2^{8}}{r_2^{27}}+\frac{416440024l_2^{6}}{r_2^{25}}-\frac{45265220l_2^{4}}{r_2^{23}}+\frac{1847560l_2^{2}}{r_2^{21}}-\frac{12155}{r_2^{19}}\right)$$

NUMERICAL FACTORS

2.	0. 0625				
3.	0. 1171875	0. 0234375			
4.	0. 2563477	0. 1708984	0. 0122070		
5.	0. 6415100	0. 7402039	0. 2018738	0. 0074768	
6.	1. 752697	2. 886795	1. 443398	0. 2220612	0. 0050468
7.	5. 087690	10. 90219	8. 033195	2. 362704	0. 2362704
					0. 0036349
8.	15. 43445	40. 74694	39. 86114	17. 71606	3. 496591
				0. 2468182	0. 0027424
9.	48. 41816	151. 9329	185. 6957	111. 4174	33. 90965
			48. 44236	25. 49598	0. 2142519
10.	155. 9334	567. 0305	832. 2544	631. 3654	263. 0689
		58. 92744	64 05156	2. 614350	0. 0171997

Term — TERMS IN $\frac{d^2r}{d\phi^2}$

2. $$\frac{a^2}{16}\frac{d^2r_2}{d\phi^2}\left(+\frac{3l_2}{r_2^4}\right).$$

3. $$\frac{a^4}{128}\frac{d^2r_2}{d\phi^2}\left(-\frac{35l_2^3}{r_2^8}+\frac{15l_2}{r_2^6}\right).$$

4. $$\frac{5a^6}{2048}\frac{d^2r_2}{d\phi^2}\left(+\frac{231l_2^5}{r_2^{12}}-\frac{210l_2^3}{r_2^{10}}+\frac{35l_2}{r_2^8}\right).$$

5. $$\frac{7a^8}{32768}\frac{d^2r_2}{d\phi^2}\left(-\frac{6435l_2^7}{r_2^{16}}+\frac{9009l_2^5}{r_2^{14}}-\frac{3465l_2^3}{r_2^{12}}+\frac{315l_2}{r_2^{10}}\right).$$

6. $$\frac{21a^{10}}{262144}\frac{d^2r_2}{d\phi^2}\left(+\frac{46189l_2^9}{r_2^{20}}-\frac{87516l_2^7}{r_2^{18}}+\frac{54054l_2^5}{r_2^{16}}-\frac{12012l_2^3}{r_2^{14}}+\frac{693l_2}{r_2^{12}}\right).$$

7. $$\frac{33a^{12}}{2097152}\frac{d^2r_2}{d\phi^2}\left(-\frac{676039l_2^{11}}{r_2^{24}}+\frac{1616615l_2^9}{r_2^{22}}-\frac{1385670l_2^7}{r_2^{20}}+\frac{510510l_2^5}{r_2^{18}}-\frac{75075l_2^3}{r_2^{16}}+\frac{3003l_2}{r_2^{14}}\right).$$

8. $$\frac{429a^{14}}{67108864}\frac{d^2r_2}{d\phi^2}\left(+\frac{5014575l_2^{13}}{r_2^{28}}-\frac{14486550l_2^{11}}{r_2^{26}}+\frac{15935205l_2^{9}}{r_2^{24}}\right.$$
$$\left.-\frac{8314020l_2^{7}}{r_2^{22}}+\frac{2078505l_2^{5}}{r_2^{20}}-\frac{218790l_2^{3}}{r_2^{18}}+\frac{6435l_2}{r_2^{16}}\right).$$

Term

9. $$\frac{715a^{16}}{2147483648}\frac{d^2r_2}{d\phi^2}\left(-\frac{300540195l_2^{15}}{r_2^{32}}+\frac{1017958725l_2^{13}}{r_2^{30}}-\frac{1368978975l_2^{11}}{r_2^{28}}\right.$$
$$\left.+\frac{929553625l_2^{9}}{r_2^{26}}-\frac{334639305l_2^{7}}{r_2^{24}}+\frac{61108047l_2^{5}}{r_2^{22}}-\frac{4849845l_2^{3}}{r_2^{20}}+\frac{109395l_2}{r_2^{18}}\right)$$

10. $$\frac{2431a^{18}}{17179869184}\frac{d^2r_2}{d\phi^2}\left(+\frac{2268783825l_2^{17}}{r_2^{36}}-\frac{8815845720l_2^{15}}{r_2^{34}}\right.$$
$$+\frac{140252091001_2^{13}}{r_2^{32}}-\frac{11763078600l_2^{11}}{r_2^{30}}+\frac{5577321750l_2^{9}}{r_2^{28}}$$
$$\left.-\frac{1487285800l_2^{7}}{r_2^{26}}+\frac{208220012l_2^{5}}{r_2^{24}}-\frac{12932920l_2^{3}}{r_2^{22}}+\frac{230945l_2}{r_2^{20}}\right)$$

NUMERICAL FACTORS

2.	0.1875				
3.	0.2734375	0.1171875			
4.	0.5639648	0.5126953	0.0854492		
5.	1.374664	1.924530	0.7402039	0.0672913	
6.	3.700138	7.010788	4.330193	0.9622650	0.0555153
7.	10.63790	25.43845	21.80439	8.033195	1.181352
					0.0472541
8.	32.05616	92.60669	101.8674	53.14819	13.28705
				1.398637	0.0411364
9.	100.0642	338.9271	455.7986	309.4929	111.4174
			20.34579	1.614745	0.0364228
10.	321.0393	1247.467	1984.607	1664.509	789.2068
		210.4551	29.46372	1.830045	0.0326794

Term TERMS IN $\left(\frac{dr}{d\phi}\right)^2$

2. $$\frac{a^2}{16}\left(\frac{dr_2}{d\phi}\right)^2\left(-\frac{12l_2}{r_2^{5}}\right).$$

3. $$\frac{a^4}{128}\left(\frac{dr_2}{d\phi}\right)^2\left(+\frac{280l_2^{3}}{r_2^{9}}-\frac{90l_2}{r_2^{7}}\right).$$

4. $$\frac{5a^6}{2048}\left(\frac{dr_2}{d\phi}\right)^2\left(-\frac{2772l_2^{5}}{r_2^{13}}+\frac{2100l_2^{3}}{r_2^{11}}-\frac{280l_2}{r_2^{9}}\right).$$

5. $$\frac{7a^8}{32768}\left(\frac{dr_2}{d\phi}\right)^2\left(+\frac{102960l_2^{7}}{r_2^{17}}-\frac{126126l_2^{5}}{r_2^{15}}+\frac{41580l_2^{3}}{r_2^{13}}-\frac{3150l_2}{r_2^{11}}\right)$$

6. $$\frac{21a^{10}}{262144}\left(\frac{dr_2}{d\phi}\right)^2\left(-\frac{923780l_2^9}{r_2^{21}}+\frac{1575288l_2^7}{r_2^{19}}-\frac{864864l_2^5}{r_2^{17}}+\frac{168168l_2^3}{r_2^{15}}-\frac{8316l_2}{r_2^{13}}\right)$$

7. $$\frac{33a^{12}}{2097152}\left(\frac{dr_2}{d\phi}\right)^2\left(+\frac{16224936l_2^{11}}{r_2^{25}}-\frac{35565530l_2^9}{r_2^{23}}+\frac{27713400l_2^7}{r_2^{21}}-\frac{9189180l_2^5}{r_2^{19}}+\frac{1201200l_2^3}{r_2^{17}}-\frac{42042l_2}{r_2^{15}}\right)$$

8. $$\frac{429a^{14}}{67108864}\left(\frac{dr_2}{d\phi}\right)^2\left(-\frac{140408100l_2^{13}}{r_2^{29}}+\frac{376650300l_2^{11}}{r_2^{27}}-\frac{382444920l_2^9}{r_2^{25}}+\frac{182908440l_2^7}{r_2^{23}}-\frac{41570100l_2^5}{r_2^{21}}+\frac{3938220l_2^3}{r_2^{19}}-\frac{102960l_2}{r_2^{17}}\right)$$

9. $$\frac{715a^{16}}{2147483648}\left(\frac{dr_2}{d\phi}\right)^2\left(+\frac{9617286240l_2^{15}}{r_2^{33}}-\frac{30538761750l_2^{13}}{r_2^{31}}+\frac{38331411300l_2^{11}}{r_2^{29}}-\frac{24168394250l_2^9}{r_2^{27}}+\frac{8031343320l_2^7}{r_2^{25}}-\frac{1344377034l_2^5}{r_2^{23}}+\frac{96996900l_2^3}{r_2^{21}}-\frac{1969110l_2}{r_2^{19}}\right)$$

10. $$\frac{2431a^{18}}{17179869184}\left(\frac{dr_2}{d\phi}\right)^2\left(-\frac{81676217700l_2^{17}}{r_2^{37}}+\frac{2997387544801_2^{15}}{r_2^{35}}-\frac{448806691200l_2^{13}}{r_2^{33}}+\frac{352892358000l_2^{11}}{r_2^{31}}-\frac{156165009000l_2^9}{r_2^{29}}+\frac{38669430800l_2^7}{r_2^{27}}-\frac{4997280288l_2^5}{r_2^{25}}+\frac{284524240l_2^3}{r_2^{23}}-\frac{4618900l_2}{r_2^{21}}\right)$$

NUMERICAL FACTORS

2.	0. 75				
3.	2. 1875	0. 703125			
4.	6. 767578	5. 126953	0. 6835938		
5.	21. 99463	26. 94342	8. 882446	0. 6729126	
6.	74. 00276	126. 1942	69. 28308	13. 47171	0. 6661835
7.	255. 3095	559. 6459	436. 0877	144. 5975	18. 90163
					0. 6615572
8.	897. 5726	2407. 774	2444. 817	1169. 260	265. 7409
				25. 17546	0. 6581819
9.	3202. 054	10167. 81	12762. 36	8046. 814	2674. 018
			447. 6074	32. 29491	0. 6556109
10.	11557. 42	42413. 88	63507. 41	49935. 27	22097. 79
		5471. 834	707. 1293	40. 26098	0. 6535874

Term	TERMS IN $\left(\frac{dl}{d\phi}\right)^2$
2.	0
3.	$\frac{a^4}{128}\left(\frac{dl_2}{d\phi}\right)^2\left(+\frac{30l_2}{r_2^7}\right)$

4. $$\frac{5a^6}{2048}\left(\frac{dl_2}{d\phi}\right)^2\left(-\frac{420l_2^3}{r_2^{11}}+\frac{140l_2}{r_2^9}\right)$$

5. $$\frac{7a^8}{32768}\left(\frac{dl_2}{d\phi}\right)^2\left(+\frac{18018l_2^5}{r_2^{15}}-\frac{13860l_2^3}{r_2^{13}}+\frac{1890l_2}{r_2^{11}}\right)$$

6. $$\frac{21a^{10}}{262144}\left(\frac{dl_2}{d\phi}\right)^2\left(-\frac{175032l_2^7}{r_2^{19}}+\frac{216216l_2^5}{r_2^{17}}-\frac{72072l_2^3}{r_2^{15}}+\frac{5544l_2}{r_2^{13}}\right)$$

7. $$\frac{33a^{12}}{2097152}\left(\frac{dl_2}{d\phi}\right)^2\left(+\frac{3233230l_2^9}{r_2^{23}}-\frac{5542680l_2^7}{r_2^{21}}+\frac{3063060l_2^5}{r_2^{19}}-\frac{600600l_2^3}{r_2^{17}}+\frac{30030l_2}{r_2^{15}}\right)$$

8. $$\frac{429a^{14}}{67108864}\left(\frac{dl_2}{d\phi}\right)^2\left(-\frac{28973100l_2^{11}}{r_2^{27}}+\frac{63740820l_2^9}{r_2^{25}}-\frac{49884120l_2^{11}}{r_2^{23}}+\frac{16628040l_2^5}{r_2^{21}}-\frac{2187900l_2^3}{r_2^{19}}+\frac{77220l_2}{r_2^{17}}\right)$$

9. $$\frac{715a^{16}}{2147483648}\left(\frac{dl_2}{d\phi}\right)^2\left(+\frac{2035917450l_2^{13}}{r_2^{31}}-\frac{5475915900l_2^{11}}{r_2^{29}}+\frac{5577321750l_2^9}{r_2^{27}}-\frac{2677114440l_2^7}{r_2^{25}}+\frac{611080470l_2^5}{r_2^{23}}-\frac{58198140l_2^3}{r_2^{21}}+\frac{1531530l_2}{r_2^{19}}\right)$$

10. $$\frac{2431a^{18}}{17179869184}\left(\frac{dl_2}{d\phi}\right)^2\left(-\frac{17631691440l_2^{15}}{r_2^{35}}+\frac{56100836400l_2^{13}}{r_2^{33}}-\frac{70578471600l_2^{11}}{r_2^{31}}+\frac{44618574000l_2^9}{r_2^{29}}-\frac{14872858000l_2^7}{r_2^{27}}+\frac{2498640144l_2^5}{r_2^{25}}-\frac{181060880l_2^3}{r_2^{23}}+\frac{3695120l_2}{r_2^{21}}\right)$$

NUMERICAL FACTORS

2.	0.					
3.	0.234375					
4.	1.025391	0.3417969				
5.	3.849060	2.960815	0.4037476			
6.	14.02158	17.32077	5.773590	0.4441223		
7.	50.87690	87.21754	48.19917	9.450817	0.4725409	
8.	185.2134	407.4694	318.8891	106.2964	13.98637	0.4936364
9.	677.8543	1823.194	1856.957	891.3394	203.4579	19.37694
						0.5099196
10.	2494.934	7938.427	9987.053	6313.654	2104.551	353.5646
						25.62063
						0.5228699

Term — TERMS IN $\left(\frac{dr}{d\phi}\frac{dl}{d\phi}\right)$

2. $$\frac{a^2}{16}\left(\frac{dr_2}{d\phi}\frac{dl_2}{d\phi}\right)\left(+\frac{6}{r_2^4}\right)$$

3. $$\frac{a^4}{128}\left(\frac{dr_2}{d\phi}\frac{dl_2}{d\phi}\right)\left(-\frac{210l_2^2}{r_2^8}+\frac{30}{r_2^6}\right)$$

4. $$\frac{5a^6}{2048}\left(\frac{dr_2}{d\phi}\frac{dl_2}{d\phi}\right)\left(+\frac{2310l_2^4}{r_2^{12}}-\frac{1260l_2^2}{r_2^{10}}+\frac{70}{r_2^8}\right)$$

5. $$\frac{7_a^8}{32768}\left(\frac{dr_2}{d\phi}\frac{dl_2}{d\phi}\right)\left(-\frac{90090l_2^6}{r_2^{16}}+\frac{90090l_2^4}{r_2^{14}}-\frac{20790l_2^2}{r_2^{12}}+\frac{630}{r_2^{10}}\right)$$

6. $$\frac{21a^{10}}{262144}\left(\frac{dr_2}{d\phi}\frac{dl_2}{d\phi}\right)\left(+\frac{831402l_2^8}{r_2^{20}}-\frac{1225224l_2^6}{r_2^{18}}+\frac{540540l_2^4}{r_2^{16}}-\frac{72072l_2^2}{r_2^{14}}+\frac{1386}{r_2^{12}}\right)$$

7. $$\frac{33a^{12}}{2097152}\left(\frac{dr_2}{d\phi}\frac{dl_2}{d\phi}\right)\left(-\frac{14872858l_2^{10}}{r_2^{24}}+\frac{29099070l_2^8}{r_2^{22}}-\frac{19399380l_2^6}{r_2^{20}}+\frac{5105100l_2^4}{r_2^{18}}-\frac{450450l_2^2}{r_2^{16}}+\frac{6006}{r_2^{14}}\right)$$

8. $$\frac{429a^{14}}{67108864}\left(\frac{dr_2}{d\phi}\frac{dl_2}{d\phi}\right)\left(+\frac{130378950l_2^{12}}{r_2^{28}}-\frac{318704100l_2^{10}}{r_2^{26}}+\frac{286833690l_2^8}{r_2^{24}}-\frac{116396280l_2^6}{r_2^{22}}+\frac{20785050l_2^4}{r_2^{20}}-\frac{1312740l_2^2}{r_2^{18}}+\frac{12870}{r_2^{16}}\right)$$

9. $$\frac{715a^{16}}{2147483648}\left(\frac{dr_2}{d\phi}\frac{dl_2}{d\phi}\right)\left(-\frac{90162058501_2^{14}}{r_2^{32}}+\frac{26466926850l_2^{12}}{r_2^{30}}-\frac{30117537450l_2^{10}}{r_2^{28}}+\frac{16731965250l_2^8}{r_2^{26}}-\frac{4684950270l_2^6}{r_2^{24}}+\frac{611080470l_2^4}{r_2^{22}}-\frac{29099070l_2^2}{r_2^{20}}+\frac{218790}{r_2^{18}}\right)$$

10. $$\frac{2431a^{18}}{17179869184}\left(\frac{dr_2}{d\phi}\frac{dl_2}{d\phi}\right)\left(+\frac{771386500501_2^{16}}{r_2^{36}}-\frac{264475326850l_2^{14}}{r_2^{34}}+\frac{364655436600l_2^{12}}{r_2^{32}}-\frac{258787729200l_2^{10}}{r_2^{30}}+\frac{100391791500l_2^8}{r_2^{28}}-\frac{20822001200l_2^6}{r_2^{26}}+\frac{2082200120l_2^4}{r_2^{24}}-\frac{71597520l_2^2}{r_2^{22}}+\frac{461890}{r_2^{20}}\right)$$

NUMERICAL FACTORS

2.	0. 375					
3.	1. 640625	0. 234375				
4.	5. 639648	3. 076172	0. 1708984			
5.	19. 24530	19. 24530	4. 441223	0. 1345825		
6.	66. 60249	98. 15103	43. 30193	5. 773590	0. 1110306	
7.	234. 0337	457. 8921	305. 2614	80. 33195	7. 088113	
					0. 0945082	
8.	833. 4602	2037. 347	1832. 334	744. 0746	132. 8705	
				8. 391819	0. 0822727	
9.	3001. 926	8812. 106	10027. 57	5570. 871	1559. 844	
			203. 4579	9. 688472	0. 0728457	
10.	10915. 34	37424. 01	51599. 77	36619. 19	14205. 72	
		2946. 372	294. 6372	10. 13125	0. 0653587	

Equation 19 may appear formidable, but as with a similar formula in the 1930 paper (eq 11, p. 1266–67), it is comparatively simple in application. It contains the same system of vertical and diagonal moduli by which the literal parts of all terms after the second can be rapidly obtained, after which the terms are completed by applying the numerical factors.

The preceding discussion has been based upon the assumption that the center of the attracted segment is on the same level as the axes of the cylinders. While in practice this is nearly true for the balls, it is not the case with the elements of the beam, and in calculating the attraction on the beam, formulas 13 to 18 require a slight modification.

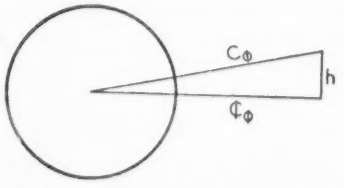

FIGURE 7.—*Geometrical constants for attraction on beam.*

In figure 7, C_ϕ is the same as C_ϕ in eq 19, the fundamental length which determines the potential of the cylinder at the center of the attracted element; h is the elevation of the center of the element above the cylinder axis, $\not{c}_\phi$ is the horizontal projection of C_ϕ, and $\not{c}_0$ the horizontal projection of C_0. The slanting line C_ϕ is not directly measured, but is calculated from $\not{c}_\phi$ and h. The plane of the angle ϕ remains horizontal. The next step is to see what difference (if any) the introduction of h will make in C_ϕ, r, l, and their derivatives which occur in formula 19.

We have the fundamental equations:

$$\left.\begin{aligned} &\not{c}_\phi=\not{c}_0+R(1-\cos\phi), \text{ whence } \frac{d\not{c}}{d\phi}=R\sin\phi \text{ and } \frac{d^2\not{c}}{d\phi^2}=R\cos\phi \\ &C_\phi{}^2=\not{c}_\phi{}^2+h^2 \\ &r^2=\not{c}_\phi{}^2+h^2+l^2 \end{aligned}\right\} \quad (20)$$

For the derivatives of C_ϕ, we have

$$\left.\begin{aligned}\frac{dC_\phi}{d\phi}&=\frac{\xi_\phi}{C_\phi}\frac{d\xi_\phi}{d\phi}=\frac{\xi_\phi}{C_\phi}R\sin\phi\\ \frac{d^2C_\phi}{d\phi^2}&=\frac{\xi_\phi}{C_\phi}\frac{d^2\xi_\phi}{d\phi^2}+\left(\frac{1}{C_\phi}-\frac{\xi_\phi^2}{C_\phi^3}\right)\left(\frac{d\xi_\phi}{d\phi}\right)^2\\ &=\frac{\xi_\phi}{C_\phi}R\cos\phi+\frac{h^2}{C_\phi^3}R^2\sin^2\phi,\end{aligned}\right\}\tag{21}$$

which assume still simpler values at the equilibrium angles.

The formulas for l_1 and l_2 and their derivatives, given by eq 15 and 16, are unaltered by the introduction of h. And this being the case, the formula for r^2 in eq 20 will give derivatives of the same form as those in eq 17, the only difference being that ξ_ϕ is written for C_ϕ.

In the case of the attraction between cylinders and balls in the present work, the value of h was always less than 1 mm, and the minimum value of ξ about 13 cm. This rendered the h-correction unnecessary for the balls, though obviously necessary for the beam.

V. DESCRIPTION OF APPARATUS

For the purpose of this work a special building was erected in a wooded section of the Bureau grounds, at a sufficient distance from parking lots and moving traffic to avoid disturbances. This building was 30 feet long and 20 feet wide, and was divided into two rooms by a partition. The walls of the building were of sheet steel with heat insulation, and were unprovided with windows. The inner partition was also heat-insulated. The front room of the building was the observing room, and contained the photographic recording apparatus. The torsion balance was in the rear room. Both rooms were electrically heated, with thermostatic control.

The torsion balance (fig. 8) was mounted on a massive concrete base in the center of the rear room. The rest of the floor was of wood, except that four concrete slabs were provided for the purpose of setting up a kathetometer for measuring vertical distances. The concrete base carried a circular steel plate 65 cm in diameter and 5 cm thick, at the center of which was the pendulum case, supported by three leveling screws. Three additional leveling screws were provided, which carried no load, but served to produce a more uniform gravitational field about the pendulum.

On the outer portion of the circular steel plate there was a circular steel ring 12 cm wide and 4 cm thick, resting on a complete ring of steel balls running in grooves. This steel ring carried the large attracting cylinders, and by rotating the ring the cylinders could be brought into the near or the far position as desired. To facilitate this adjustment the outer rim of the circular steel plate was provided with graduations and the rim of the circular ring carried a reference mark.

The cylinders were kept in place on the steel ring by four small aluminum wedges. As these wedges weighed about 0.21 g each, and the cylinders about 66,000 g, no correction for the attraction of the wedges was necessary.

The pendulum case and its lid were made of soft iron, for magnetic shielding. Windows were provided for observing the elevation of the

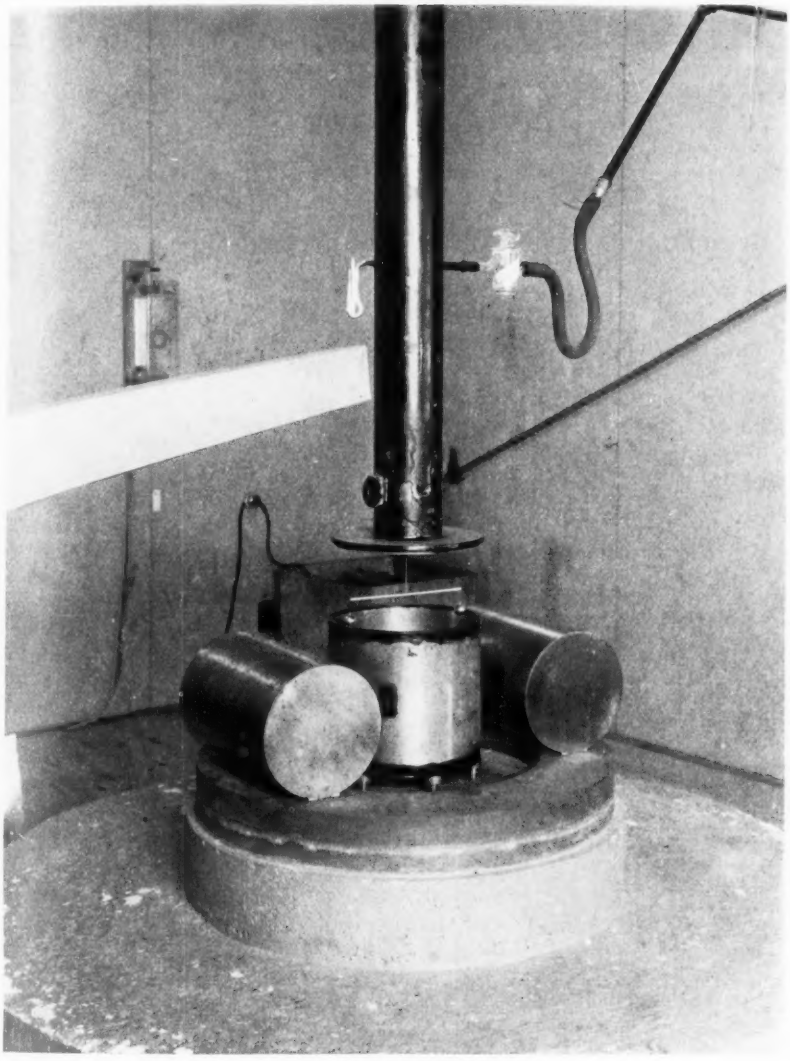

FIGURE 8.—*Torsion balance.*

balls. The joint between the case and lid was sealed with Peixene wax. A brass tube attached to the lid carried the suspending filament. This tube was provided near the lower end with an observing window and four smaller windows for centering the filament. At the upper end the tube contained the movable torsion head described in the 1930 paper, by which the resting point of the filament could be adjusted from outside by means of a magnet without breaking the vacuum.

The beam of the pendulum with its attached balls can be seen in place in figure 8. The beam was an aluminum tube 20 cm long and 0.5 cm in outside diameter. The beam was provided at its center with a vertical brass rod 5.5 cm long. A phosphor-bronze truss wire was run through the tube and its ends soldered to the upper end of the vertical brass rod. A piece of annealed tungsten filament, 0.0012 in. in diameter, was also run through the tube to provide a suspension for the balls, the centers of which were about 4 cm below the center of the beam. The balls were of platinum, provided with platinum hooks, and weighed about 87 g each. They were shaped to a spherical form by scraping through a steel die plate, as described in the 1930 paper.

The upper point of the beam truss was not joined directly to the suspending filament, but to a short piece of thin brass rod which carried a small optically flat silvered mirror at the level of the observing window. The connections with the filament at each end were made by small clamps.

The total mass of the beam was about 5.7 g. The vacuum masses per unit length of the different parts were as follows, in grams per centimeter:

Aluminum tube	0.21254
Truss wire	.00261
Filament supporting balls	.00015

Two different tungsten filaments were used as a suspension for the pendulum. One of these was ordinary commercial lamp filament, hard-drawn, of diameter 0.0012 in. and tensile strength 288 g. This filament had been coiled in the drawing process, and consequently exhibited considerable drift when first set up. The measurements with this filament were not begun until 3 months after setting up, by which time the drift of the resting point had been reduced to 0.04 cm in 15 hours, the photographic plate being 490 cm from the filament. The total load on the filament was about 182 g.

After the completion of the measurements with this filament, we obtained, through the cooperation of W. E. Forsythe, of the General Electric Lamp Works at Cleveland, several pieces of specially annealed filament which had been kept straight in drawing and shipping. This filament, on account of being annealed, had a lower tensile strength than the hard-drawn filament, and a diameter of 0.0014 in. was necessary to give a tensile strength of 284 g. This filament, although care was taken not to bend it in the process of setting up, showed a slight drift, which after 2 months' time was reduced to about half that of the hard-drawn filament.

The experience of Bearden [2] of Johns Hopkins University with straight-drawn and especially annealed tungsten filament, in his work on the viscosity of air, led us to expect more precise results from the

[2] Phys. Rev. **56** [2] 1023 (Nov. 15, 1939).

annealed filament than from the hard-drawn one. The reverse, however, was the case. The average departure from the mean in our measurements with the hard-drawn filament was about half that obtained with the annealed filament, because of the fourth-power law of torsion. The times of swing with the annealed filament of diameter 0.0014 in. were about 1,880 and 1,640 sec in the far and near positions, respectively, with a difference of 240 sec. With the hard-drawn filament, of diameter 0.0012 in., the times of swing were increased to 2,920 and 2,200 sec, with a difference of 720 sec. This threefold increase in sensitivity with the hard-drawn filament apparently overbalanced any slight advantage of stability on the part of the annealed filament.

Of course, in geophysical surveying, where it is of importance to occupy as many stations as possible in the course of a week, it is out of the question to allow a month or more for a filament to stabilize itself; and in Bearden's work it was not necessary to determine the difference between two times of swing.

The vacuum used in the pendulum case was always less than 0.5 mm. Experiments were made with a molecular pump giving a much lower pressure, but it was found that at pressures below 0.5 mm the damping factor of the pendulum became constant, indicating that at such pressures the air resistance was negligible compared to the internal friction in the filament.

VI. METHOD OF OBSERVING

1. ADJUSTMENTS

(a) ADJUSTMENT OF CYLINDERS

The ideal adjustment of the cylinders requires that they be symmetrical with respect to a certain circle, which, of course, includes the condition of mutual parallelism. The tolerance for this adjustment is much greater than might be supposed. In all cases of asymmetry, one half of a cylinder will be a little nearer a ball than it should be and the other half a little too far away, and these two inaccuracies will partly cancel each other. For instance, calculation shows that, in the near position, a difference of 0.3 mm in the distance between the cylinders at their ends (28 cm apart) will affect only the seventh significant figure in the value of $d^2V/d\phi^2$, and for the far position the effect will be still less. It is, in fact, quite practicable to adjust for parallelism by a few trials to an accuracy of 0.1 mm.

The cylinders were so accurately shaped that their lengths differed by only 0.01 mm, and consequently it was easy to set them with their end faces in the same plane with an accuracy of 0.1 mm by laying a straightedge across the faces.

It was found also that the circular steel ring was sufficiently accurate to serve as the circle of reference for the cylinders and the pendulum. Measurements of the inside and outside diameters of the ring showed that no error greater than 0.2 mm existed in these dimensions. By means of the graduated circle around the rim of the steel plate it was possible to complete the adjustment of the cylinders for symmetry with respect to the circle.

(b) ADJUSTMENT OF PENDULUM

For the pendulum three adjustments are necessary—azimuth, longitudinal, and transverse. These adjustments, as was found in the 1930 work, have a rather large tolerance, which in some cases, as in the azimuth setting in the near position, is increased by the changed position of the cylinders. Calculation gives the following errors in the result introduced by neglecting the errors in the separate adjustments in the near position. In the far position there will be still less effect in the result.

Transverse centering, error 0.5 mm____1 part in 27,000
Longitudinal centering, error 0.5 mm___1 part in 26,000
Azimuth centering, error 0.1°_____1 part in 65,000

The original adjustments for centering could be made to 0.1 mm and 0.1°. The centering adjustments were checked at intervals during the

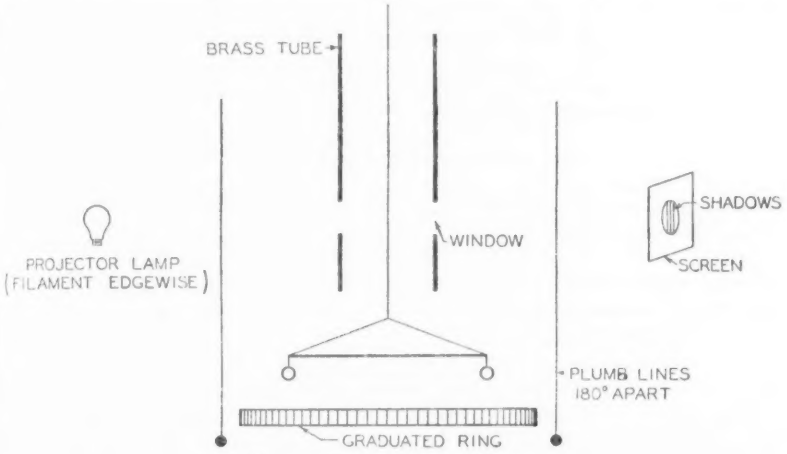

FIGURE 9.—*Centering device.*

work, and such errors as arose in the course of the work were recorded and allowed for in the computations.

The azimuth setting was made in the present work by direct observation. The lid of the pendulum case was lifted sufficiently to allow the beam to be held against two supports in such a position that the normal to the mirror passed approximately through the center of the recording apparatus, as determined by visual observation. Then by means of two plumb lines the azimuths of the centers of the ends of the beam were found to be 285.6° and 107.2°, with a difference of 178.4° instead of 180°. This showed that a transverse adjustment was necessary. Imagining such an adjustment to be made so that the azimuth at each end will be altered by 0.8°, the correct azimuth readings were found to be 286.4° and 106.4°. Then, by turning the steel ring carrying the cylinders until the centers of the cylinders were at these azimuth readings, the cylinders could be set in the near position, and by turning 90° farther, in the far position.

The pendulum case was then closed and the filament centered longitudinally and transversely, making use of the four observation

windows in the tube carrying the filament (fig. 9). For this purpose two plumb bobs were hung close to the graduations on the circular steel plate, 180° apart. A projector lamp was placed in line with these plumb bobs at a distance of about 3 m from the filament, giving approximately a point source of light, and a white cardboard screen was placed on the opposite side of the pendulum case, on which three sharp shadows could be obtained, two of the wire plumb lines and one of the filament. By moving the plumb lines around, always keeping them 180° apart, their shadows could be made to coincide, and then by tilting the pendulum case by means of its leveling screws the shadow of the filament could be brought into coincidence with the shadow of the plumb lines. By carrying out this process in two positions 90° apart, the filament could be centered with respect to the circular steel plate with an accuracy of 0.1 mm.

This centering was made at first with the glass panes of the observing windows removed. The glass panes were then replaced and the case was exhausted. No apparent change was observed in the centering. From time to time as the observations were made the centering was checked, and slight variations were observed, the maximum being 0.9 mm. No attempt was made to correct these changes, but they were recorded and allowed for in the computations.

2. LENGTH MEASUREMENTS

The lengths to be measured, horizontal and vertical, in the present work were essentially the same as those in the earlier work, and except for the device of the previously described rayon-filament plumb bobs in measuring the distance between the cylinders, were carried out with the same instruments and in the same manner as described in the 1930 paper.

3. TIME MEASUREMENTS

The choice of a photographic method for recording the transits of the pendulum was prompted by several considerations. Perhaps the most important of these was the desire to obtain an accurate record of transits at small amplitudes, as these have the greatest influence in the reduction of the time of swing to infinitesimal amplitude. Moreover, by making the method completely automatic, the necessity for the continuous presence of the observer was eliminated.

(a) STANDARD OF TIME

The standard of time employed was the primary frequency standard maintained by the radio laboratory of the National Bureau of Standards. This standard originates in a 100-kc quartz oscillator, from which, by a submultiple generator, a 60-cycle current was obtained. This standard 60-cycle current was amplified sufficiently to operate the signaling mechanism of the photographic recording apparatus. The frequency of the primary oscillator was constant to better than 1 part in 10 million.

The signals used in the recording apparatus were flashes of light at 5-sec intervals. These were obtained by a revolving shutter in the form of a brass disk with radial slits cut in its periphery. This disk was rotated at a speed of one revolution a minute by means of

a synchronous clock motor driven by the standard 60-cycle current. The disk carried 11 slits at intervals of 30°, the twelfth being omitted to mark the minutes.

(b) OPTICAL SYSTEM

Two slightly different optical systems were used. The first system, used with the hard-drawn filament, was an adaptation of a system previously used for visual observations. In this system the light from a 200-watt projector lamp was focused on a narrow slit close to the revolving disk. The light from the slit then entered the eyepiece of a telescope and was directed to the plane mirror carried by the torsion pendulum. After reflection at this mirror, the light was brought to a focus to form an image of the signaling slit on a photographic plate. As the pendulum swung, an image was recorded on the plate every 5 sec. The distance from mirror to plate was 490 cm, and a deflection of 1° at the mirror corresponded to a distance of 17 cm at the plate. The sharpness of the lines obtained was such that three lines per millimeter could easily be resolved by a low-power microscope.

For the measurements with the annealed filament the optical system was improved to give sharper images on the photographic plate (fig. 10). Here the light flashes from the revolving disk were focused on a stationary slit by means of an achromatic lens. It was found that the presence of this second slit gave a much sharper image on the plate. After passing through a concave lens of 25 cm focal length, the light fell on a convex lens of 400-cm focal length mounted on the outside of the pendulum case just in front of the mirror carried by the pendulum. The light was reflected by the mirror back through the convex lens and was brought to a focus on the photographic plate. The sharpness of the lines obtained with this second system was such that five lines per millimeter could easily be resolved.

Except for the mirror on the pendulum and the convex lens on the outside of the pendulum case, the whole optical system, including the camera, was mounted on a concrete pier in the observing room (fig. 11). It was found that even though the apparatus and observing rooms were closed up and the temperature thermostatically controlled, there was sufficient turbulence caused by convection currents to be noticeable in the photographic record. For this reason a series of paper tubes was set up enclosing the light path in both directions. Undesirable reflections from the inner surfaces of these tubes, which would have fogged the plate, were prevented by a system of interior baffles.

A reference mark was provided on the photographic plate as a basis for measurements of the positions of the recorded images. This mark was the shadow of a fine wire fastened to the front panel of the camera (fig. 12). The shadow was made by the light from a neon lamp behind a pinhole in the optical path about 200 cm in front of the camera. The plate being continuously illuminated by the faint red light was fogged just enough to show the shadow of the wire as a white line, without interfering perceptibly with the definition of the recorded images.

(c) THE CAMERA

The camera consisted of a metal box in which the plateholder could move only in a vertical direction (fig. 12). A spring on the

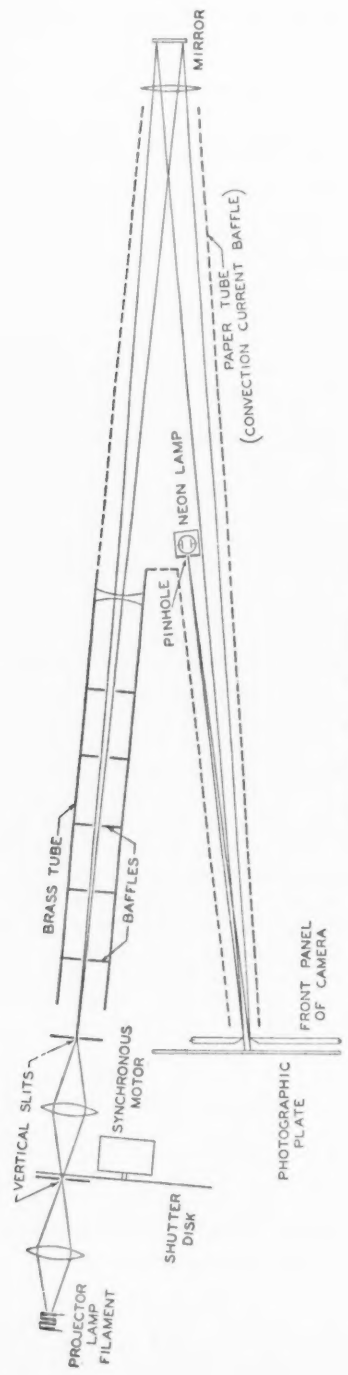

FIGURE 10.—*Optical system.*

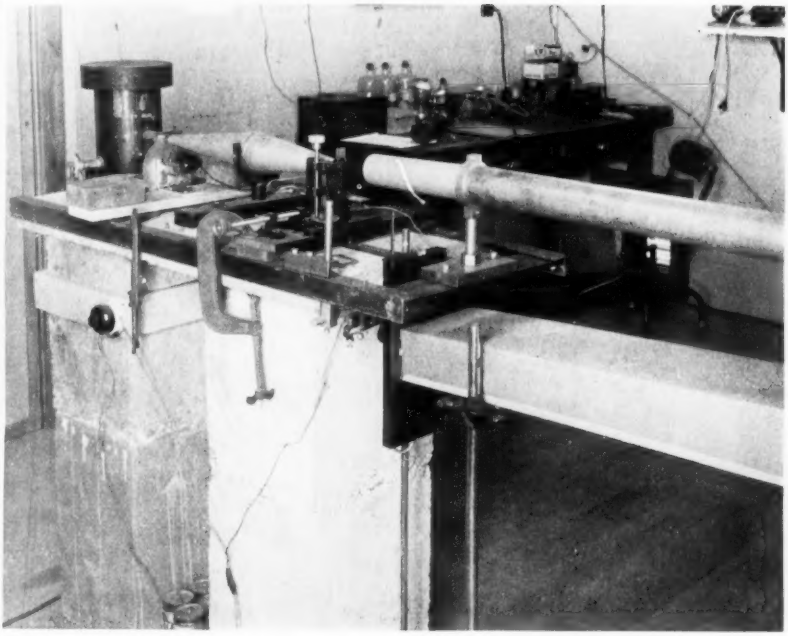

FIGURE 11.—*Photographic recording apparatus.*

UNIV. OF MICH.

plateholder bearing against the side of the camera prevented any sidewise motion of the plateholder. The beam of light reflected from the moving mirror entered through a horizontal slot cut through the front panel of the camera. With the pendulum at rest, the image of the illuminated slit was centered vertically across this slot and the motion of the mirror made the beam traverse the length of the slot. Thus, only as much of the plate was exposed during a given transit as was exposed by the slot during the transit. A guillotine safety

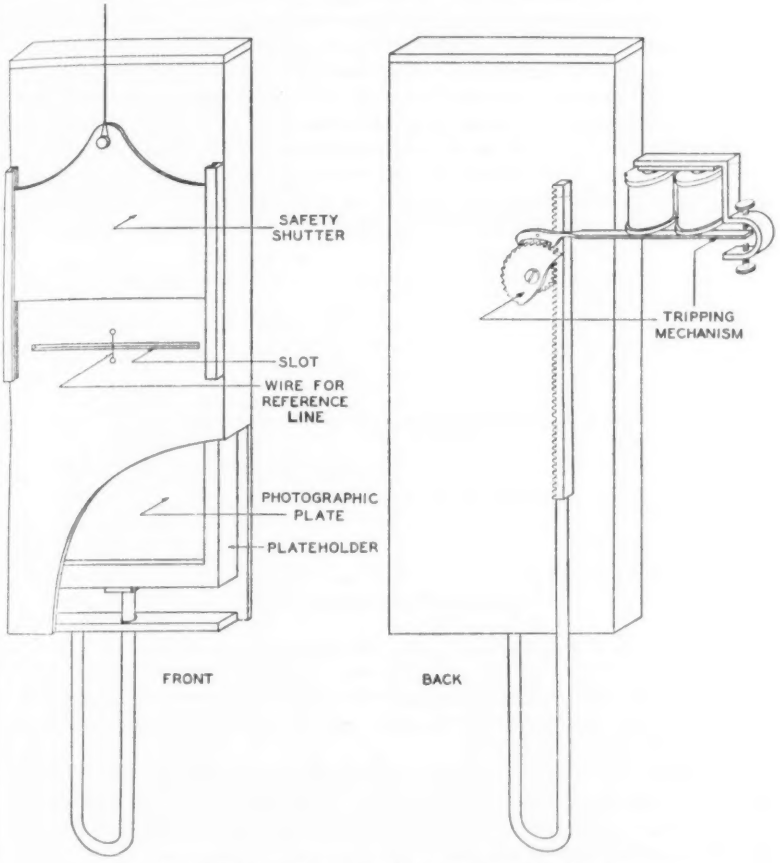

FIGURE 12.—*Camera and tripping mechanism.*

shutter on the front panel could be dropped to cover the slot whenever it was desired to make the camera light-tight.

Between transits, the vertical position of the plateholder was changed automatically by means of a tripping mechanism mounted on the back of the camera (fig. 12). Essentially, the mechanism consisted of a pawl-and-ratchet escapement. The pawl was actuated by an electromagnet. The ratchet was rigidly connected to a pinion which in turn was geared to a rack sliding in ways. The rack formed one prong of a fork whose other prong entered the camera through a

hole in its bottom. The plateholder rested on the end of the prong within the camera. Thus, when a pulse of current from a timing device actuated the electromagnet, the escapement permitted the plateholder to drop by gravity through a predetermined distance.

The camera accommodated 4- by 5-in. photographic plates. The choice of this particular size was dictated by the availability of a traveling microscope whose screw was 10 cm in length. The plate emulsion was of the modern high-speed panchromatic variety. Over 80 transits could be recorded on a single plate.

The pulse of current through the electromagnet was obtained when a timing device (fig. 13) momentarily closed a switch as the pendulum reached the end of its swing. The timing device consisted of an endless rubber belt running over two pulleys, one of which was driven by a synchronous motor suitably geared down, and the other idled in a set of pivot bearings. A balance wheel from a watch, lightly pivoted to reduce friction, was fastened to one arm of a spring-leaf switch. This balance wheel, acting merely as a pressure wheel, was brought to bear against the rubber belt opposite the idler pulley. The switch,

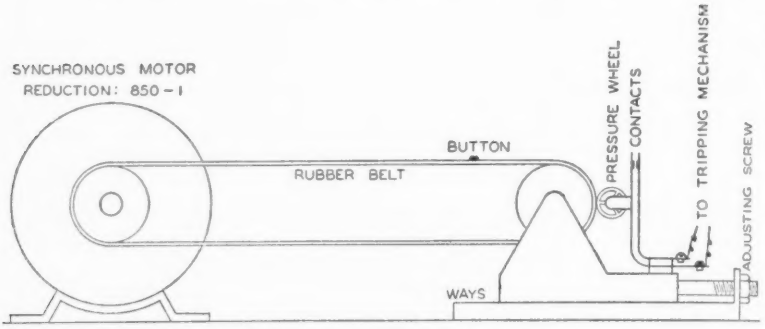

FIGURE 13.—*Timing device.*

in series with a battery and the electromagnet, was normally open, but when a rubber button which was cemented to the outer surface of the rubber belt came in contact with the pressure wheel, the switch contacts were momentarily closed and a pulse of current was sent through the electromagnet.

The base on which the idler pulley and the switch were mounted moved in ways parallel to the belt. The length of the rubber belt, and therefore the interval between contacts, could be varied by means of an adjusting screw.

A different driving pulley was used with each type of swing, since the difference in the half period in the "near" and "far" positions was more than could be taken care of by the adjusting screw.

Using a pulley of the proper size, the length of the rubber belt was adjusted so that the interval between contacts was very nearly equal to the mean half period of the pendulum. The button on the rubber belt was brought into position to make contact, and the motor was started as the pendulum reached the end of its swing. Then throughout a series of 60 to 70 transits the time of contact and the time the pendulum reached the end of its swing remained very nearly synchronized.

Records were made at night, from five o'clock in the afternoon until eight o'clock the next morning. The pendulum was started swinging (by movable weights outside the case, as in the 1930 paper) and the plateholder adjusted in the camera. The guillotine safety shutter was dropped and the room darkened. The operator then pulled the slide of the plateholder, and going outside of the house and closing the door, pulled a wire which lifted the guillotine shutter, and the run was on. This process was reversed the next morning, the safety shutter being dropped before the door was opened.

The precision obtainable by this method of photographic recording can be seen from the following examples (table 1), taken from observations in the near position with the annealed filament. Measurement of the photographic record by a traveling microscope gave the following figures, for two transits, one near the beginning and one near the end of a 14-hour run, the central reference line on the record being taken as 50 mm.

TABLE 1.—*Time-scale relation*

TRANSIT 5			TRANSIT 66		
Time	Scale reading	Scale difference	Time	Scale reading	Scale difference
sec	*mm*	*mm*	*sec*	*mm*	*mm*
40	15.92		30	44.33	
		6.33			0.57
35	22.25		35	44.90	
		6.34			.58
30	28.59		40	45.48	
		6.33			.58
25	34.92		45	46.06	
		6.38			.55
20	41.30		50	46.61	
		6.36			.56
15	47.66		55	47.17	
		6.38			.57×2
10	54.04		5	48.31	
		6.38			.56
5	60.42		10	48.87	
		6.34×2			.58
55	73.10		15	49.45	
		6.28			.57
50	79.38		20	50.02	
					.55
			25	50.57	
					.57
			30	51.14	

It will be seen that although the speeds in these transits differ by a factor of 11, the speed in each transit is practically uniform within the space covered by each record, and interpolation is safe. By interpolation we next obtain for each transit of the run a table with integral values of the scale readings and nonintegral values of the time, such as would be obtained by chronographic recording of visual observations.

It was found that with 60 or more transits in each record, considerable time could be saved by making a change in the procedure of the 1930 paper. The calculation was carried out in the usual way up to the point where the mean midpoint of the swing was determined as the average of five separate values. The next step, the sinusoidal corrections, took a great deal of time, and it was found that this could be avoided.

The alternative procedure adopted can be illustrated by an example. Taking transit 5, we obtain by the aid of transits 4 and 6 the following midpoints on the scale in millimeters:

47.39
.39
.39
.38
.36
Mean 47.38

From the time-scale relation for this transit (table 1), we find by interpolation the following values of the time at the mean midpoint:

28 min 15.22 sec.
.23
.23
.23
.21
Mean 28 min 15.22 sec.

The corresponding value for transit 7 is found to be 55 min 35.45 sec, and the difference of these times, 27 min 20.23 sec, gives us one value for the damped period of the pendulum. From this point the procedure is the same as that in the 1930 paper.

VII. RESULTS

The computations for the present work are much too extensive to be given here. The complete computations and original notebooks are preserved in the Library at the National Bureau of Standards. As an illustration of the general procedure, we may summarize the calculation of one result in table 2.

TABLE 2.—*Calculation of G*

[Hard-drawn filament]

Far position, May 15–18, 1940. Periodic time = T_F = 2924.20 sec. Temp. 24.1° C.

I = moment of inertia = 17735.4

Values of KG

Balls and cylinders	349253.6 G
Beam and cylinders	2951.5 G
	352205.1 $G=(KG)_F$

Near position, May 22–24, 1940. T_N = 2200.12 sec. Temp. 24.1° C.

I = 17735.4

Values of KG

Balls and cylinders	−584323.1 G
Beam and cylinders	−3924.6 G
	−588247.7 $G=(KG)_N$

$$(KG)_F-(KG)_N=4\pi^2\left(\frac{I}{T_N^2}-\frac{I}{T_F^2}\right)$$

940453 G = 0.0627647

$G=6.6739\times10^{-8}$

Five values of G were obtained with each filament, hard-drawn and annealed. These values are given in table 3, with their average departures from the mean.

TABLE 3.—*Values of G*

Hard-drawn filament		Annealed filament	
	Δ		Δ
6.6739	0.0016	6.6670	0.0015
56	1	667	18
69	14	703	18
62	7	707	22
51	4	680	5
6.6755	0.0008	6.6685	0.0016

It will be seen that the precision of the results with the hard-drawn filament is twice that of the results with the annealed filament. Weighting the results in this proportion, we obtain for the weighted mean:

$$6.6732 \pm 0.0031.$$

In view of the fact that the average departure from the mean appears in the third decimal place, the fourth decimal place may be dropped, and we obtain for the final result:

$$\mathbf{6.673 \pm 0.003 \times 10^{-8}\ cm^3\ g^{-1}\ sec^2.}$$

The final result in the 1930 paper was:

$$\mathbf{6.670 \pm 0.005 \times 10^{-8}\ cm^3\ g^{-1}\ sec^{-2}.}$$

These two results agree well with each other, but it is to be noted that the increase in precision in the present work is hardly appreciable. It will also be noted that the present results show the same peculiarity of pattern as did those in the 1930 paper. The results with the hard-drawn filament differ from those with the annealed filament by an amount greater than can be accounted for by the departures from the mean.

It is difficult to explain this anomaly. The only point of difference in the two series of measurements was the difference in the filament, and while irregular variations in the torsion constant of the filament are to be expected, and would account for random variations in the individual results with any one filament, what is needed to account for the observed anomaly in the results with the two filaments is a regular variation of such a nature as to be incredible.

Comparing the 1930 results with those of the present work, the outstanding feature is that a carefully planned and executed attempt to increase the precision of the 1930 results has met with but slight success. The conclusion may be drawn that the limit of the possibilities of the torsion balance has been reached.

WASHINGTON, March 30, 1942.

463607—42——3

U. S. Department of Commerce National Bureau of Standards

RESEARCH PAPER RP1481

Part of Journal of Research of the National Bureau of Standards, Volume 29, July 1942

INFLUENCE OF INITIAL STRUCTURE AND RATE OF HEATING ON THE AUSTENITIC GRAIN SIZE OF 0.5-PERCENT-CARBON STEELS AND IRON-CARBON ALLOY

By Thomas G. Digges and Samuel J. Rosenberg

ABSTRACT

Tests were made to determine the influence of variations in initial structure and rate of heating through the transformation temperature range on the grain sizes at 1,475° and 1,600° F of a high-purity alloy of iron and carbon and two commercial steels each containing 0.5 percent of carbon. Variations in initial structure had no effect on the grain size of the iron-carbon alloy. Although the initial structure had some influence on the grain size of the steels, no correlation was found between the grain size and the spacing of pearlite or the form and distribution of the carbides. The rate of heating had a pronounced effect on the grain size of the iron-carbon alloy, and in some cases the rate of heating also influenced the grain size of the steels. However, the trend in the steels was the reverse of that of the iron-carbon alloy in that the finest grains were obtained in the steels with slow rates of heating.

CONTENTS

	Page
I. Introduction	33
II. Experimental materials and procedure	33
III. Results	37
1. Iron-carbon alloy	37
2. Noncontrolled steel	37
3. Controlled steel	38
IV. Discussion of results	38
V. Summary	39

I. INTRODUCTION

In a previous study [1] made with high-purity alloys of iron and carbon and plain carbon steels, it was shown that in certain cases the austenitic grain size was markedly affected by the rate of heating through the transformation temperature range. It was recognized at that time that variation in the initial structure was also a factor that should be considered in a study of austenitic grain size. The work reported herein is concerned with the influence of both the initial structure (i. e., the structure that existed just prior to heating to the temperature establishing the austenitic grain size) and the rate of heating upon the grain size of certain of the materials used in the previous investigation.

II. EXPERIMENTAL MATERIALS AND PROCEDURE

The chemical compositions of the alloy and steels used in the present study are given in table 1. The iron-carbon alloy was prepared in

[1] Samuel J. Rosenberg and Thomas G. Digges, *Effect of rate of heating through the transformation range on austenitic grain size*, J. Research NBS **25**, 215 (1940) RP1322; Trans. Am. Soc. Met. **29**, 638 (1941).

the laboratory [2] and contained less than 0.031 percent of identifiable impurities. The two steels were commercial heats differing principally in the amounts of aluminum oxide and aluminum. Heat designated *C–1*, with the lower proportion of aluminum, was produced under conditions which resulted in noncontrol of austenitic grain size, whereas heat *C–2* was produced under conditions intended to control the austenitic grain size. Each heat was representative of good commercial practice. In this report, these two steels are occasionally indicated by the terms "noncontrolled grain size" applied to steel *C–1* and "controlled grain size" applied to steel *C–2*.

The iron-carbon alloy was treated for three different initial structures, which consisted of (a) coarse pearlite, (b) fine pearlite (sorbite), and (c) spheroidized cementite (fig. 1). All of these treatments were carried out in vacuum, and the pearlitic structures were not produced by isothermal reactions.

TABLE 1.—*Chemical composition of iron-carbon alloy and steels used*

Identification	Element (percentage by weight)												
	C	Mn	P	S	Si	Ni	Co	Al_2O_3	Acid soluble Al	Total Al	[1]H_2	O_2	N_2
Iron-carbon alloy [2]	0.50	0.002	<0.001	0.004	0.002	0.007	0.007	[3]ND	ND	ND	0.0002	0.003	0.001
Noncontrolled steel (*C–1*)	.49	.79	.023	.023	.22	.....	.....	.001	.002	.0025	.0002	.004	.004
Controlled steel (*C–2*)	.49	.80	.022	.028	.21	.....	.....	.007	.016	.0195	.0002	.003	.004

[1] Values for gaseous elements obtained by the vacuum-fusion method.
[2] Total identifiable impurities, less than 0.031 percent, obtained by spectrochemical, chemical, and vacuum-fusion analyses.
[3] ND means not detected.

Each of the two commercial steels was treated to give initial structures differing in the interlamellar spacing of pearlite or in the form and distribution of the carbides (figs. 2 and 3). These initial structures were (a) coarse pearlite obtained by pack-annealing at 1,700° F; (b) medium pearlite obtained by air-cooling after hot-rolling; (c) fine pearlite (sorbite) formed by isothermal reaction at about 1,010° F; (d) bainite formed by isothermal reaction at 720° to 750° F; and (e) spheroidized cementite produced by prolonged heating of sorbitized steel in the temperature range of 1,200° to 1,300° F.

An interesting feature of the spheroidized structure of the iron-carbon alloy was the tendency of the carbides to coalesce in the form of a network, as is shown in figure 1, C.

The experimental procedure used was the same as that described in detail in the previous report (see footnote 1). Essentially, it consisted in heating small specimens, approximately 1/10 inch square by 0.04 inch thick, in a lead bath or in vacuum at various rates to 1,475° or 1,600° F. The specimens were held at these temperatures for 15 minutes and then cooled in a manner suitable for delineating the austenite grains with proeutectoid ferrite.

For the fastest rates of heating, the specimens were plunged into a lead bath maintained at a temperature of either 1,475° or 1,600° F.

[2] Thomas G. Digges, *Effect of carbon on critical cooling rate of high-purity iron-carbon alloys and plain carbon steels*, J. Research NBS **20**, 571 (1938) RP1092; also, *Effect of carbon on the hardenability of high-purity iron-carbon alloys*, Trans. Am. Soc. Metals **26**, 408 (1938).

For the specimens heated in vacuum, the rates of heating through the transformation range were taken as the average rates required to heat through the temperature range from 1,325° to 1,450° F. Two or more specimens were frequently used for any selected condition of test. The average grain sizes obtained are shown by representative micrographs at 100 diameters in figures 4 to 29, and the estimated American Society for Testing Materials grain numbers are summarized in table 2. This table is included as an aid in comparing the effect of the variables studied. The grain-size numbers enumerated were obtained by estimation on larger micrographs than are shown in the figures. It is not always possible to show small differences in grain size by numbers; comparison of micrographs conveys a more definite picture. This is particularly true where the grain sizes are small (compare, for instance, figs. 21, *D*, and 22, *D*, both of which were rated as grain No. 8).

TABLE 2.—*Influence of initial structure and rate of heating on austenitic grain size*

Initial structure	Estimated ASTM grain size number at 1,475° F				Estimated ASTM grain size number at 1,600° F			
	Rate of heating [1]				Rate of heating [1]			
	Very rapid	Rapid	Medium	Slow	Very rapid	Rapid	Medium	Slow
Iron-carbon alloy								
Coarse pearlite	7	6	4	−2 to 1, 30%; coalesced, 70%.	2 to 4, 40%; 5 to 7, 60%	5 to 6	4	0 to 1.
Fine pearlite	7	4	2	−2 to 1, 90%; coalesced, 10%.	2 to 3, 25%; 5 to 7, 75%	4 to 5	4	1.
Spheroidized cementite	7	6	3 to 4	−2 to 1, 90%; coalesced, 10%.	4 to 7	5 to 7	4	−2 to −1.
Noncontrolled steel (*C–1*)								
Coarse pearlite	6	5	5	5	6 (some 5)	5 to 6	4	5.
Medium pearlite	6	5 (some 8)	8 (some 5)	8 (some 6)	6	5	6	5 to 6.
Fine pearlite	4	4	8 (some 4)	8 (some 6)	5	4 to 5	4 to 5	4 to 5.
Bainite	(*A*) 6 to 7. (*AA*) 5	4 to 5	6 to 8	6 to 8	5	4 to 5	5 to 6	4 to 5.
Spheroidized cementite	6	6	5 to 6	4 to 5	5	5	5	5.
Controlled steel (*C–2*)								
Coarse pearlite	7	6 to 8	8	8	7 to 8	6	7 to 8	7 to 8.
Medium pearlite	6	8	8	8	6	8 (some 4 to 6)	8	7 to 8 (few 6).
Fine pearlite	6	8 (few 3)	8	8	6 to 7	5	8	8.
Bainite	6 to 7	8 (some 5 to 6)	8	8	6 to 7	8 (some 5 to 6)	8 (some 4 to 5)	8.
Spheroidized cementite	6	6 to 8	7 to 8	7 to 8	7	6 to 7	6 to 8	6 to 8.

[1] The rate of heating was not a constant for each condition listed. Values for some of the rates used are summarized in figures 4 to 29.

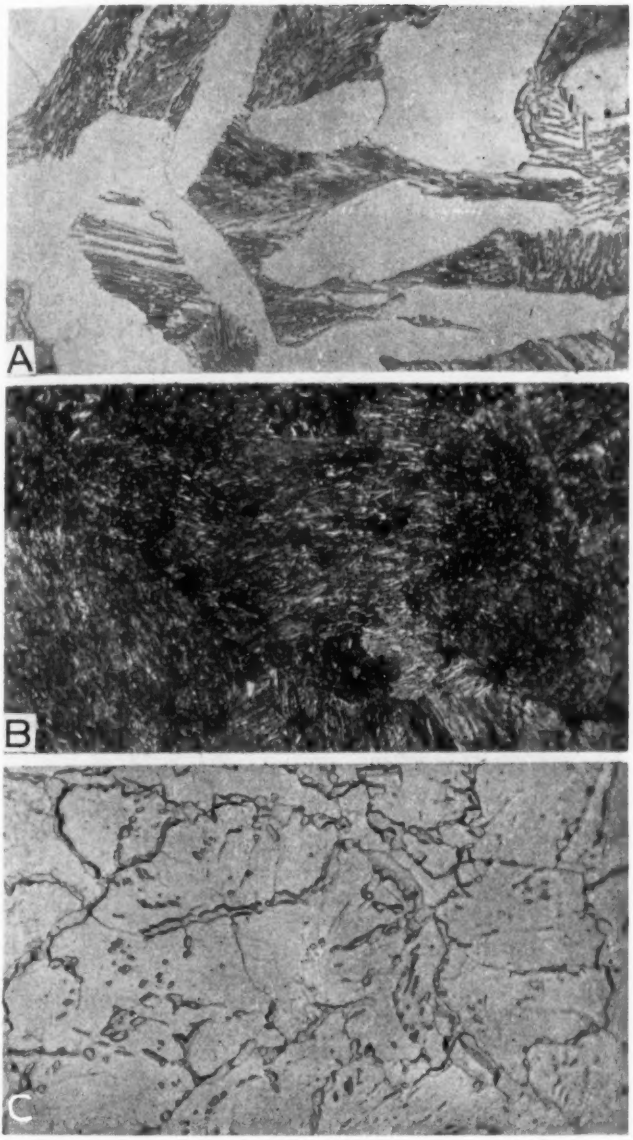

FIGURE 1.—*Initial structures of the iron-carbon alloy.*

A, coarse pearlite; *B*, fine pearlite; *C*, spheroidized cementite. Etched with 1-percent nital. ×500.

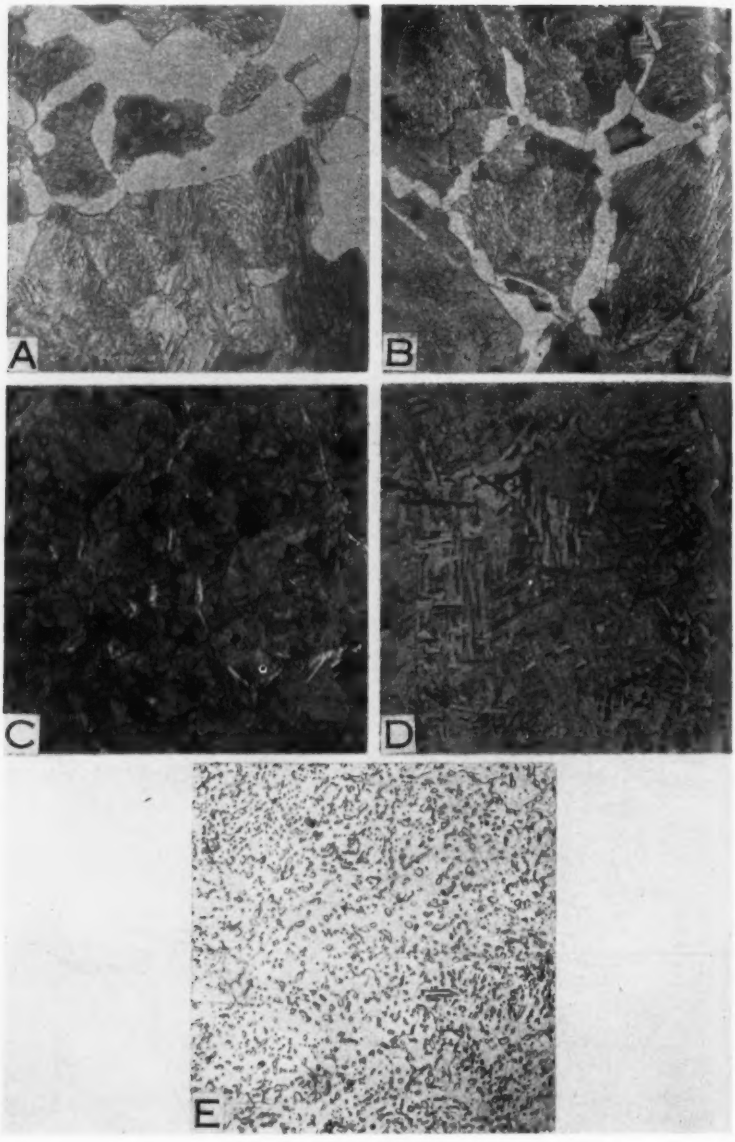

FIGURE 2.—*Initial structures of noncontrolled steel C–1.*

A, coarse pearlite; *B*, medium pearlite; *C*, fine pearlite; *D*, bainite; *E*, spheroidized cementite. Etched with 1-percent nital, ×500.

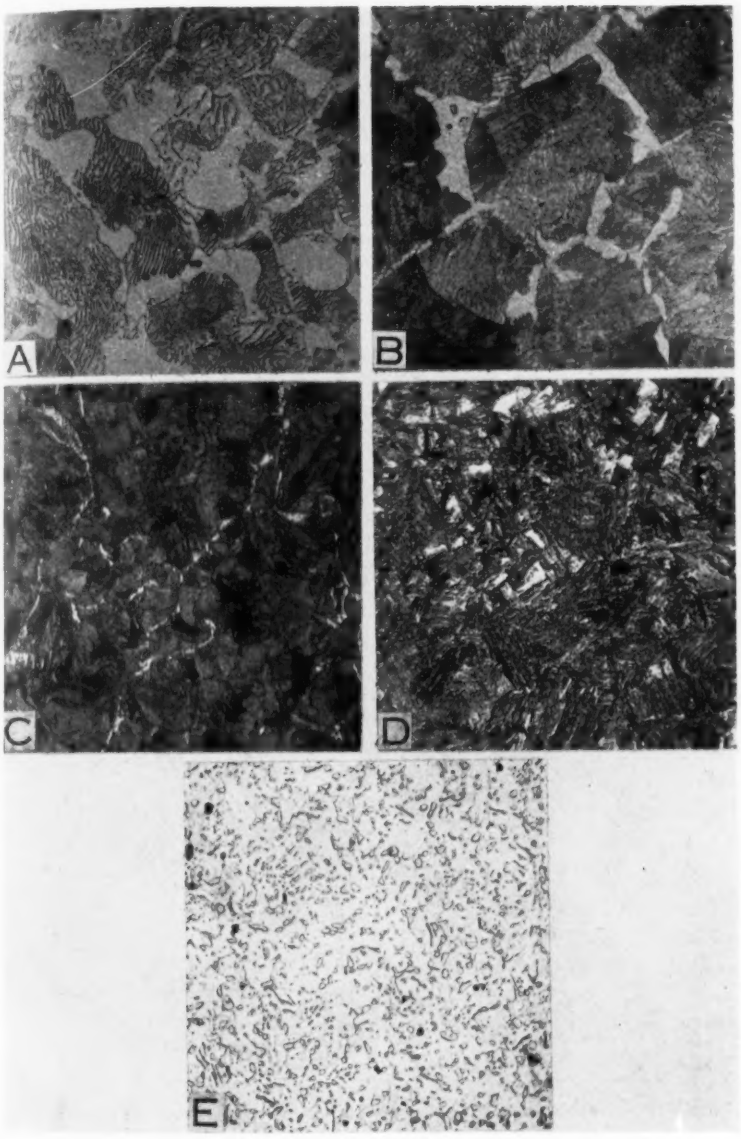

FIGURE 3.—*Initial structures of controlled steel C 2.*

A, coarse pearlite; *B*, medium pearlite; *C*, fine pearlite; *D*, bainite; *E*, spheroidized cementite. Etched with 1-percent nital, ×500

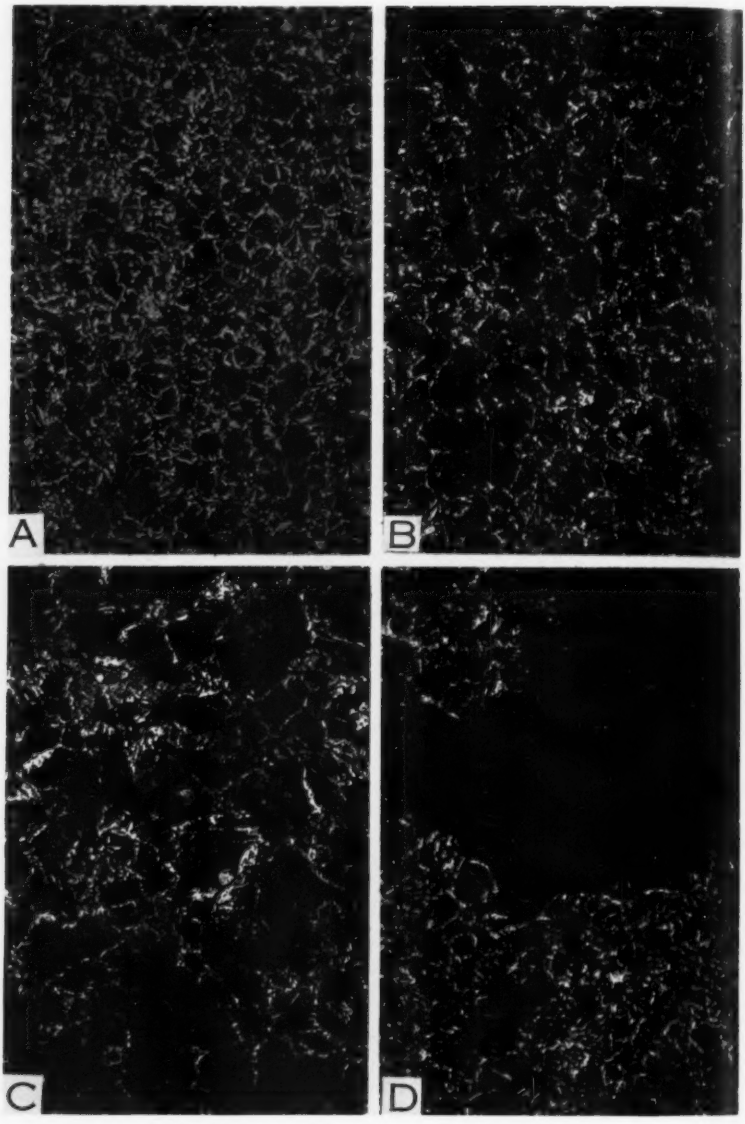

FIGURE 4.—*Austenitic grain size at 1,475° F of iron-carbon alloy with initial structure of coarse pearlite.*

A, heated in lead bath; *B*, heated at 540° F/min; *C*, heated at 80° F/min; *D*, heated at 5° F/min. Etched with 1-percent nital, ×100.

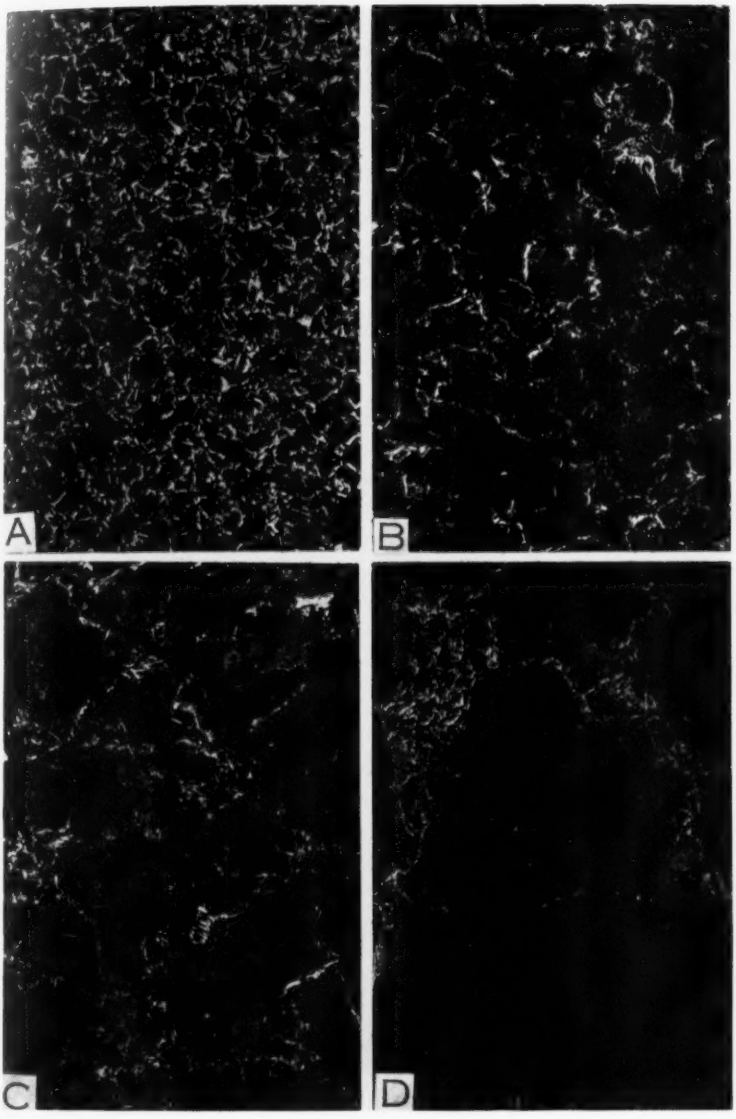

FIGURE 5.—*Austenitic grain size at 1,475° F of iron-carbon alloy with initial structure of fine pearlite.*

A, heated in lead bath; *B*, heated at 620° F/min; *C*, heated at 80° F/min; *D*, heated at 8° F/min. Etched with 1-percent nital, ×100.

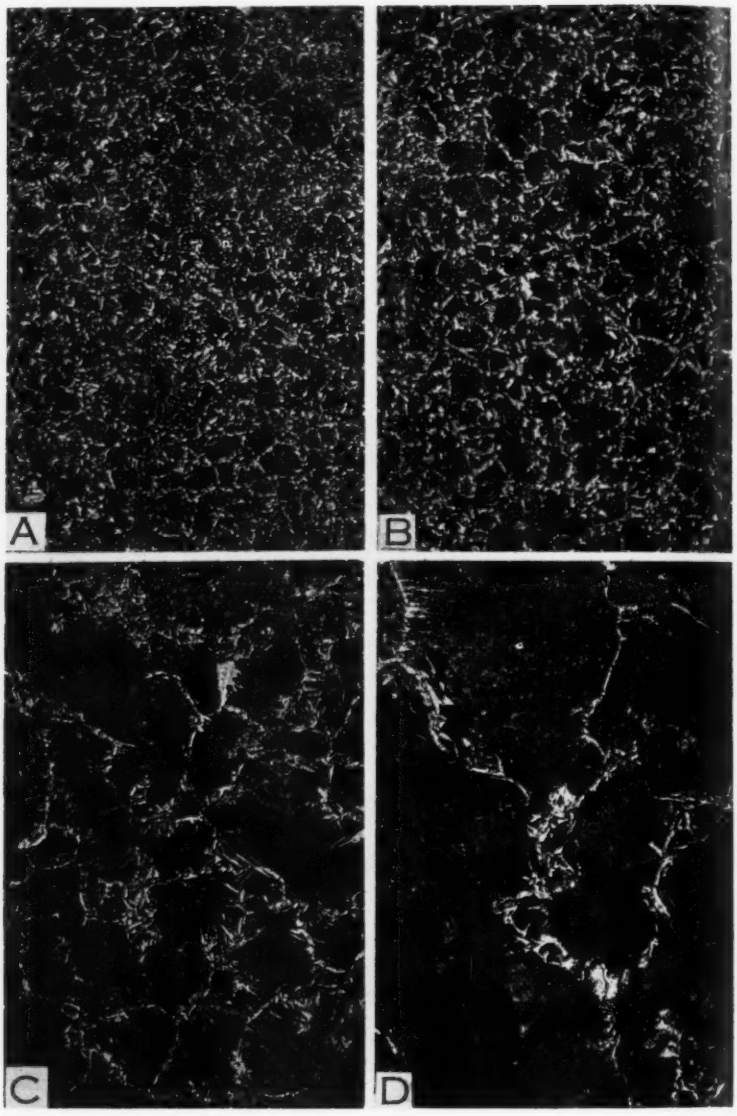

FIGURE 6.—*Austenitic grain size at 1,475° F of iron-carbon alloy with initial structure of spheroidized cementite.*

A, heated in lead bath; *B*, heated at 1,070° F/min; *C*, heated at 80° F/min; *D*, heated at 5° F/min. Etched with 1-percent nital. ×100.

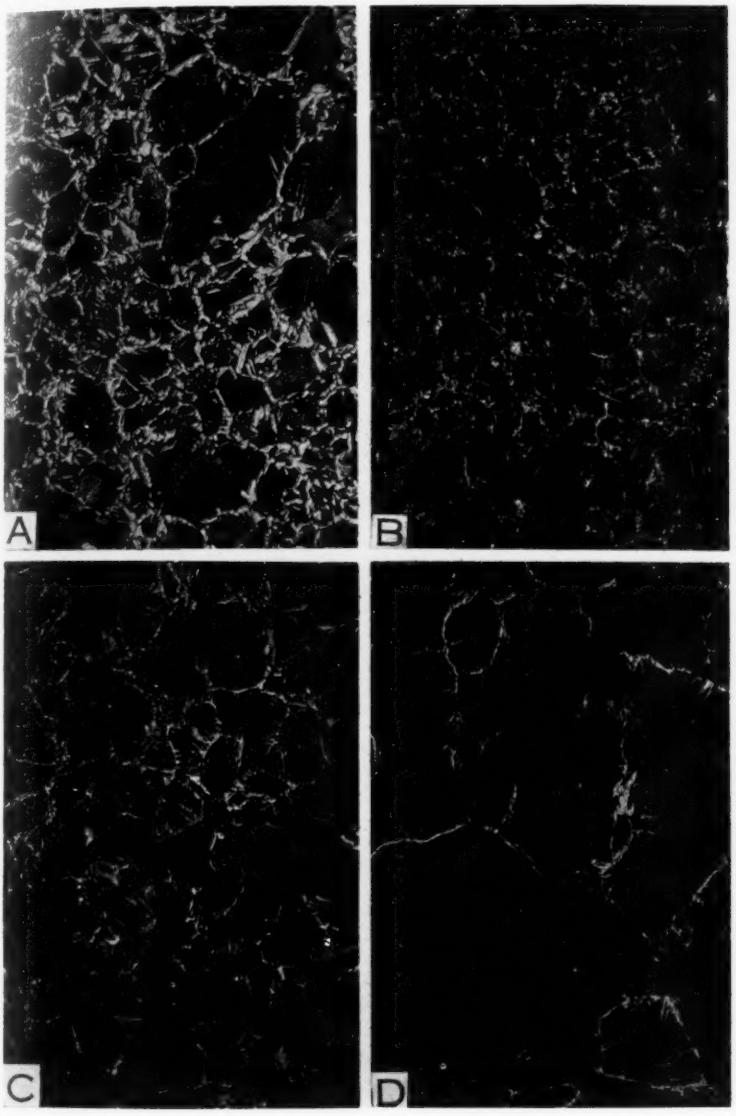

FIGURE 7.—*Austenitic grain size at 1,600° F of iron-carbon alloy with initial structure of coarse pearlite.*

A, heated in lead bath; *B*, heated at 1,070° F/min; *C*, heated at 130° F/min; *D*, heated at 5° F/min. Etched with 1-percent nital, ×100.

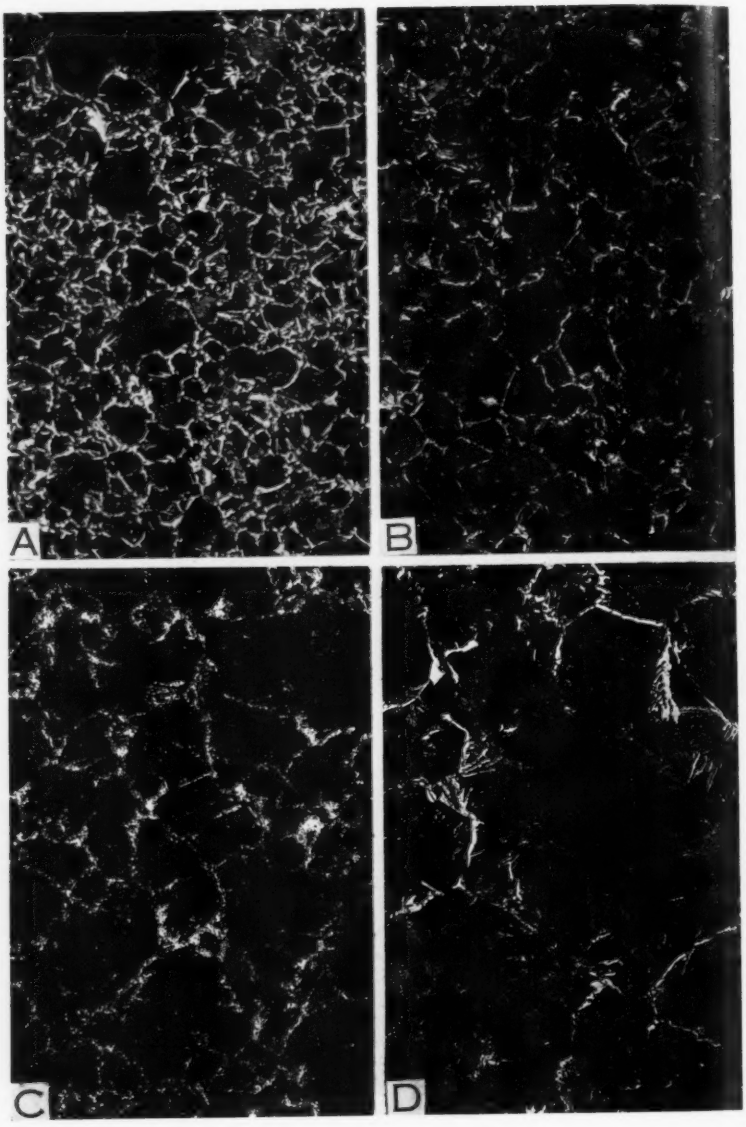

FIGURE 8.—*Austenitic grain size at 1,600° F of iron-carbon alloy with initial structure of fine pearlite.*

A, heated in lead bath; *B*, heated at 1,500° F/min; *C*, heated at 280° F/min; *D*, heated at 3° F/min. Etched with 1-percent nital. ×100.

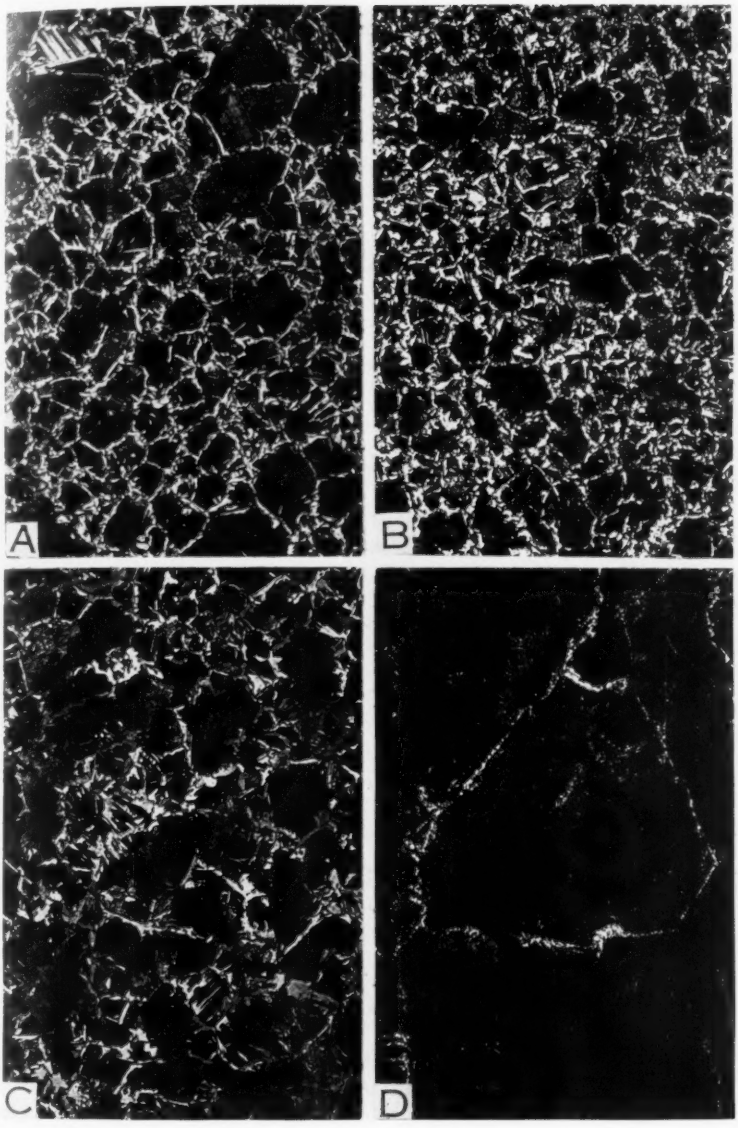

FIGURE 9.—*Austenitic grain size at 1,600° F of iron-carbon alloy with initial structure of spheroidized cementite.*

A, heated in lead bath; *B*, heated at 1,250° F/min; *C*, heated at 150° F/min; *D*, heated at 5° F/min. Etched with 1-percent nital, ×100.

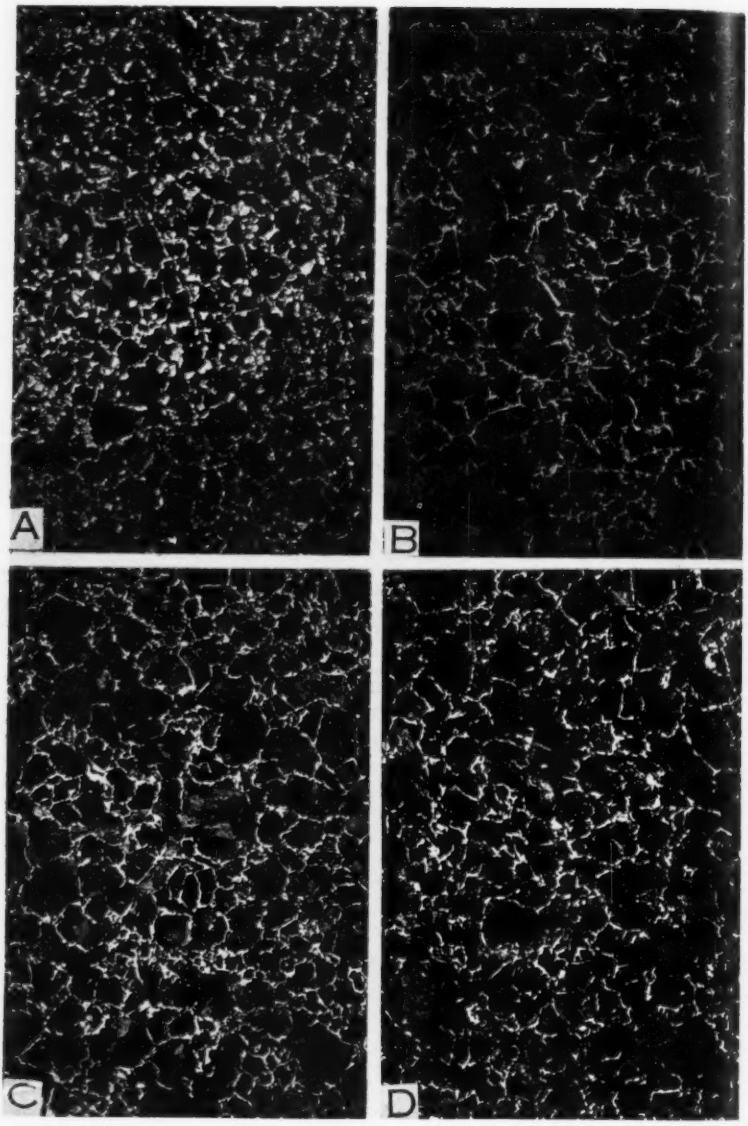

FIGURE 10.—*Austenitic grain size at 1,475° F of noncontrolled steel C–1 with initial structure of coarse pearlite.*

A, heated in lead bath; *B*, heated at 1,070° F/min; *C*, heated at 120° F/min; *D*, heated at 6° F/min. Etched with 1-percent nital, ×100.

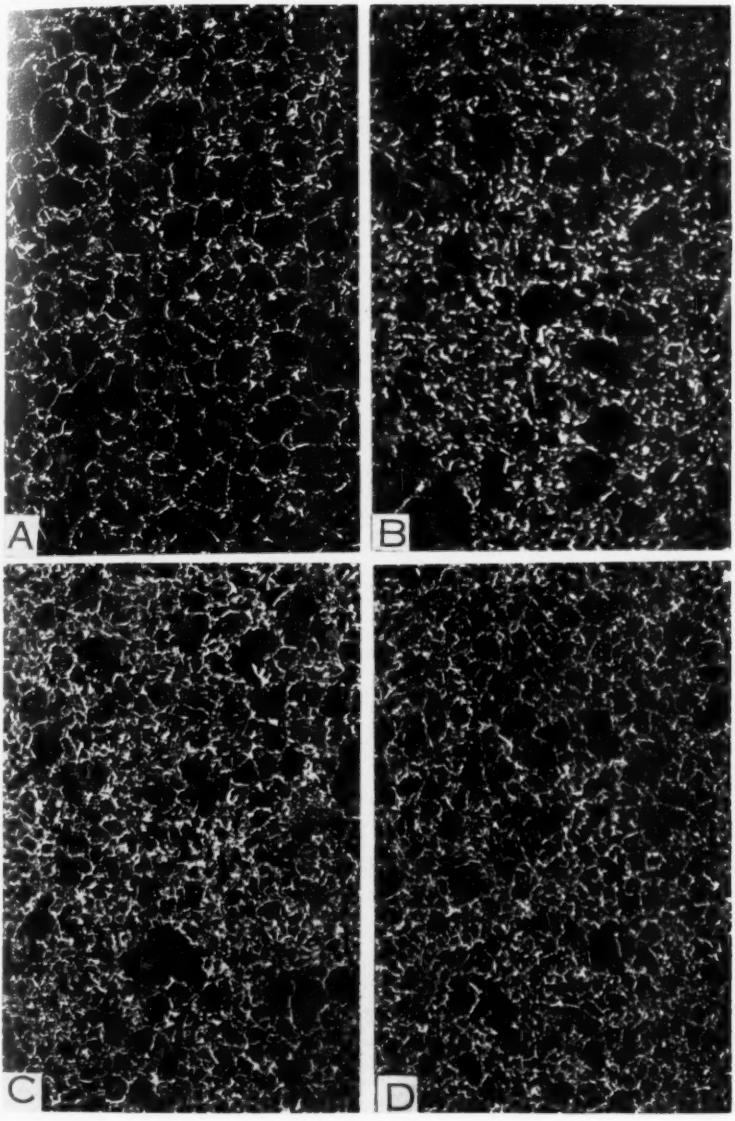

FIGURE 11.—*Austenitic grain size at 1,475° F of noncontrolled steel C–1 with initial structure of medium pearlite.*

A, heated in lead bath; *B*, heated at 830° F/min; *C*, heated at 180° F/min; *D*, heated at 4° F/min. Etched with 1-percent nital. ×100.

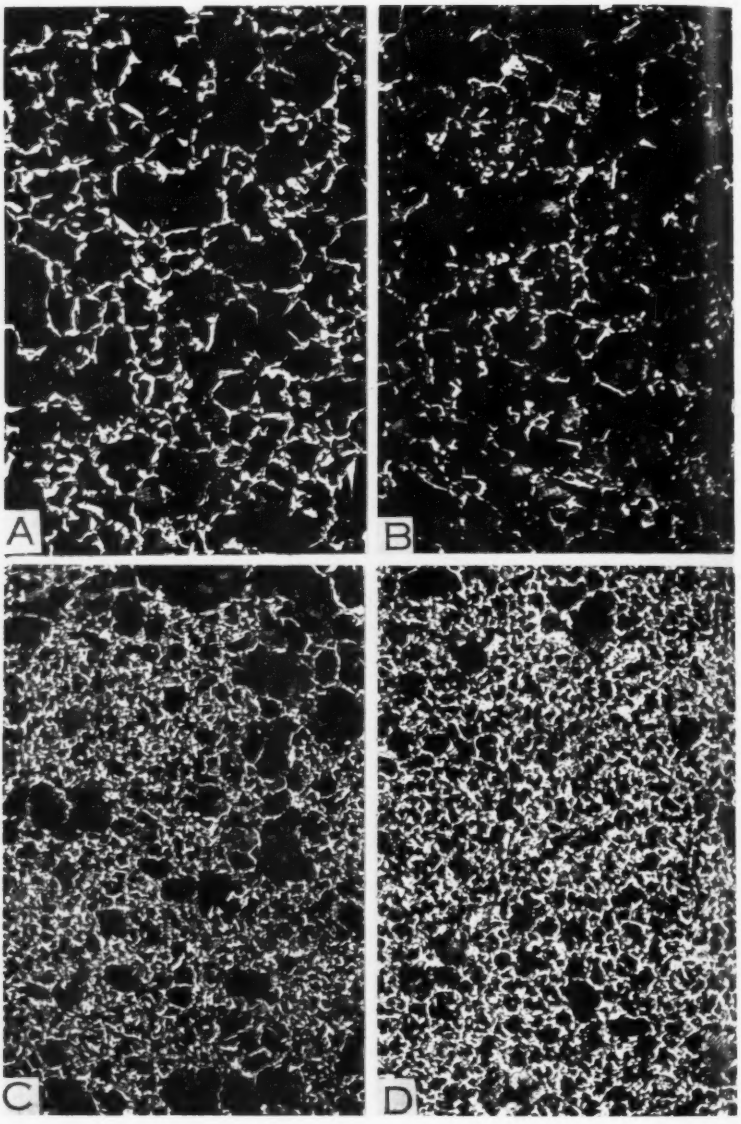

FIGURE 12.—*Austenitic grain size at 1,475° F of noncontrolled steel C–1 with initial structure of fine pearlite.*

A, heated in lead bath; *B*, heated at 680° F/min; *C*, heated at 160° F/min; *D*, heated at 6° F/min. Etched with 1-percent nital, ×100.

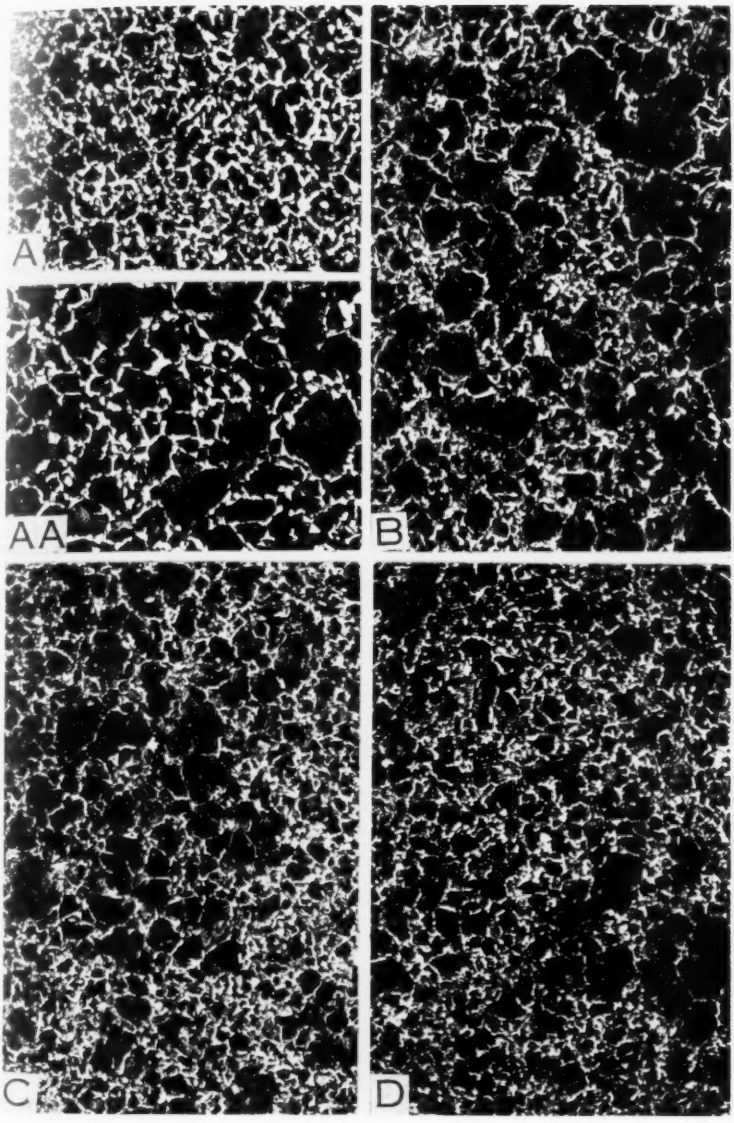

FIGURE 13.—*Austenitic grain size at 1,475° F of noncontrolled steel C–1 with initial structure of bainite.*

A and *AA*, heated in lead bath; *B*, heated at 570° F/min; *C*, heated at 110° F/min; *D*, heated at 6° F/min. Etched with 1-percent nital, ×100.

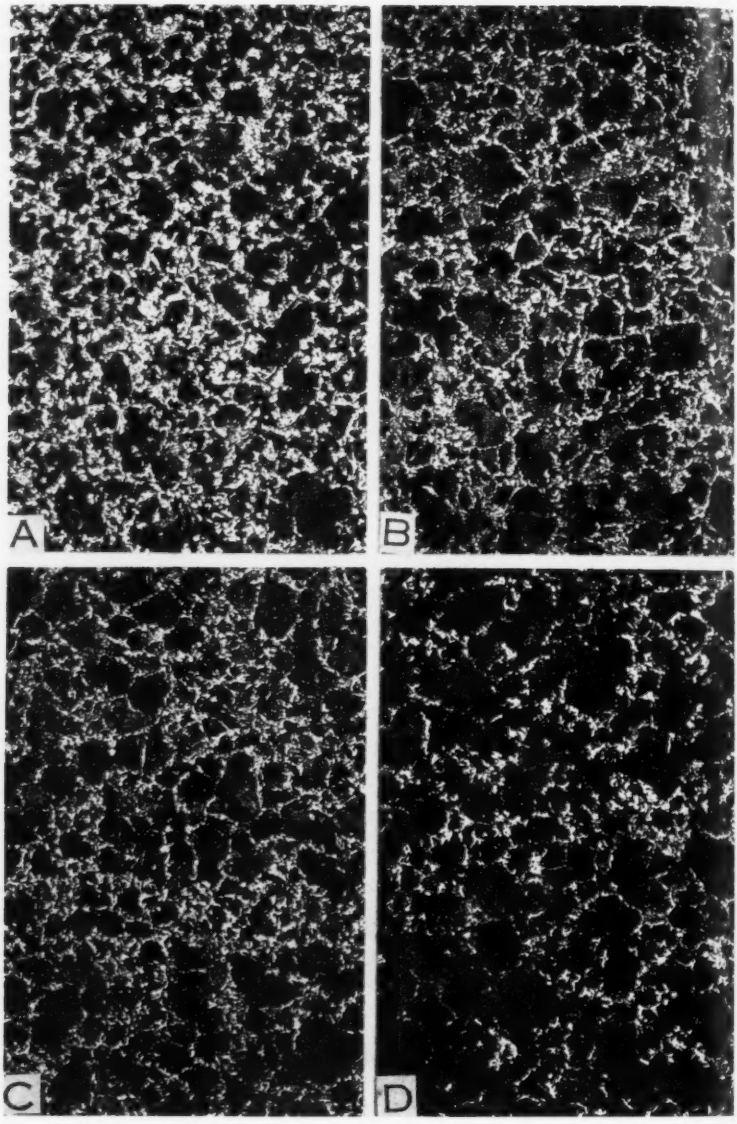

FIGURE 14.—*Austenitic grain size at 1,475° F of noncontrolled steel C–1 with initial structure of spheroidized cementite.*

A, heated in lead bath; *B*, heated at 940° F/min; *C*, heated at 80° F/min; *D*, heated at 5° F/min. Etched with 1-percent nital, ×100.

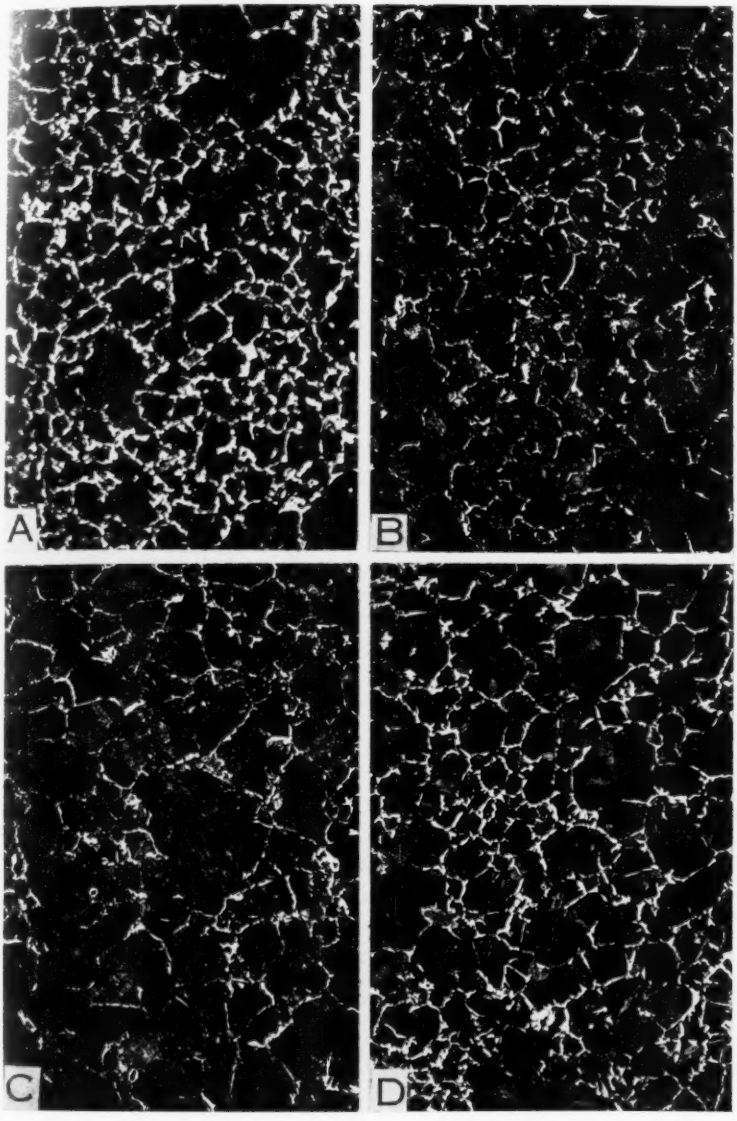

FIGURE 15.—*Austenitic grain size at 1,600° F of noncontrolled steel C–1 with initial structure of coarse pearlite.*

A, heated in lead bath; *B*, heated at 1,320° F/min; *C*, heated at 110° F/min; *D*, heated at 5° F/min. Etched with 1-percent nital, ×100.

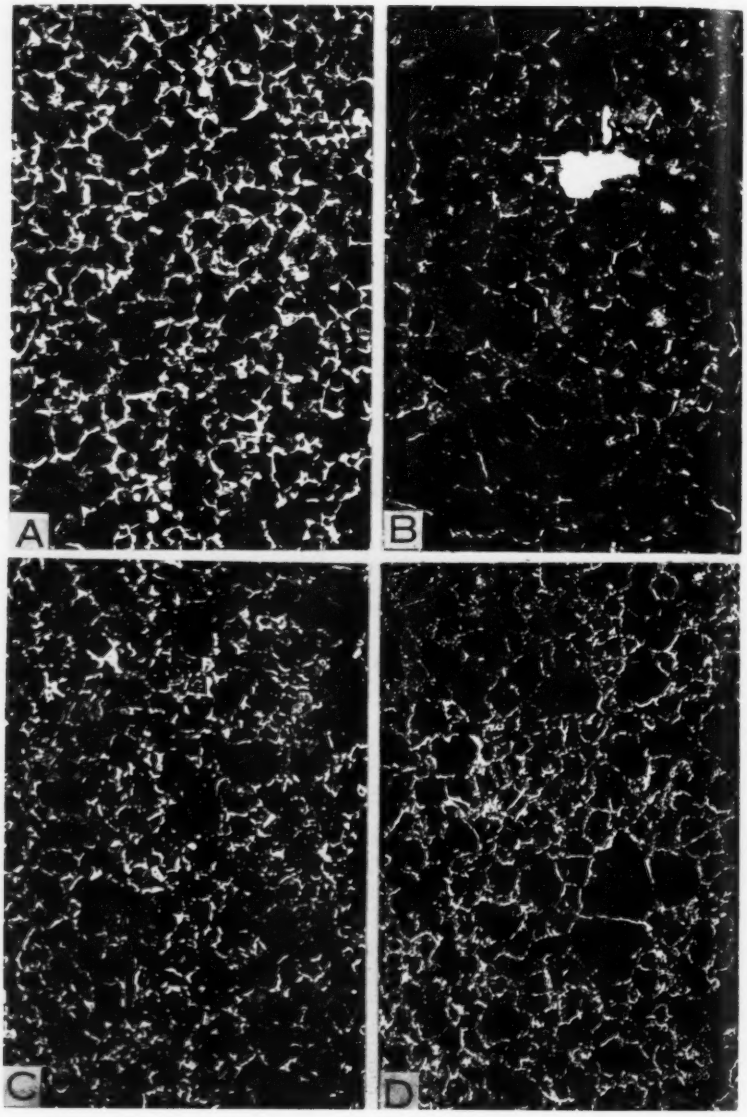

FIGURE 16.—*Austenitic grain size at 1,600° F of noncontrolled steel C–1 with initial structure of medium pearlite.*

A, heated in lead bath; *B*, heated at 1,070° F/min; *C*, heated at 110° F/min; *D*, heated at 4° F/min. Etched with 1-percent nital, ×100.

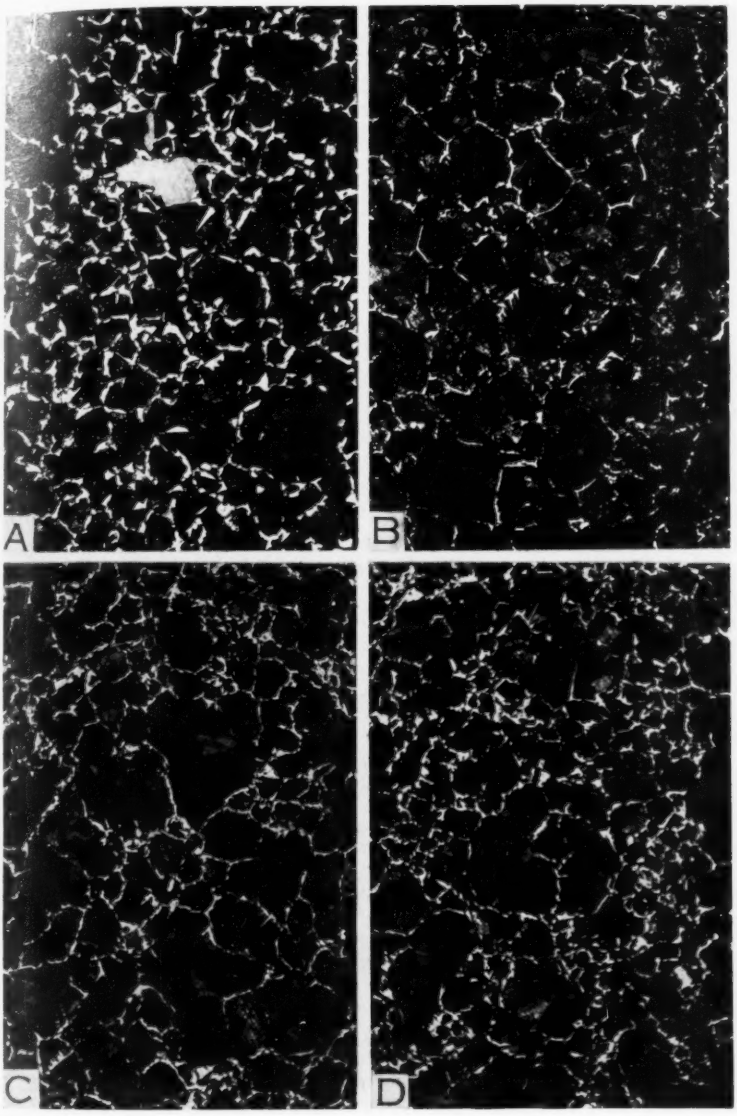

FIGURE 17.—*Austenitic grain size at 1,600° F of noncontrolled steel C–1 with initial structure of fine pearlite.*

A, heated in lead bath; *B*, heated at 940° F/min; *C*, heated at 90° F/min; *D*, heated at 5° F/min. Etched with 1-percent nital, ×100.

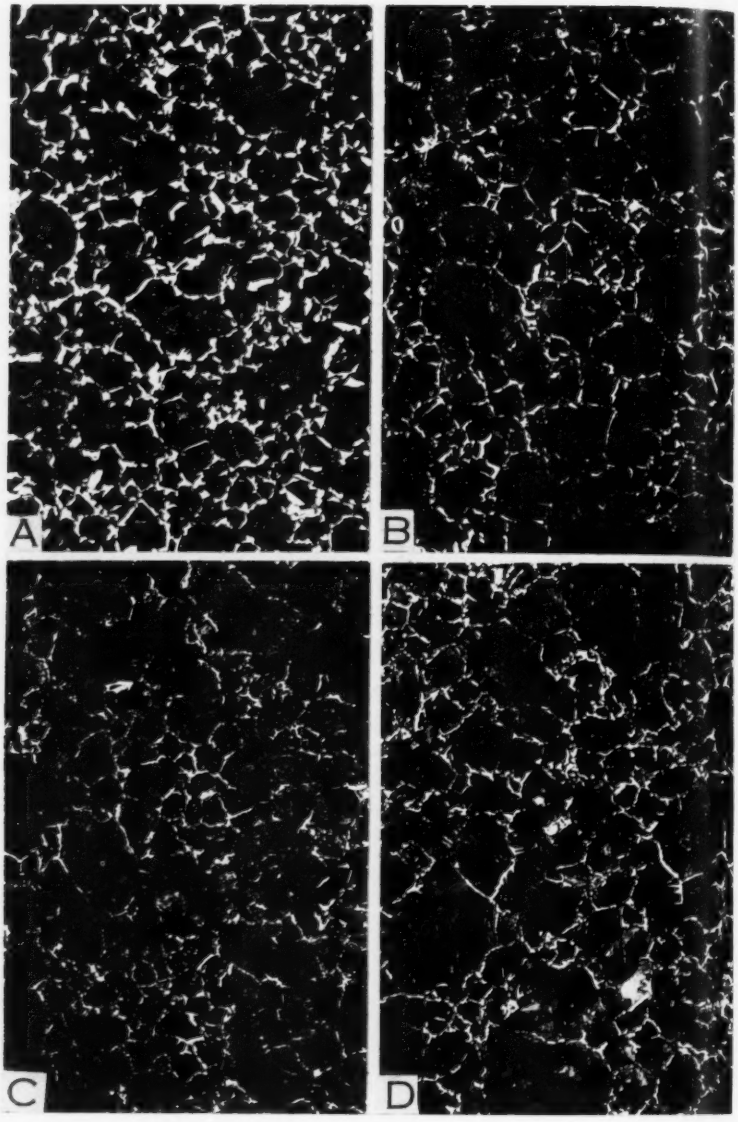

FIGURE 18.—*Austenitic grain size at 1,600° F of noncontrolled steel C–1 with initial structure of bainite.*

A, heated in lead bath; *B*, heated at 830° F/min; *C*, heated at 280° F/min; *D*, heated at 9° F/min. Etched with 1-percent nital, ×100.

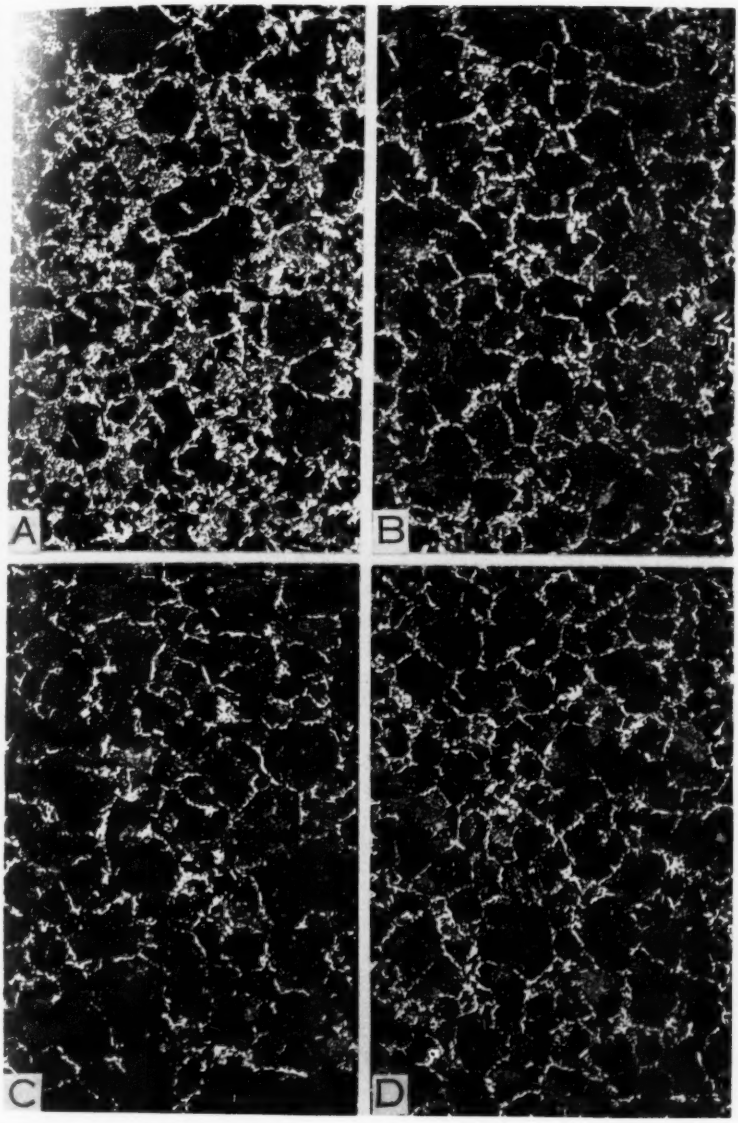

FIGURE 19.—*Austenitic grain size at 1,600° F of noncontrolled steel C–1 with initial structure of spheroidized cementite.*

A, heated in lead bath; *B*, heated at 750° F/min; *C*, heated at 20° F/min; *D*, heated at 7° F/min. Etched with 1-percent nital, ×100.

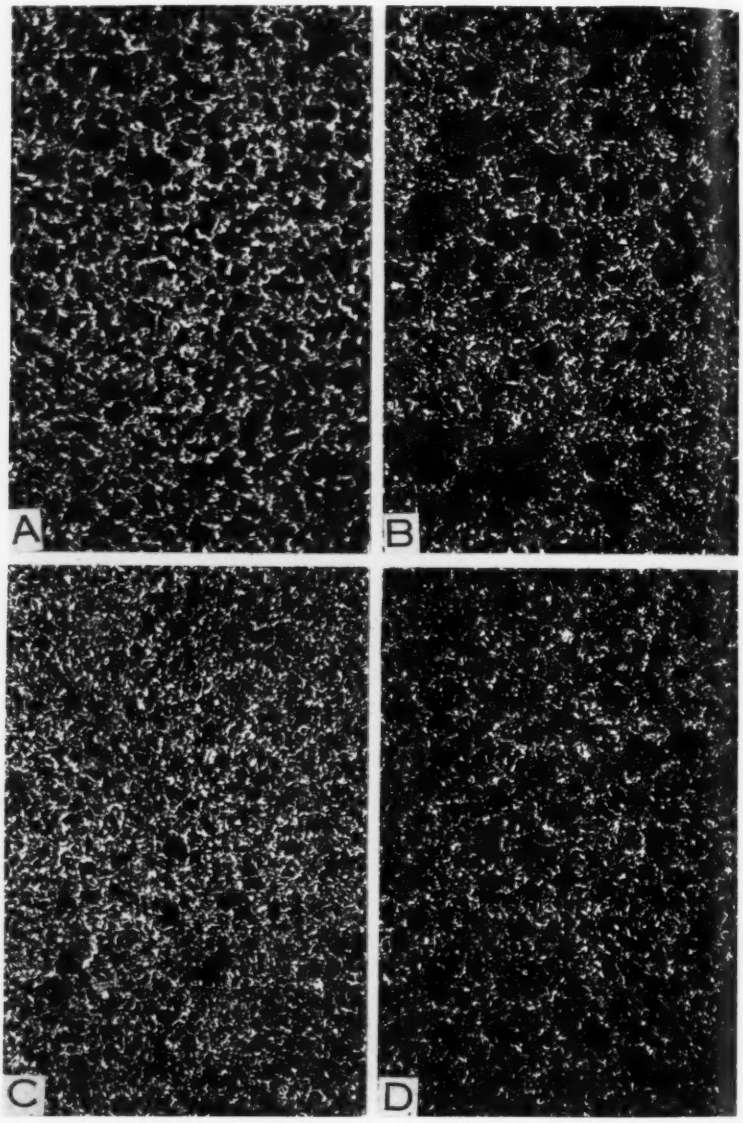

FIGURE 20.—*Austenitic grain size at 1,475° F of controlled steel C–2 with initial structure of coarse pearlite.*

A, heated in lead bath; *B*, heated at 750° F/min; *C*, heated at 110° F/min; *D*, heated at 3° F/min. Etched with 1-percent nital, ×100.

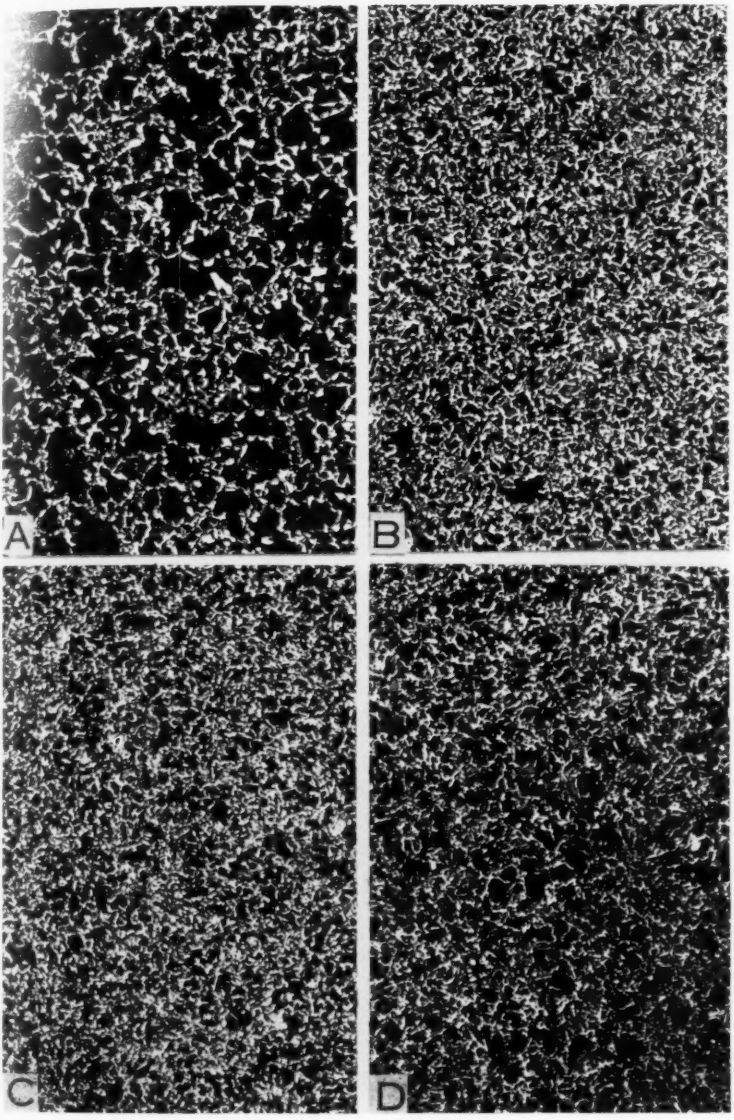

FIGURE 21.—*Austenitic grain size at 1,475° F of controlled steel C–2 with initial structure of medium pearlite.*

A, heated in lead bath; *B*, heated at 420° F/min; *C*, heated at 120° F/min; *D*, heated at 3° F/min. Etched with 1-percent nital, ×100.

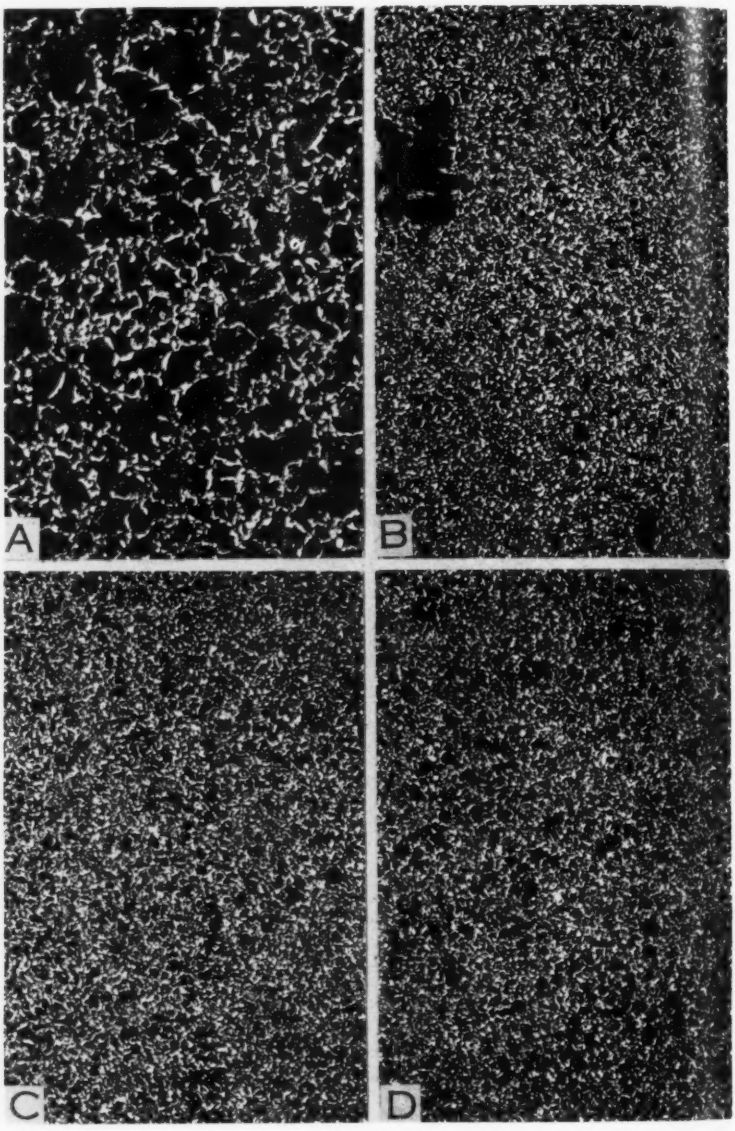

FIGURE 22.—*Austenitic grain size at 1,475° F of controlled steel C–2 with initial structure of fine pearlite.*

A, heated in lead bath; *B*, heated at 750° F/min; *C*, heated at 130° F/min; *D*, heated at 4° F/min. Etched with 1-percent nital. ×100.

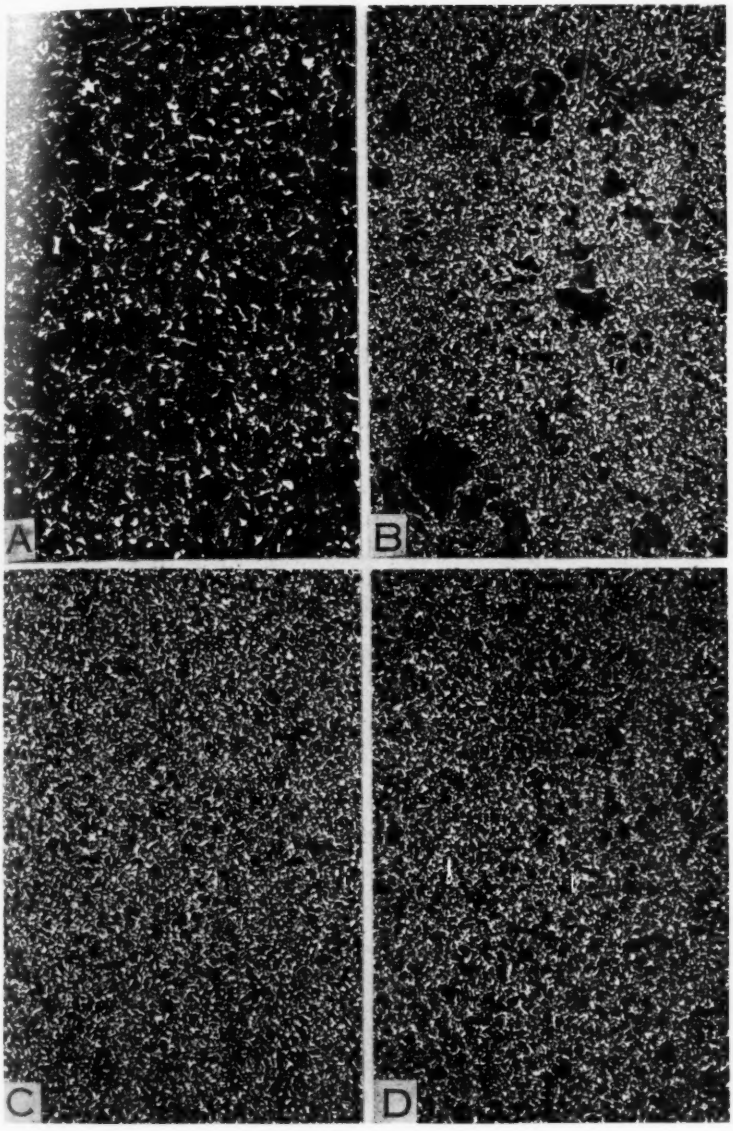

FIGURE 23.—*Austenitic grain size at 1,475° F of controlled steel C–2 with initial structure of bainite.*

A, heated in lead bath; *B*, heated at 680° F/min; *C*, heated at 130° F/min; *D*, heated at 4° F/min. Etched with 1-percent nital, ×100.

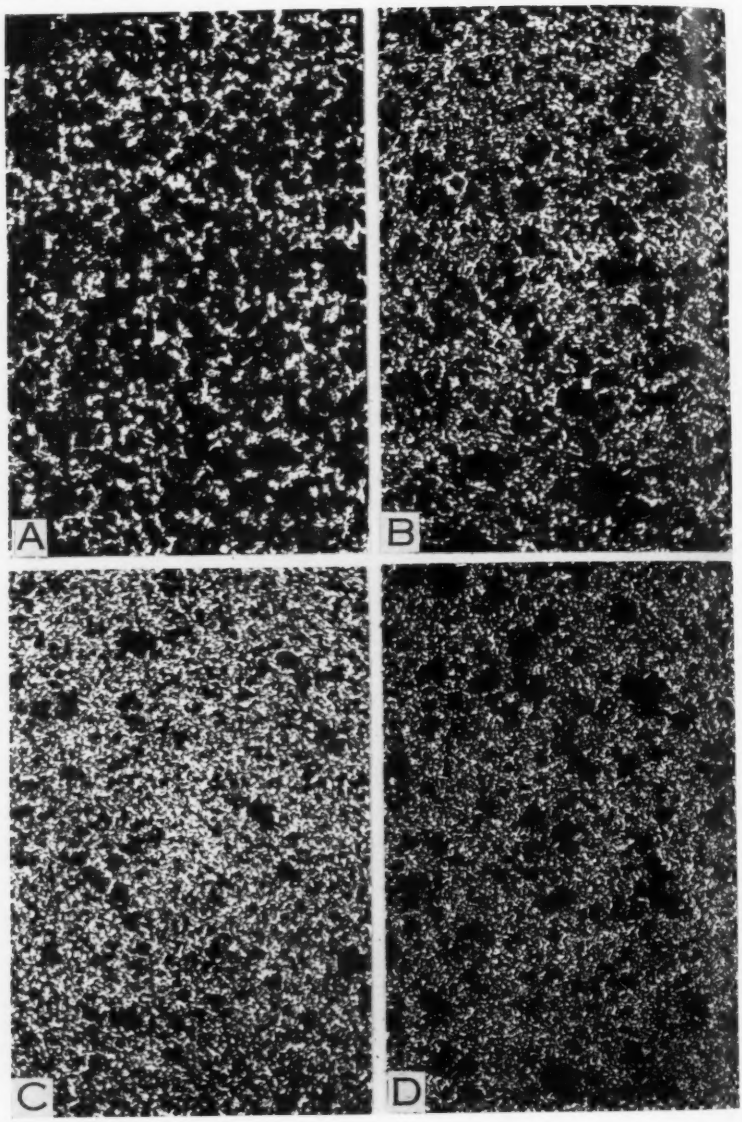

FIGURE 24.—*Austenitic grain size at 1,475° F of controlled steel C–2 with initial structure of spheroidized cementite.*

A, heated in lead bath; *B*, heated at 1,080° F/min; *C*, heated at 90° F/min; *D*, heated at 4° F/min. Etched with 1-percent nital, ×100.

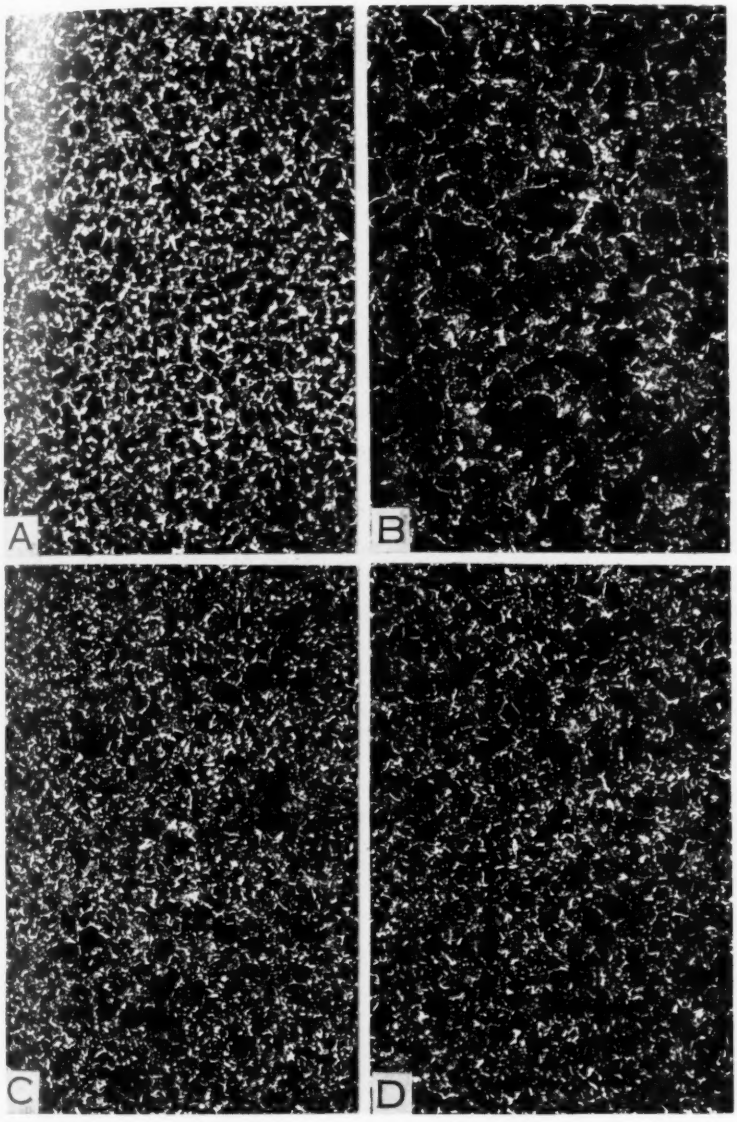

FIGURE 25.—*Austenitic grain size at 1,600° F of controlled steel C–2 with initial structure of coarse pearlite.*

A, heated in lead bath; *B*, heated at 1,250° F/min; *C*, heated at 140° F/min; *D*, heated at 7° F/min. Etched with 1-percent nital, ×100.

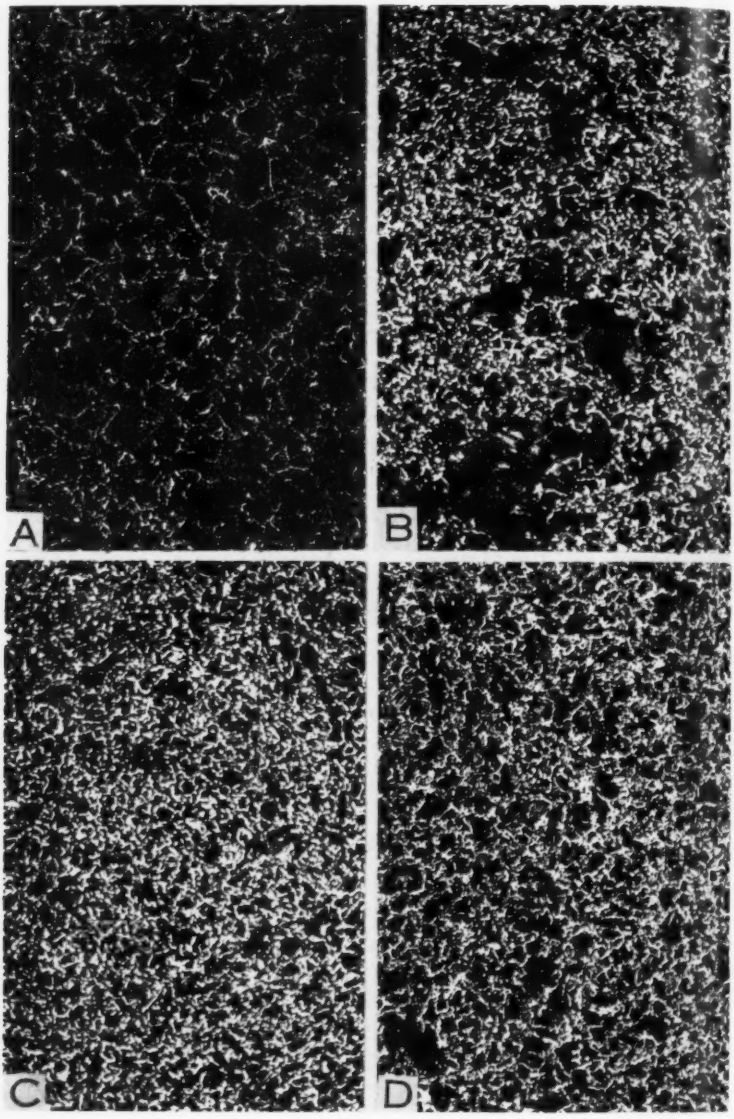

FIGURE 26.—*Austenitic grain size at 1,600° F of controlled steel C–2 with initial structure of medium pearlite.*

A, heated in lead bath; *B*, heated at 1,500° F/min; *C*, heated at 100° F/min; *D*, heated at 3° F/min. Etched with 1-percent nital, ×100.

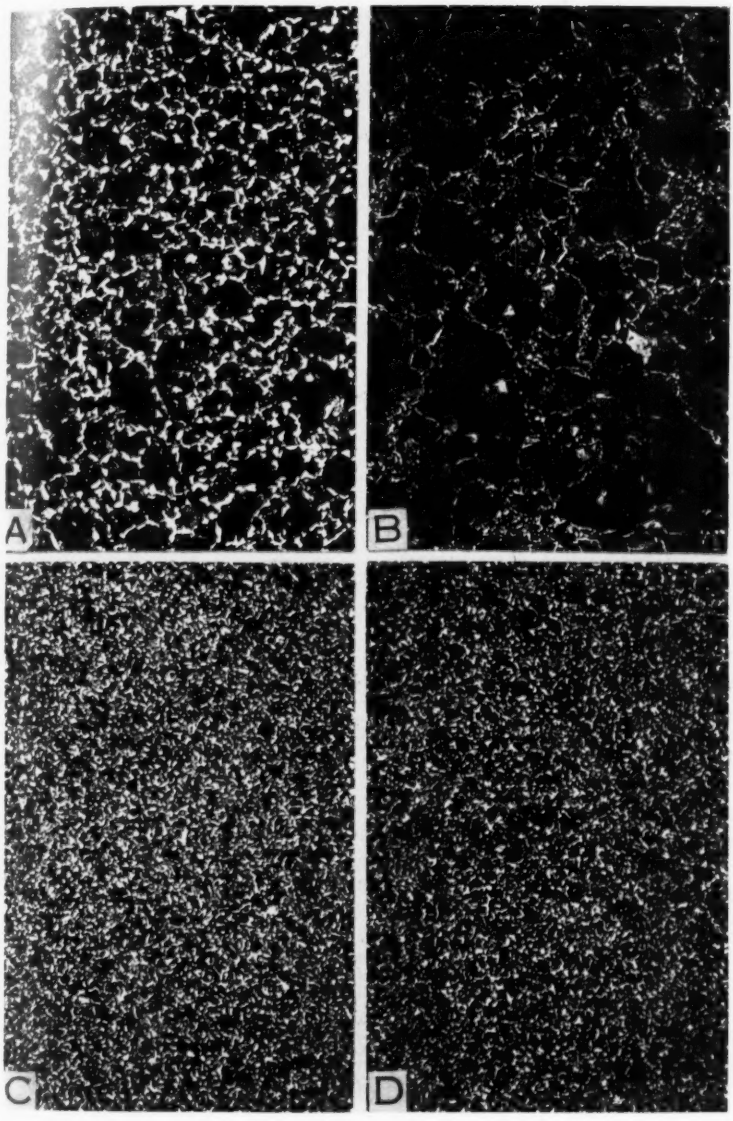

FIGURE 27.—*Austenitic grain size at 1,600° F of controlled steel C–2 with initial structure of fine pearlite.*

A, heated in lead bath; *B*, heated at 940° F/min; *C*, heated at 150° F/min; *D*, heated at 4° F/min. Etched with 1-percent nital, ×100.

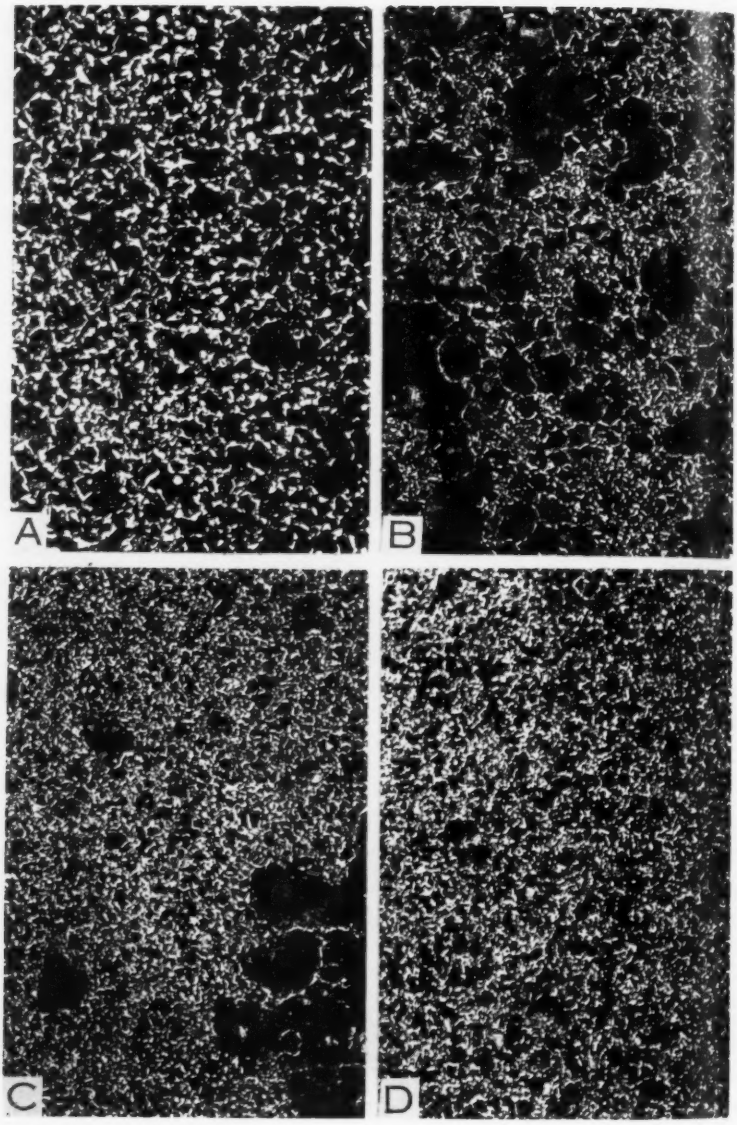

FIGURE 28.—*Austenitic grain size at 1,600° F of controlled steel C–2 with initial structure of bainite.*

A, heated in lead bath; *B*, heated at 830° F/min; *C*, heated at 120° F/min; *D*, heated at 7° F/min. Etched with 1-percent nital. ×100.

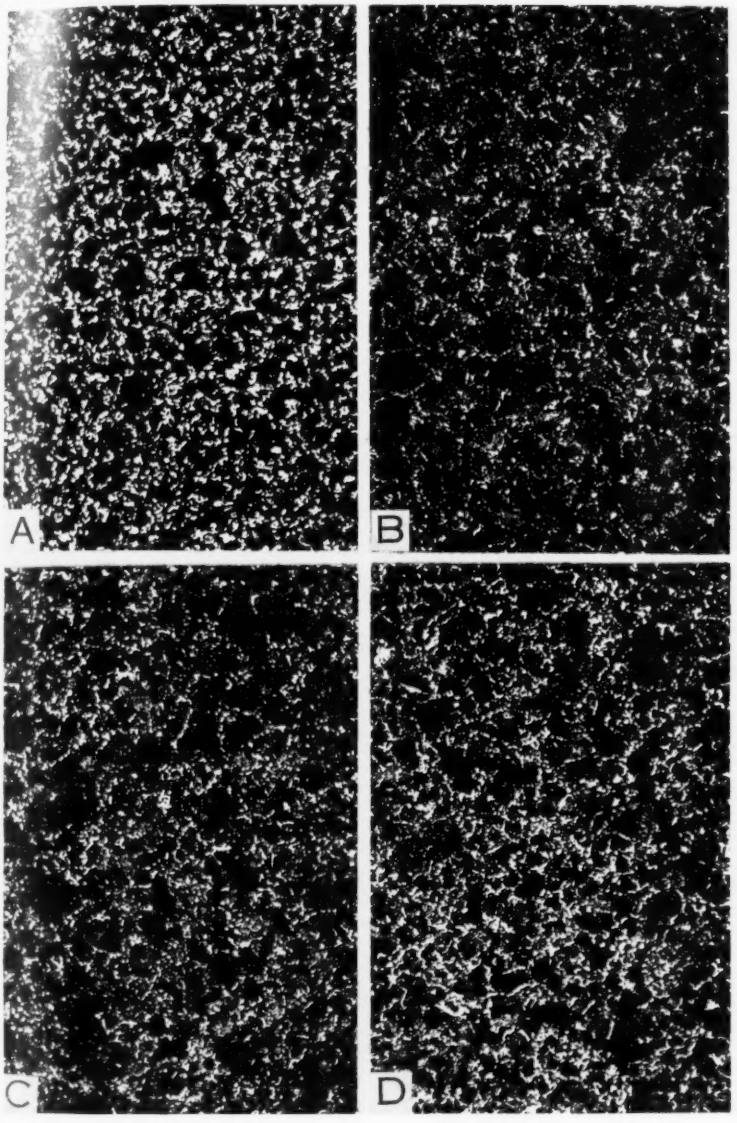

FIGURE 29.—*Austenitic grain size at 1,600° F of controlled steel C–2 with initial structure of spheroidized cementite.*

A, heated in lead bath; *B*, heated at 1,500° F/min; *C*, heated at 130° F/min; *D*, heated at 7° F/min. Etched with 1-percent nital, ×100.

UNIV. OF MICH.

III. RESULTS

1. IRON-CARBON ALLOY

The interlamellar spacing of the pearlite or the form and distribution of the carbides in the initial structures had no appreciable influence on the grain sizes established at 1,475° and 1,600° F in the high-purity alloy of iron and carbon (figs. 4 to 9).

With each initial structure investigated, relatively fine grains were obtained at 1,475° F, provided the rate of heating was extremely fast. The grain size at this temperature, however, increased with decrease in the rate of heating until extremely coarse grains (ASTM grain No. −2 to 1) were produced. The coarse-grained specimens often contained areas of coalesced ferrite (fig. 5, *D*).

At 1,600° F, the average size of the grains obtained also was a minimum when the rate of heating was rapid (fig. 7, *B;* 8, *A*; and 9, *B*), although the fastest rate did not produce the smallest grains when the initial structure was either coarse pearlite or spheroidized cementite. The specimens heated in a lead bath (fastest rate) always showed mixed-size grains at 1,600° F, some of the grains being very coarse (figs. 7, *A;* 8, *A;* and 9, *A*). With slow rates of heating, coarse grains of the same order of magnitude were obtained at all temperatures (1,475° and 1,600° F) and with all initial structures (coarse pearlite, fine pearlite, and spheroidized cementite).

It is apparent that the dominant factor in establishing the grain size in this iron-carbon alloy, either at 1,475° or 1,600° F, was the rate of heating and not the initial structure. The effect of the rate of heating was so pronounced that it also overshadowed the effect of the austenitizing temperature. Although it is generally understood that the higher the temperature, the coarser the austenitic grain size, it was possible to produce considerably coarser grains in this alloy at 1,475° F, merely by heating slowly, than at 1,600° F by heating rapidly.

2. NONCONTROLLED STEEL

The influence of initial structure and rate of heating on the grain sizes at 1,475° and 1,600° F of the noncontrolled steel (*C–1*) is shown in figures 10 to 19, inclusive.

With the fastest rate of heating, slightly coarser grains were obtained at 1,475° F with initial structures of fine pearlite or bainite (figs. 12, *A;* and 13, *AA*) than with coarse or medium pearlite or spheroidized cementite (figs. 10, *A;* 11, *A*; and 14, *A*). The observed difference was not considered significant, however, because its order of magnitude was no greater than that obtained with duplicate specimens, as for example, with an initial structure of bainite (fig. 13, *A* and *AA*). With the slowest rates, however, finer grains were obtained at 1,475° F with initial structures consisting of medium pearlite, fine pearlite, and bainite (figs. 11, *D;* 12, *D;* and 13, *D*), than were obtained with coarse pearlite or spheroidized cementite (figs. 10, *D;* and 14, *D*). With intermediate rates, a grain-size contrast was often obtained in this steel.

The rate of heating showed some minor influence on the grain size at 1,475° F when the initial structure was medium pearlite, fine pearlite, or bainite (figs. 11, 12, and 13), but was without effect when the initial structure was coarse pearlite or spheroidized cementite (figs. 10 and 14).

The grain size of this steel at 1,600° F was not markedly affected by variations in the initial structure or rate of heating, although some minor variations in grain size were observed.

3. CONTROLLED STEEL

The influence of initial structure and rate of heating on the grain size at 1,475° and 1,600° F of the controlled steel (*C–2*) is shown in figures 20 to 29, inclusive.

Although variations in the initial structure influenced the grain size of this steel at 1,475° and 1,600° F, the effects observed depended chiefly upon the rate of heating; no definite relation could be established between the initial structure and the grain size at either of these temperatures. For example, with the fast rates of heating, somewhat finer grains were obtained at both 1,475° and 1,600° F when the initial structure was coarse pearlite (figs. 20, *A*, and *B*; and 25, *B*) than when the initial structures were medium pearlite, fine pearlite, bainite, or spheroidized cementite; but with the slowest rates of heating, the finest grains were obtained with initial structures of fine pearlite and bainite (figs. 22, *D;* 23, *D;* 27, *D;* and 28, *D*). Occasionally, particularly with intermediate rates of heating, marked contrast in the grain size was obtained in this steel.

The grain size at 1,475° F was influenced by the rate of heating, regardless of the initial structure (figs. 20, 21, 22, 23, and 24). The grain size at 1,600° F was also influenced by the rate of heating when the initial structure was either medium pearlite, fine pearlite, or bainite (figs. 26, 27, and 28). In all cases where the rate of heating influenced the grain size of this steel, the *finest* grains were obtained with *slow* rates, a relationship which is the reverse of that obtained with the iron-carbon alloy.

It is noteworthy that by varying the rates of heating, finer grains may be obtained in this controlled steel at 1,600° F than at 1,475° F.

IV. DISCUSSION OF RESULTS

It is apparent that both initial structure and rate of heating can affect the grain size at a particular temperature. Of these two variables, the data presented in this paper indicate that the rate of heating is the more important. The effect of this variable is pronounced in the case of the iron-carbon alloy investigated. Although very rapid rates of heating result in the formation of rather small austenitic grains in this alloy, very slow rates of heating cause the formation of extremely coarse grains.

From a commercial viewpoint, fortunately, the two steels investigated did not exhibit a similar phenomenon. Slight differences in grain size were obtained with variations in initial structure and rate of heating. A definite correlation between initial structure and grain size could not be established. However, some indication of a correlation between the rate of heating and the grain size could be observed; the slow rates often caused the formation of the smaller austenitic grains. This trend was slight in the case of the noncontrolled steel, but was more marked in the controlled steel. Attention should be directed to the fact that the rate of heating not only had a much more pronounced effect upon the grain size of the iron-carbon alloy than upon the steels, but that the effect was *opposite* in the two materials.

It is realized that the iron-carbon alloy and the steels differed widely from each other in chemical composition, especially with regard to P, S, Mn, Si, Al, and gaseous elements, and that the iron-carbon alloy was relatively free from materials that are classified as grain-growth inhibitors. Although the observed difference in behavior must be attributed to these differences in chemical composition, the present results do not show which of the elements, either individually or in combination, are responsible.

The iron-carbon alloy used in this investigation is being utilized in a study of the mechanism of the transformation of different initial structures to austenite. The results of preliminary tests indicate that the austenitic grains initially formed in this alloy are relatively small regardless of the rate of heating and that the grains grow rapidly in the transformation-temperature range.

The controlled steel was relatively fine-grained in the McQuaid-Ehn test (ASTM grain No. 8), whereas the noncontrolled steel was coarse-grained (ASTM grain No. 3). It is interesting, therefore, to observe that the controlled steel (fine-grained when carburized at 1,700° F) may have some coarse grains at the recommended quenching temperature of 1,475° F. (figs. 22, *B*; and 23, *B*) or at the normalizing temperature of 1,600° F (figs. 26, *B*; 27, *B*; 28, *B*; and 28, *C*).

V. SUMMARY

A study was made of the influence of initial structure and rate of heating on the grain sizes at 1,475° and 1,600° F of a high-purity alloy of iron and carbon and two plain carbon steels each containing about 0.5 percent of carbon. The two steels were commercial heats which differed principally in the amounts of alumina and aluminum. The steel with the lower percentage of aluminum was produced under conditions which resulted in noncontrol of the austenitic grain size, whereas the other heat was produced under conditions intended to control the grain size.

The different initial structures (that is, the structure that existed just prior to heating to the temperature establishing the grain size) consisted of either coarse pearlite, fine pearlite or spheroidized cementite in the iron-carbon alloy and either coarse pearlite, medium pearlite, fine pearlite, bainite, or spheroidized cementite in each of the commercial steels.

Wide variations in the rate of heating were obtained by plunging small specimens into a lead bath or by heating them in vacuum. Except for the specimens heated in lead (most rapid rates), the rate of heating was taken as the average rate to heat from 1,325° to 1,450° F, which included the transformation-temperature range.

Variations in the initial structure of the iron-carbon alloy had no appreciable effect on the grain size at 1,475° or 1,600° F. Although the initial structure had some influence on the grain size of the commercial steels, no definite correlation was found between the grain size and the interlamellar spacing of pearlite, or the form and distribution of carbides.

The rate of heating had a marked influence on the grain sizes at 1,475° and 1,600° F of the iron-carbon alloy. At each temperature relatively fine grains were produced by rapid heating and coarse grains by slow heating.

With some of the initial structures, the rate of heating affected the grain size at 1,475° F in the noncontrolled and controlled steels, and at 1,600° F in the controlled steel. In all cases where the rate of heating influenced the grain size of the commercial steels, the finest grains were obtained with slow rates, the reverse of the relation found with the iron-carbon alloy.

WASHINGTON, March 18, 1942.

U. S. Department of Commerce National Bureau of Standards

RESEARCH PAPER RP1482

Part of Journal of Research of the National Bureau of Standards, Volume 29, July 1942

MICROSCOPIC STRUCTURE OF FLAX AND RELATED BAST FIBERS

By Charles W. Hock [1]

ABSTRACT

The microscopic structure of flax and of related bast fibers was investigated. The stem of the flax plant consists of two main parts, a central woody core, and a surrounding cortex which contains the bast fibers. The cambium layer lies between these regions. Retting involves, essentially, a softening of the tissues to permit separation of the fibers from the other parts of the stem. The cambium layer is attacked first during this treatment, followed later by attack on other thin-walled cells in the cortex.

Flax and related bast fibers, such as hemp, jute, and ramie, have a similar origin and structure. They are obtained from the stem in the form of long filaments, each of which is made up of cells. In this respect they differ from cotton fibers, which are single plant cells.

A flax cell has a primary and a secondary wall. The former constitutes the surface of each cell and consists largely of wax and other material, much of which has generally been assumed to be of a pectic nature. The secondary wall, which comprises the bulk of the fiber, is made up of innumerable cellulose fibrils, the outermost layer of which winds in one direction, whereas the majority of the fibrils beneath this layer wind in the opposite direction. These fibrils are grouped so as to give the wall a lamellar pattern. There is a greater number of these layers in the walls of the cells at the base of the stem than in the cells from the growing tip. A corresponding increase in thickness of the wall, from the tip of the stem where the cells originate to the base where they mature, also prevails. All the bast fibers have essentially similar structures. Flax and ramie, however, differ from hemp and jute in the directions of fibrillate orientation, and this accounts for some of the differences in the physical properties of the two groups.

CONTENTS

	Page
I. Introduction	41
II. Materials	42
III. Experimental procedure and results	43
1. Flax fibers in cuprammonium reagent	43
2. Lamellas	44
3. Fibrillate structure	46
4. Retting	47
5. Comparison of flax with other bast fibers	48
IV. References	49

I. INTRODUCTION

Flax fibers are obtained from the stem of the flax plant. The stem consists essentially of a central woody core, and a surrounding cortex which contains the flax or bast fibers. The thin cambium layer lies between these regions. The fibers are obtained from the plant in the form of long filaments, each of which is made up of cells. Other bast

[1] Research Associate at the National Bureau of Standards, representing the Textile Foundation.

fibers, such as hemp, jute, and ramie, have a similar origin and structure. Although the bast fibers have many structural details like those in cotton, they differ from it in one important respect, namely, a cotton fiber is a single plant cell, whereas a bast fiber is made up of a group of cells.

A flax cell has a primary and a secondary wall. In accordance with the terminology used by Bailey [1],[2] the primary wall is considered to be the outer sheath of the fiber, or that portion of the wall which is laid down during the period of active elongation of the cell. The secondary wall is that part which is subsequently deposited on the inside of the primary wall, and which is largely responsible for the useful properties of the fiber. The adjacent cells are held together by a layer of intercellular substance.

At the tip of a growing flax stem all the cells are essentially alike. They are relatively small and uniform, and have a tenuous primary wall. A short distance back from the growing point the cells that are to develop into fibers increase in dimensions, and deposition of the secondary wall is initiated.

Considerable information concerning the structure of flax is available from the work of Tammes [2], Nodder [3, 4], Searle [5], Herzog [6], Anderson [7], Osborne [8], and others. In the present investigation many of these earlier observations have been confirmed and extended by applying to the flax fiber those methods and techniques which have recently been used to advantage in studying the structure of the cotton fiber.

II. MATERIALS

Two varieties of *Linum usitatissimum*, Martin and Jlord, were used for most of the experiments. The samples of the former variety consisted of dried flax plants, flax straw, retted straw, scutched line fiber, and machine-hackled line fiber. This material was grown in Oregon and supplied through the courtesy of the Bureau of Plant Industry, U. S. Department of Agriculture.[3] Plants of the second variety were grown from seed, in pots in the laboratory. For comparison, about 15 other samples each of flax, hemp, jute, and ramie were used. This material included fibers which had received various treatments during manufacture.

A few experiments were carried out with commercially retted fibers, but for the most part the investigation was limited to fibers that had received as few treatments as possible. This was accomplished by careful dissection of single fibers from flax straw, such fibers being termed "raw fibers." The natural waxes were removed from some of the raw fibers by extraction with alcohol and ether for 24 hours each. These fibers are termed "dewaxed fibers." A portion of the dewaxed material was further purified by boiling with 5-percent sodium hydroxide until the fibers were practically free of intercellular substance, and of much of the primary wall. These fibers, after removal of the material which has generally been assumed to be pectic in nature [1, 9], are designated "depectinized fibers."

The cuprammonium hydroxide solution, used for dissolving and for swelling the cellulose, was prepared according to the recommendation of Mease [10]. Trimethylbenzylammonium hydroxide was used in

[1] Figures in brackets indicate literature references at the end of this paper.
[2] Acknowledgment is made to B. B. Robinson and E. G. Nelson for supplying this material.

some of the experiments. The stock solution, which was 2.5 *N*, was diluted with water just before using to about 2.2 *N*. For staining cellulose, iodine and sulfuric acid [11], zinc chloride-iodine [11], and an alkaline solution of Congo red (0.5 percent of dye in a 0.5-percent solution of sodium hydroxide) were used. Aqueous solutions of ruthenium red were suitable for staining pectic compounds [12]. Although ruthenium red is not a specific stain for pectic substance, native pectic compounds are invariably colored by it [13].

III. EXPERIMENTAL PROCEDURE AND RESULTS

1. FLAX FIBERS IN CUPRAMMONIUM REAGENT

In an earlier investigation on the behavior of cotton in cuprammonium hydroxide solution it was shown that the cellulose of the fibers dissolves, leaving residues which vary in amount and in structure, depending upon the extent of purification of the fibers [14]. In the present study similar results were obtained with flax. When raw and dewaxed fibers were placed on microscope slides and then treated with cuprammonium reagent the fibers swelled and twisted, and separation of the individual cells occurred. The fibers were attacked first at the characteristic surface markings, which Osborne [8] has shown to be fissures in the wall. That these markings are actual fissures explains why they became more prominent when the fibers were given microchemical color tests for cellulose (fig. 1), and also why the cuprammonium reagent attacked these regions first. The latter phenomenon was especially noticeable when the observations were made with the crossed nicols of a polarizing microscope. The fibers, originally bright against a dark field, became progressively dimmer as the cellulose dissolved. After several minutes the field was black, which indicated that the birefringent material had disappeared. Under the conditions of this experiment, balloon-like swellings which commonly arise when cotton fibers are similarly treated [15], were not observed.

The raw and dewaxed flax fibers were practically identical in their behavior. The residue which remained after treating them with cuprammonium reagent was isotropic and stained deeply with ruthenium red (fig. 2). It consisted of intercellular substance, and of material from the primary wall and lumen, and parts of the secondary wall. When handled and dissected with microneedles this residue appeared gelatinous and rubbery, and was less readily torn apart than similar residues from cotton. Whereas in cotton the pectic substances are usually restricted to the primary wall and to the lumen [15], in flax cells this material, which appears to be of a pectic nature and which stains with ruthenium red, is present in the secondary wall also. It is distributed in narrow lamellas, which are especially prominent around the lumen (fig. 3, *A*). The existence of these lamellas can be verified by focusing, shading, and gently moving the specimen by applying pressure to the cover glass.

The individual cells of depectinized fibers separated from each other more easily than the cells of raw and dewaxed fibers. In cuprammonium reagent they dissolved almost completely, leaving only a small amount of residue, which exhibited no definite cellular structure.

The examination of cross sections of raw, dewaxed, and depectinized

fibers confirmed the results obtained with single fibers. By means of the device of Hardy [16], fibers were cut into sections about 10 microns thick. The sections were placed on microscope slides and then examined as cuprammonium hydroxide solution was drawn under the cover glass. The sections swelled, and in a short time the cellulose appeared to be dissolved. The residue from sections of raw and dewaxed flax was relatively large in amount, isotropic, stained with ruthenium red, and consisted in part of insoluble material from the region around the lumen (fig. 3, B). Cross sections of depectinized flax fibers dissolved in the reagent, leaving only a small amount of disorganized residue.

2. LAMELLAS

Under high magnification the secondary walls of plant fibers exhibit diverse structural patterns which are sometimes visible in untreated cells, but which usually stand out clearly only after the cells have been swollen. The presence of concentric lamellas in the cell wall of the cotton fiber has been clearly established [15, 17, 18]. That the wall of the flax cell has a similar configuration is suggested by the work of Tammes [2], Nodder [3], Searle [5], Anderson [7], Aldaba [19], and others. Additional evidence in support of such a structure was obtained in the present investigation.

Cuprammonium reagent dissolves the cellulose of the fibers in a relatively short time. In suitable dilutions of the reagent, however, complete dissolution of the cellulose does not occur; instead the fibers swell considerably and thereby reveal many details of structure. When single cells or small groups of flax cells were placed in cuprammonium hydroxide which had been diluted with 3 to 4 volumes of concentrated ammonium hydroxide, they swelled to several times their original diameter. Upon focusing midway between the upper and lower surfaces of such a swollen flax cell, layers or lamellas running parallel to the axis were discernible in the wall (fig. 4, A and B). Lamellas were similarly observed in swollen cross sections of the cells (fig. 5). Individual lamellas varied in thickness from 0.1 to 0.2 micron.[4] In both cases, upon staining with Congo red, alternating layers of densely and of lightly stained cellulose became prominent. Between crossed nicols these sections showed alternating layers of strongly and of weakly birefringent material.

Although in longitudinal view the lamellas usually ran parallel to the long axis of the cell, this pattern was occasionally altered. At certain points the lamellas did not maintain their cylindrical shape but converged over the lumen to form dome-shaped structures, or "caps." As shown in figure 4, B, two of these domes lay next to each other. Usually, only the innermost lamellas formed these structures, the outermost layers continuing parallel to the axis of the cell and enclosing the "compartments" within. These observations appear to be in agreement with those of Aldaba [19], who studied the development of the cell wall in bast fibers of *Boehmeria* (ramie) and *Linum* (flax). Apparently in the earlier stages of cellular differentiation the protoplasm of a single cell behaves more or less as a unit, thereby giving rise to lamellas which extend usually along the entire length of the cell wall. In the later stages of development the compartments

[4] The width of the lamellas was obtained by dividing the thickness of the wall of the unswollen fiber by the number of layers counted after swelling.

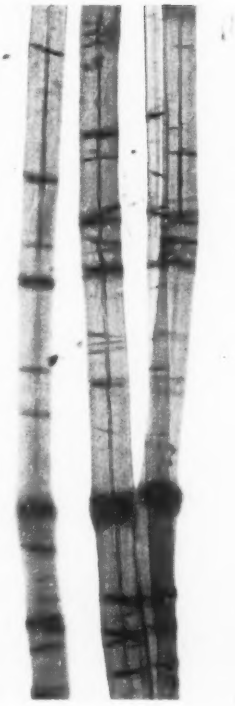

FIGURE 1.—*Transverse markings of flax fibers.*

Several flax cells separated from a fiber and treated with zinc chloride-iodine to show the transverse markings. Magnification ×100.

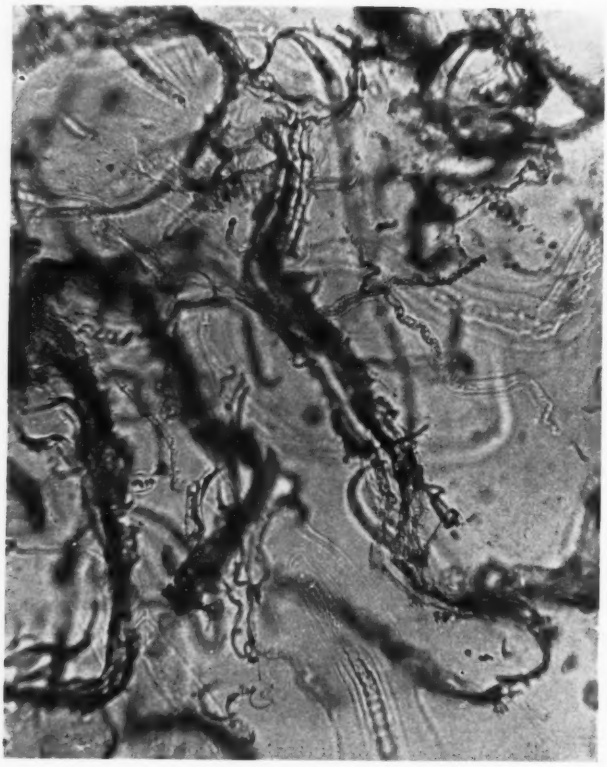

FIGURE 2.—*Dewaxed flax fibers in cuprammonium hydroxide solution.*
Residue which remains after the cellulose of the fibers has dissolved in the reagent. Stained with ruthenium red. Magnification ×100.

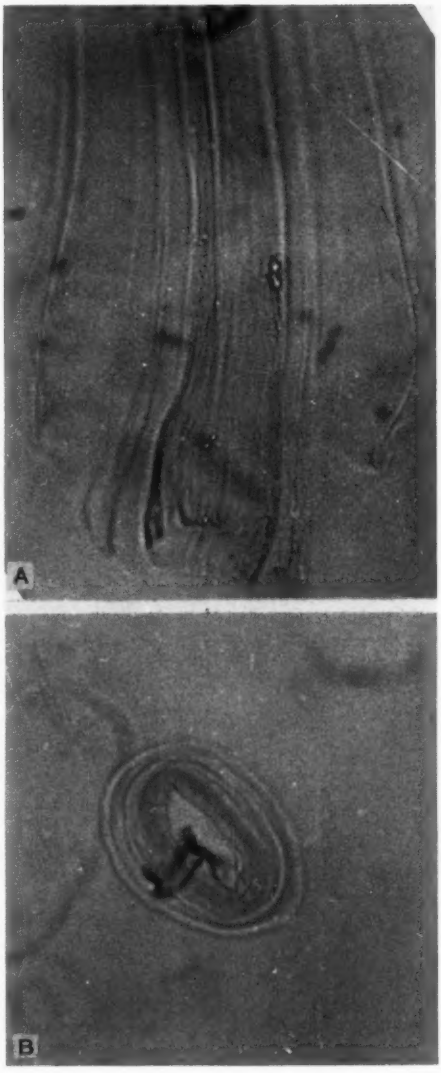

FIGURE 3.—*Residue from dewaxed fibers after treatment with cuprammonium reagent.*

A, Longitudinal view of residue from part of a cell; *B*, cross section of residue from a single cell. Stained with ruthenium red. Magnification ×500.

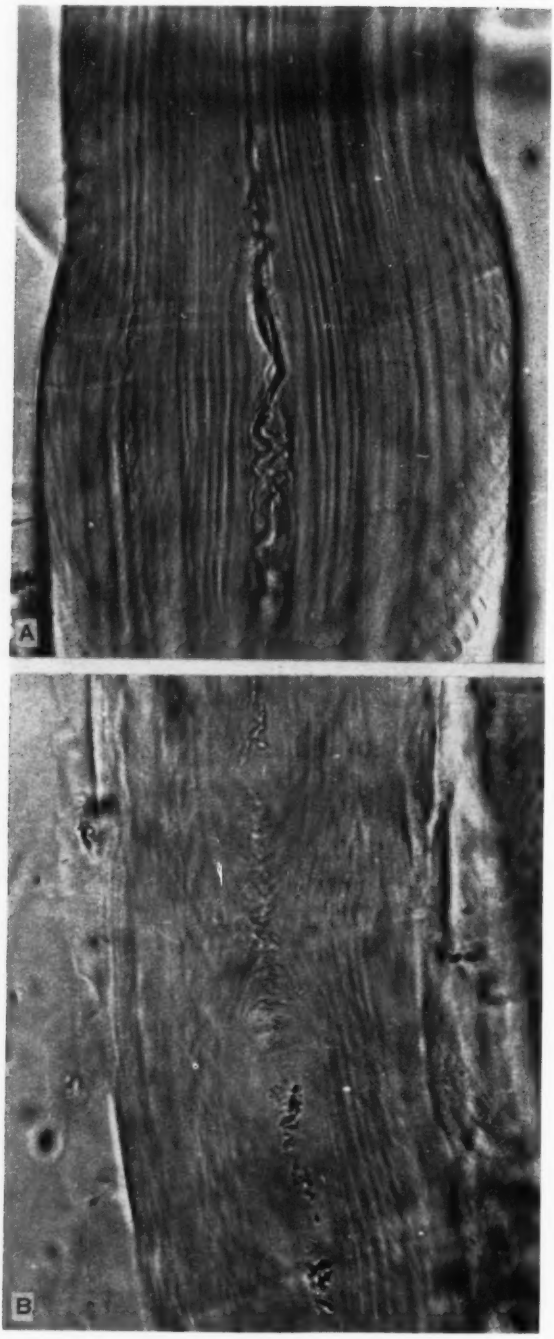

FIGURE 4.—*Lamellas in longitudinal view.*

A, Single cell, showing lamellas parallel to the long axis; *B*, single cell, showing formation of "compartments" by some of the inner lamellas. Cells swollen in dilute cuprammonium hydroxide and stained with Congo red. Magnification ×500.

FIGURE 5.—*Lamellas in cross section.*

Two adjacent cells after swelling in dilute cuprammonium hydroxide and staining with Congo red. Magnification ×500.

UNIV. OF MICH.

are formed in localized regions of the cell, which give rise to additional lamellas enclosed within those previously deposited.

In order to investigate the lamellar structure of flax fibers from different regions of the plant, several flax stems each about 96 cm in length, were selected and divided into 16 segments in the following manner. Starting at the base, fifteen 6-cm segments were cut off. The remaining part, which included the branching tip and which sometimes slightly exceeded 6 cm, constituted the 16th segment. Several series of experiments were then run on the fibers, which were manually separated from each of these regions. First, the fibers were cut into thin cross sections, and the width of the cell walls was measured with a calibrated ocular micrometer. Although considerable variation was found, the measurements indicated that the wall is thicker in the cells at the base of the stem than in those at the tip (table 1). As the cells mature, an initial rapid increase in thickness of the wall appears to be followed by a further more gradual increase. Second, cross sections were swollen in dilute cuprammonium hydroxide, and the lamellas were counted. Finally, the lamellas were counted in longitudinal view in swollen cells from each region. Although there was an appreciable variation in the number of lamellas at any one level of the stem, the number was greater in the cells at the base of the stem than in those at the tip. Figure 6 shows graphically the number of lamellas in relation to the position of the cell in the stem.

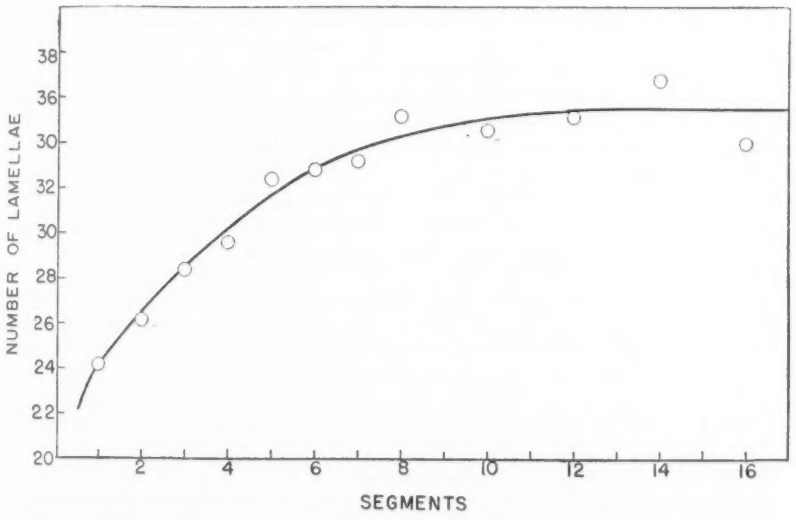

FIGURE 6.—*Number of lamellas in cells from various regions of the stem.*

The segments represent a distance of 6 cm each, and are numbered from the tip to the base of the stem. (Each point of the curve represents the average of 20 counts.)

The examination of cross sections (fig. 7) and of cells from living plants confirmed the above observations. The wall often showed a lamellar pattern even in unswollen sections. The lumens of the growing fibers were sharp and irregular in outline, and in some cells the lamellas of the secondary wall appeared wrinkled and folded and

TABLE 1.—*Thickness of the wall of cells from fibers in various regions of the stem*

[The segments represent a distance of 6 cm each and are numbered from the tip to the base of the stem.]

Segment	Thickness (microns) arithmetic mean of 40 measurements	Standard deviation (microns)	Segment	Thickness (microns) arithmetic mean of 40 measurements	Standard deviation (microns)
1	5.5	±1.4	8	7.5	±1.8
2	6.5	±1.3	10	7.3	±1.4
3	7.1	±1.4	12	8.4	±1.6
4	7.0	±1.5	14	8.2	±1.7
5	7.4	±1.0	16	7.7	±1.5
6	7.0	±2.2			

only loosely held together. At the tip of the stem, where the cell walls were thin, there were fewer lamellas than in the walls of mature fibers from the base.

Because of the similarity in the lamellar structure of the flax and cotton fibers, it seems probable that the deposition of lamellas in flax may be related to environmental factors, as has been shown for cotton [15, 17, 18]. However, because of the complex structure of the flax stem, the time at which the fibers originate in the stem is unknown and their development cannot be followed.

3. FIBRILLATE STRUCTURE

A fibrillate structure has been described for many different plant-cell walls, and probably accounts for many of their useful properties. In order to study the fibrillate structure of flax, raw and depectinized flax cells were treated with dilute cuprammonium hydroxide (diluted with 3 to 4 volumes of ammonium hydroxide), trimethylbenzylammonium hydroxide, or approximately 10 percent sodium hydroxide. Upon swelling, the wall of each cell was found to consist of innumerable exceedingly fine fibrils which made an acute angle with respect to the axis. As the cell continued to swell, this angle increased until, in extreme cases, the outermost layer of fibrils lay in a nearly transverse position. In agreement with the observations of Nodder [3] and Osborne [8], it was found that upon focusing on the upper half of a swollen cell the majority of the fibrils appeared to make an S twist.[5] Under favorable conditions, however, it can be shown that although most of the fibrils in the secondary wall have an S twist, the outermost layer has a Z twist (fig. 8). In other words, the first layer of fibrils laid down in the secondary wall winds in an opposite direction from those which are deposited subsequently, making flax comparable to cotton in this respect. Although it is difficult to determine whether all the fibrils in the inner layers wind in one direction, this appeared to be the case. Anderson [7], however, found a reversal in direction of fibrillate orientation in alternate lamellas. With continued swelling in the reagent, the outermost layer of fibrils frequently lost its even distribution over the surface of the fibres and became clumped in a few places, thereby restricting the uniform lateral expansion of the swelling fiber (fig. 9).

[5] According to ASTM Standards on Textile Materials [20], a yarn or cord has an S twist if, when held in a vertical position, the spiral conforms in slope to the central portion of the letter S, and a Z twist if the spiral conforms to the central portion of the letter Z. In the present paper, the same terminology will be applied to fibrils.

The fibrillate structure of the secondary wall was examined further with the aid of the needles of a micromanipulator. Flax cells were first swollen in trimethylbenzylammonium hydroxide and then handled with the microneedles. The cells were flattened, stretched, dissected, and otherwise handled so as to reveal their structural details. By this technique the apparent fibrillate structure of the flax fibers was verified. In some cases, small groups of fibrils were pulled away from the cell, whereas at other times practically all the fibrils were separated from each other and spread out in a thin sheet (fig. 10). When examined with the polarizing microscope the fibrils themselves appeared to be birefringent.

4. RETTING

In order to study the changes in structure which take place during retting, comparisons were made of commercially retted flax and of samples which were observed continuously during retting in the laboratory.

The commercially retted (tank-retted) flax straw was darker in appearance and more brittle than the untreated stems of the same variety. The bast fibers were often only loosely held to the central woody portion of the retted stem, and could be removed easily for further examination. These fibers stained rather uniformly with ruthenium red and left a large residue of isotropic material upon treatment with cuprammonium hydroxide solution. As observed in cross section, spaces were sometimes evident around the individual bast cells as if the intercellular substance and the primary wall had been attacked, but for the most part the small groups of cells were still held together in their natural arrangement. Cross sections were also made of retted flax straws in order to observe the changes in all the cells of the stem, and not just in the commercially useful bast fibers. Retting was found to take place first in the cambium layer, and later in certain of the cortical cells which surround the fibers. The cells in these regions are thin-walled, with a high proportion of intercellular substance and primary wall, and are easily accessible to retting agents. In the retted samples these layers still gave a positive test with ruthenium red although the individual cell walls were distorted and crushed. The weakening of these regions allows easy separation of the bast fibers from the woody portion of the stem and from the nonfibrous cells of the cortex.

Similar experiments were also carried out on samples retted in the laboratory. The specimens were placed in water at 95° F and were observed daily thereafter for 2 weeks. Observations were made on entire flax straws and on their cross sections. The results of these experiments confirmed and extended the observations made on commercially retted samples. The first cells to be attacked by the retting microorganisms were the thin-walled cells of the cortex and cambium layers [21]. Where the process was continued for a longer time, the primary walls of the flax cells were attacked also (fig. 11), but this did not appear to be the essential feature of retting. The observations suggest that, while retting may depend in part on the removal of intercellular substance and of material from the primary walls of the bast cells, the weakening of the cambium and cortical layers is of greater importance [21, 22].

463607—42——4

5. COMPARISON OF FLAX WITH OTHER BAST FIBERS

While less attention has been paid to the other bast fibers—hemp, jute, ramie—it appears that their structures are similar to those of flax. Upon treatment with cuprammonium reagent the cellulose dissolves, leaving a disorganized isotropic residue resembling that from flax. All of these fibers show transverse surface markings, which become more prominent after treatment with zinc chloride-iodine. Whereas in flax, hemp, and sometimes in ramie, these markings often form the letter "X", this does not occur in jute. After swelling to many times their original diameter, all the bast fibers show both lamellas and fibrils in their cell walls.

The identification of bast fibers by ordinary microscopic techniques is often difficult and uncertain. The moisture test, in which the direction of movement of one end of the fiber is observed during wetting and drying, has been suggested as a further means of distinguishing them [11]. Accordingly, it was decided to examine all of the available samples of these fibers in order to determine the usefulness of this test. Samples of raw fibers, and others which had been processed in various ways, were used. The test was carried out in the following manner. A small piece of paper was cemented to one end of the fiber perpendicular to its axis. This refinement of technique was helpful, although not essential, in accurately determining the twist. The fiber was then placed in water for 30 sec to 1 min to ensure thorough wetting, whereupon it was removed and allowed to dry in air. The fiber was held vertically and the direction of twist observed by looking down at the paper indicator. By alternate wetting and drying, the test may be repeated many times on a single fiber. During wetting, the fibers usually show a twist opposite to that observed during drying. With few exceptions, the following generalizations, in agreement with those of Nodder [3] and Reimers [23], appear to hold. The drying twist of flax and ramie is counterclockwise, whereas the twist for hemp and jute is clockwise. The speed of twisting was not uniform for any one type of fiber. For example, some hemp fibers twisted clockwise very rapidly, whereas others moved only slowly in that direction. Generally, however, the motion is more rapid in flax and ramie than in hemp and jute.

The results of the moisture test suggest that the variations in drying behavior may be caused by differences in the fundamental structure of the two groups of fibers. That differences in structure do exist was revealed by noting the direction of orientation of the fibrils in swollen fibers. As described in an earlier section of this paper, a flax cell consists of many fibrils, oriented at an acute angle with respect to the long axis of the fiber. The majority of these fibrils have an S twist, but the outermost layer has a Z twist (fig. 8). The fibrillate structure of cells from ramie fibers was found to be identical. Swelling treatments did not reveal the fibrillate structure in hemp and jute as clearly as in flax and ramie. However, with microneedles, fibrils were dissected from the former. The outermost layer of fibrils showed a Z twist, as in flax and ramie, but unlike them, the majority of the fibrils appeared to be oriented nearly parallel to the axis. Figure 12 shows, diagrammatically, the direction of fibrillate orientation in the bast fibers and is similar to sketches of the micellar orientation in these fibers as reported by Reimers [23].

FIGURE 7.—*Cross section of the flax stem.*

Part of a cross section of the stem of a growing flax plant, showing the thick-walled fiber cells surrounded by other tissues. Magnification ×500.

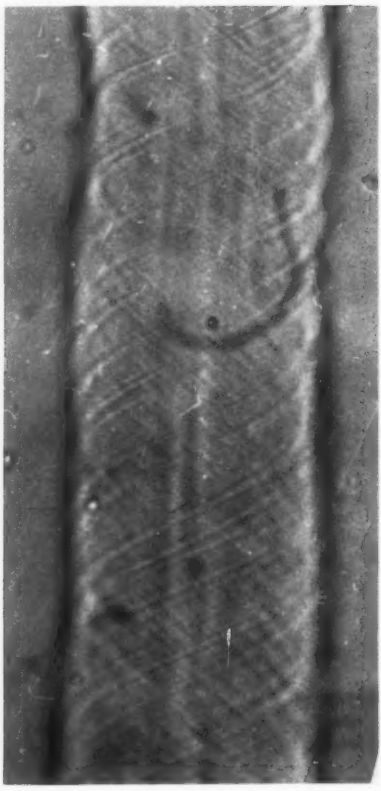

FIGURE 8.—*Fibrillate structure of flax.*

A single cell swollen in dilute cuprammonium hydroxide, showing the Z twist of the fibrils in the outer layer and S twist of the fibrils in the layers beneath. Magnification ×500.

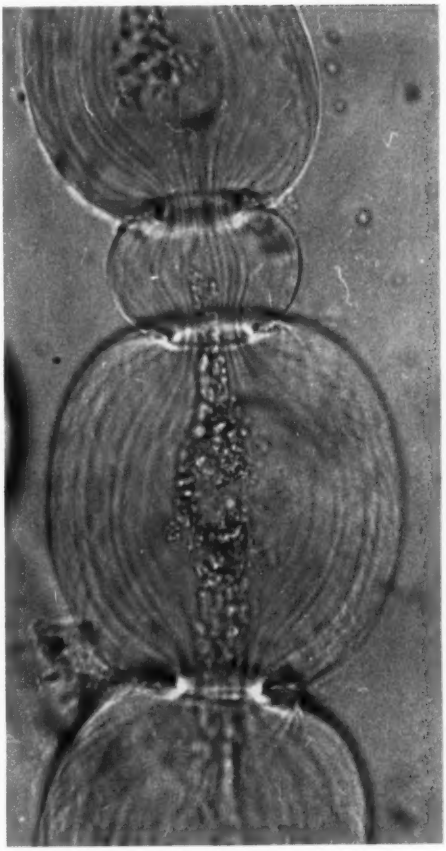

FIGURE 9.—*Irregular swelling of a flax cell.*

A depectinized cell in dilute cuprammonium hydroxide, showing irregular swelling because of the constricting influence of the outermost layer of fibrils. Lamellas, as well as some protoplasmic material in the lumen, are also shown.

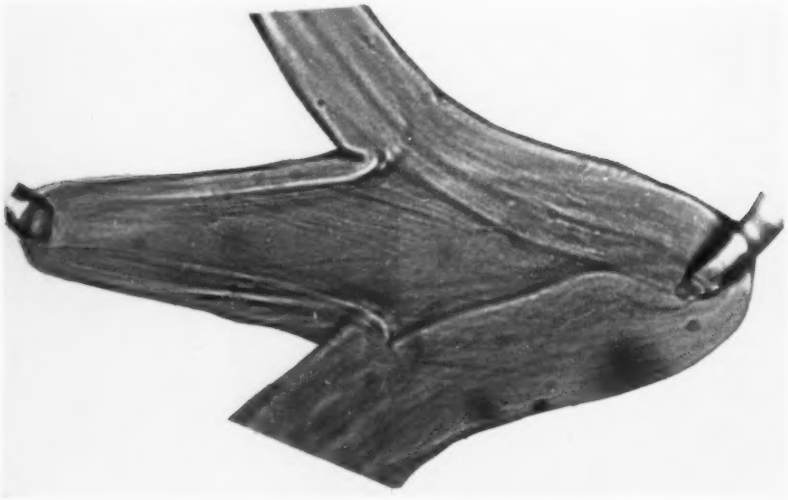

FIGURE 10.—*Microdissection of a single flax cell.*

Cell swollen in trimethylbenzyl ammonium hydroxide and dissected with microneedles. Magnification ×360.

FIGURE 11.—*Retted flax straw.*

Part of a cross section of a retted flax stem, showing the break-down of the cells surrounding the fibers, and in this case the separation of the fiber cells from each other because of overretting. Compare with figure 7. Stained with ruthenium red. Magnification ×500.

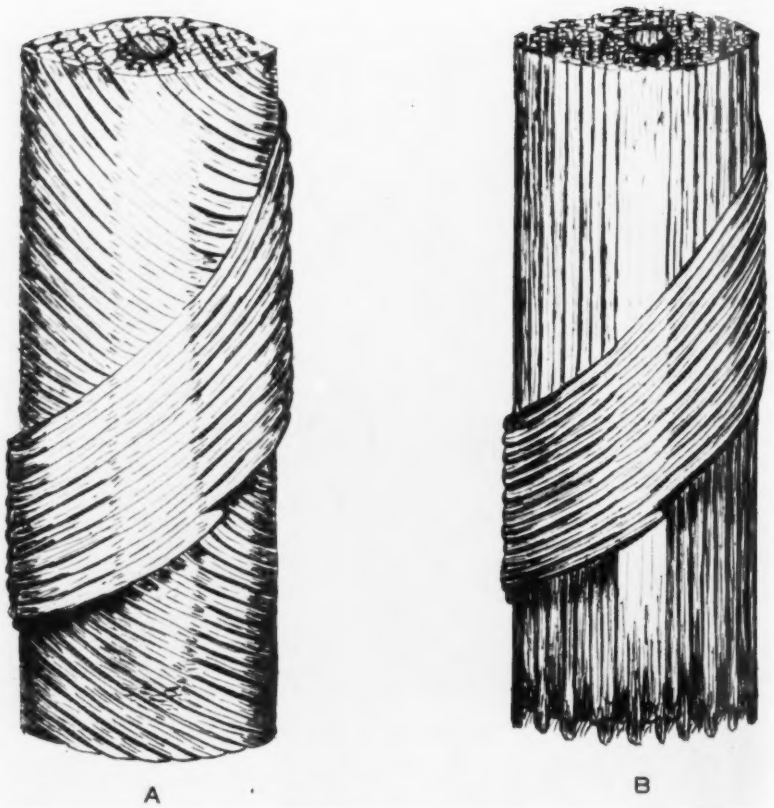

FIGURE 12.—*Schematic drawing of the arrangement of fibrils in the cells of bast fibers.*
A, Flax and ramie; *B*, hemp and jute.

In order to see whether there was any similarity between the behavior of yarns with various twists, and fibers with different fibrillate orientations, several yarns with S and Z twists were given the moisture test. Yarns with an S twist were found to turn counterclockwise when losing moisture and clockwise when taking it up. The reverse was true for yarns with a Z twist. This suggests the following analogy with bast fibers. In flax and ramie the direction of twist appears to be determined largely by the bulk of fibrils, which make an S twist. When drying, for instance, the tendency of the outermost layer of fibrils with the Z twist to turn the fiber in a clockwise direction is overcome by the very many more fibrils whose orientation favors a counterclockwise movement. In hemp and jute the parallel orientation of the majority of fibrils does not influence the fiber to turn either one way or the other during moisture changes. In these fibers the Z twist of the fibrils in the outer later appears to be the determining factor, thereby causing a clockwise drying twist and a counterclockwise twist during wetting.

While it is recognized that during swelling the angle which the fibrils make with the fiber axis may be changed in magnitude, studies with the polarizing microscope indicate that the general direction of orientation is unaltered. When the fibers were mounted in water and examined between crossed nicols and a selenite plate some of the fibers were opposite in appearance to others. Flax and ramie were indigo at 0° and orange red at 90°, whereas hemp and jute were orange red at 0° and indigo at 90°. Upon rotating the fibers the color changes were more pronounced in the first than in the second of the above groups. In both groups color variations occurred in different fibers and even in different regions of the same fiber, but in general when flax and ramie were placed at 0° the interference colors rose in the color scale, whereas for hemp and jute the interference colors fell. These observations, which are in agreement with those of Herzog [6], indicate an opposite orientation of the cellulose in the two groups of fibers. In cotton, contrasting colors indicative of differences in orientation occur within a single fiber and upon swelling it is seen that in a single fiber the direction of fibrillate orientation is frequently reversed [15]. It is interesting to note, accordingly, that when the moisture test was applied to single cotton fibers they twisted either clockwise or counterclockwise during drying, and sometimes different parts of the same fiber twisted in opposite directions. Occasionally no movement was observed. These experiments indicate that a close correlation exists between the fibrillate orientation of the fibers and some of their physical properties.

IV. REFERENCES

[1] I. W. Bailey, Ind. Eng. Chem. **30,** 40 (1938).
[2] T. Tammes, Natuurkundige Verhandelingen van de Hollandshe Maatschappij der Wetenschappen te Haarlem. De Erven Loosjes, Haarlem (1908).
[3] C. R. Nodder, J. Textile Inst. **13,** T161 and 213 (1922).
[4] C. R. Nodder, Trans. Faraday Soc. **20,** 251 (1924).
[5] G. O. Searle, J. Textile Inst. **15,** T371 (1924).
[6] A. Herzog, Die Unterscheidung der Flachs- und Hanffaser. Julius Springer, Berlin (1926).
[7] D. B. Anderson, Am. J. Bot. **14,** 187 (1926).
[8] G. G. Osborne, Textile Research **5,** 351 and 431 (1935).

[9] M. H. Branfoot (M. H. Carrè). Dept. of Scientific and Industrial Research Food Investigation, Special Report No. 33 for 1928. His Majesty's Stationery Office, London (1929).
[10] R. T. Mease, J. Research NBS **22,** 271 (1939) RP1179.
[11] T. M. Plitt, Circular of the National Bureau of Standards C423 (1939).
[12] L. Mangin, Compt. rend. **116,** 653 (1893).
[13] D. B. Anderson and T. Kerr, Ind. Eng. Chem. **30,** 48 (1938).
[14] C. W. Hock and M. Harris, J. Research NBS **24,** 743 (1940) RP1309; Am. Dyestuff Rptr. **29,** No. 12, 287–292 (1940).
[15] C. W. Hock, R. C. Ramsay and M. Harris, J. Research NBS **26,** 93 (1941) RP1362; Am. Dyestuff Rptr. **30,** 53 (1941).
[16] J. I. Hardy, U. S. Dept. of Agriculture Circular 378 (1935).
[17] W. L. Balls, Proc. Roy. Soc. (London) [B] **90,** 342 (1919).
[18] T. Kerr, Protoplasma **27,** 229 (1937).
[19] V. C. Aldaba, Am. J. Bot. **14,** 17 (1927).
[20] A. S. T. M. Standards on Textile Materials, Am. Soc. for Testing Materials, Philadelphia (1941).
[21] R. L. Davis, U. S. Dept. of Agric. Bul. No. 1185 (1923).
[22] J. V. Eyre and C. R. Nodder, J. Textile Inst. **15,** T237 (1924).
[23] H. Reimers, Textilberichte **2,** 367, 381, and 420 (1931).

WASHINGTON, April 3, 1942.

U. S. Department of Commerce National Bureau of Standards

RESEARCH PAPER RP1483

Part of Journal of Research of the National Bureau of Standards, Volume 29, July 1942

ACCELERATED AGING OF LACE LEATHERS

By Joseph R. Kanagy and Philip E. Tobias

ABSTRACT

Alum-, indian-, and chrome-tanned lace leathers, submitted by various manufacturers, were tested for deterioration under accelerated-aging conditions. In addition, the physical and chemical properties of these leathers were determined according to the tests prescribed by the Federal specification for lace leathers. The alum-tanned lace leathers were much less stable under the conditions of accelerated aging than the indian- and chrome-tanned leathers. Several types of chrome-tanned leathers, including chrome-tanned lace leather, showed intermediate stability. From the results of these tests, it appears that measurements of physical properties such as strength, stretch, and flexibility, together with an accelerated-aging test, may be expected to give more valuable information about the performance characteristics of lace leathers than the measurements required by the present Federal specification.

CONTENTS

	Page
I. Introduction	51
II. Materials and experimental procedure	52
III. Results and discussion	52
IV. References	56

I. INTRODUCTION

Two of the more important physical properties desired for lace leathers are high strength and high flexibility. These properties are found in leathers which have been tanned lightly, with the hides in an unswollen condition, followed by treatment with large amounts of oils and greases in the finishing processes. Another essential property for lace leather, as well as for any other type of leather, is durability. Durability is not necessarily imparted by the same tanning processes which yield high strength and high flexibility. Therefore, it is important that specifications for lace leathers should require a direct determination of their aging characteristics.

In the Federal specification for lace leather, KK–L–201, durability is judged from a number of chemical tests. To make these tests requires considerable time, and the significance of some of them has been questioned. An accelerated-aging test would be a more accurate index of the durability, since such a test would approximate the conditions of actual service, and would also save time in testing and simplify

such specifications. For this reason, a study of the accelerated-aging properties of alum-, indian-,[1] and chrome-tanned lace leathers was made. Methods were used which were developed at the National Bureau of Standards [1] [2], and these have been shown to give results similar to those obtained with vegetable-tanned leathers under normal aging conditions.

II. MATERIALS AND EXPERIMENTAL PROCEDURE

The samples tested included indian-, alum-, and chrome-tanned lace leathers. A total of 15 samples of these leathers were submitted by various manufacturers, and it was assumed that they were fairly representative of the lace leather on the market.

From each block, measuring 7 by 14 inches, 12 tensile-strength specimens were cut. These blocks were cut from the best area of the hide available, however, no regard was given to using the corresponding areas from all of the hides in a given test. The specimens were numbered 1 to 12, consecutively. The even-numbered specimens were aged, whereas the odd-numbered ones were used as controls. In all but one experiment the samples were allowed to dry for 6 hours before aging. This drying procedure is described in a previous publication [1]. The effect of degreasing before aging on some of the samples was also studied.

The apparatus used in making the tests was the same as that described in a previous publication [1]. Air which had been saturated with water at 45° C was passed over the leather specimens. This furnished an atmosphere having a relative humidity of about 9.5 percent at 100° C. The temperature and time of aging were varied.

III. RESULTS AND DISCUSSION

The results of the accelerated-aging tests on the lace leathers, expressed as percentage loss in breaking strength, are given in table 1. The temperature, time, and other conditions of aging are also given. The results indicate that the alum-tanned lace leathers are extremely unstable under all of the aging conditions. The relative order of stability of each of the alum-tanned leathers is the same for nearly all sets of conditions tried. Alum leather 6 is most stable under all conditions; alum leather 4 is correspondingly least stable. Degreasing the leathers decreases the rate of deterioration, but the relative rates of deterioration are unchanged.

Indian- and chrome-tanned lace leathers are much more resistant to accelerated aging than the alum-tanned leathers, as shown in table 1. In these cases, as was also observed with alum leathers, the relative order of resistance to aging as measured by loss in breaking strength for each of the samples is the same under nearly all of the conditions. Leathers 1 and 14 are most resistant to aging, whereas leather 10 is least resistant. The chrome-tanned lace leathers show comparatively low resistance to aging. Chrome leather 11 gives a high percentage loss in breaking strength in comparison with any of the indian-tanned leathers, whereas chrome lace leather 15 is equal in performance to the indian-tanned leathers, which give intermediate results.

[1] Alum-tanned leather retanned with a suitable vegetable tanning material.
[2] Figures in brackets indicate the literature references at the end of this paper.

TABLE 1.—*Results of accelerated aging*

Percentage loss in breaking strength

Leather number	Conditions of aging—air saturated with water vapor at 45° C					
	100° C; 7 days; dried	90° C; 4 days; dried	90° C; 2 days; dried	80° C; 4 days; dried	90° C; 4 days; dried; degreased	100° C; 7 days; not dried
ALUM-TANNED						
2	88	74	57	66	64	
4	95	89	80	81	69	88
6	81	65	51	60	41	
9			72	66	43	
INDIAN-TANNED						
1	14	[a]4			[a]3	22
3	42	210, 18			11	
5	44	17, 17			8	33
7	58	33, 23			9	35
10		43, 46, 54				49
13	26					
14	4					
CHROME-TANNED						
11		74			24	
15					8	34

[a] Gain.

Since the low resistance to aging of the chrome lace leathers was unexpected, several additional experiments were made, in which other types of chrome-tanned leathers were included. Chrome-tanned ski leather, chrome-tanned lace leather, and chrome-, chestnut-, and quebracho-tanned steer-hide leathers were aged at 60°, 70°, 80°, 90°, and 100° C in air which had been saturated with water at 60° C, thus producing a relative humidity of approximately 19.5 percent at 100° C. Chrome-tanned steer hide, chrome-tanned lace leather, and chrome-tanned ski-leather, previously dried, were aged at 80°, 100°, and 120° C in air saturated with water at 45° C. The steerhide leathers were tanned in the experimental tannery at the National Bureau of Standards.

The results of the accelerated aging are shown in table 2, and in comparing the losses in breaking strength, the chrome-tanned leathers show less stability under the conditions of this test than quebracho leather and are about equal in stability to chestnut leather. The losses in breaking strength, for the chrome-tanned leathers, increase with temperature, continuing up to 120° C, the highest temperature at which the tests were made. Slightly higher losses in breaking strength were obtained at 60° than at 70° C. This was possibly caused by the condition of 100-percent relative humidity at 60° C. The amounts of soluble nitrogenous materials extractable by a 0.1 *N* sodium carbonate solution from the aged chrome-tanned leathers do not parallel the losses in breaking strength. The aged samples yield small amounts of soluble nitrogenous materials, which are nearly constant for every temperature except 120° C. Similar results for losses in breaking strength and for amounts of soluble nitrogenous materials for chrome-tanned leathers were obtained by Frey and

Beebe [4] in their studies on acid deterioriation in the sulfur dioxide gas chamber. They suggested that the soluble nitrogenous material values might not be a reliable index of the deterioration of chrome-tanned leathers and also mentioned the possibility of a mechanism of deterioration, different for chrome- than for vegetable-tanned leathers. The fact that a mechanism of deterioration, different for chrome- than for vegetable-tanned leathers, may exist emphasizes the importance of the selection of suitable conditions and the proper criterion of deterioration for comparing the aging qualities of vegetable- and chrome-tanned leathers. The conditions of aging should be similar to those which the leathers will undergo in service. The belief that chrome leather is superior to vegetable-tanned leather originated principally from the fact that well-tanned chrome leather when heated in water has a higher shrinkage temperature than vegetable-tanned leather. This condition parallels few circumstances of actual service. From the results of this work in which the test method approximates more nearly normal aging conditions, it appears that for use as lace leather, where breaking strength is important, either vegetable- or the so-called indian-tanned leather, if well made, would be as serviceable as chrome-tanned leather.

TABLE 2.—*Results of accelerated aging tests*

Type of leather	Conditions of aging—air saturated with water vapor at 60° C. Samples not dried. Aging time—7 days							
	60° C	70° C	80° C		90° C		100° C	
	Loss in breaking strength	Loss in breaking strength	Loss in breaking strength	Soluble nitrogen	Loss in breaking strength	Soluble nitrogen	Loss in breaking strength	Soluble nitrogen
	%	%	%	%	%	%	%	%
Quebracho-tanned steer hide	5	2	9	1.0	9	1.0	16	1.5
Chestnut-tanned steer hide	6	3	13	4.0	24	6.4	29	11.0
Chrome-tanned steer hide	[a] 3	7	10	0.6	20	1.0	31	0.9
Chrome-tanned lace	6	0	10, 15	.6	27	0.7	34	1.0
Chrome-tanned ski				1.5	15	.6	26	1.1

Type of leather	Conditions of aging—air saturated with water vapor at 45° C. Samples dried. Aging time—7 days					
	80° C		100° C		120° C	
	Loss in breaking strength	Soluble nitrogen	Loss in breaking strength	Soluble nitrogen	Loss in breaking strength	Soluble nitrogen
	%	%	%	%	%	%
Chrome-tanned steer hide	[a] 3	0.6	26		51	2.0
Chrome-tanned lace [b]	7	.6	32		70	7.1
Chrome-tanned ski [b]	8	.4	29		70	6.7

[a] Gain.
[b] Degreased.

The chemical and physical analyses of the lace leathers are shown in table 3. These analyses were made by the methods described in Federal Specification KK–L–201 for lace leathers. Tensile-strength measurements were made in a tension machine, using the full-length lace. The degree of tannage of the indian-tanned lace leathers was determined by the ALCA method for vegetable-tanned leathers.

Wallace [2] has shown that the amount of the nitrogenous materials extractable from vegetable-tanned leathers decreases as the degree of tannage increases. In general, such a trend is shown by comparing the corresponding values for these factors given in table 3. There is no apparent correlation between the results of the aging tests and the amounts of the nitrogenous materials extractable from the unaged leathers by water at 70° C. Leather 3, which yields far more nitrogenous material than the other indian-tanned leathers, shows as much resistance to aging as leathers 5 or 7, and considerably more than 10. Leather 3 contains a high amount of R_2O_3, consisting principally of aluminum oxide. Frey and Beebe [3] have shown that leathers tanned with a combination of alum and vegetable tanning materials are more resistant to aging than those tanned with vegetable tanning materials alone. They found that the resistance to aging increases as the alum content is increased. Therefore, the amounts of nitrogenous materials extractable from any unaged leathers at 70° C may not be a reliable criterion of the stability of those tanned with a combination of alum and vegetable tanning materials.

TABLE 3.—*Properties of lace leather*

Leather number	Chemical							Physical					
	Ash	Grease	R_2O_3	Extractable nitrogen	Cr_2O_3	pH	Degree of tannage	Hide area	Maximum thickness	Stretch[1] ¼ in.	Stretch[2] ½ in.	Break load ¼ in.	Break load ½ in.
ALUM-TANNED													
	%	%	%	*mg/7.5 g leather*	%			*ft.²*	*in.*	%	%	*lb.*	*lb.*
2	5.2	34.8	2.2	.....	.....	3.9	.....	18	0.120	14.5	18.6	97	221
4	5.2	28.2	1.3	.....	.....	4.0	.....	18	.140	11.7	11.9	109	284
6	9.0	32.8	2.2	.....	.....	3.9	.....	17	.140	12.8	13.1	164	363
9	4.2	33.8	1.1	274.1	0.04	4.1	.....	15	.135	22.2	22.2	51	170
INDIAN-TANNED													
1	2.3	41.6	1.0	2.7	0.06	3.8	30.8	24¾	0.125	6.7	8.1	118	233
3	10.7	27.9	7.1	103.0	.....	3.9	5.5	17	.125	9.4	13.6	111	256
5	9.5	25.7	2.5	43.1	.....	3.9	8.1	16	.130	11.9	14.2	151	314
7	7.2	31.3	1.7	25.5	.....	4.0	21.6	16	.150	12.2	12.5	138	332
10	8.5	19.0	1.5	44.7	.....	4.2	13.3	19	.090	13.6	13.1	92	234
13	6.1	33.7	1.5	34.0	.....	3.6	31.9	.....	.....	.....	.....	.....	.....
14	1.7	20.5	0.2	2.1	.....	3.7	71.9	.....	.....	.....	.....	.....	.....
CHROME-TANNED													
11	5.5	24.7	0.3	2.3	4.8	4.3	.....	19	0.160	16.1	20.0	121	314
15	5.2	21.7	.5	.....	2.8	3.9	.....	.....	.142	16.7	19.7	89	206

[1] Measured at 32.5 lb.
[2] Measured at 85 lb.

By accelerated aging, and by the determination of the physical properties, leather 1 appears to be the best type of lace leather. It was completely penetrated with vegetable tanning materials at the low degree of tannage of 30.8. Leather 14 also resisted aging well but had a high degree of tannage, which, for most leathers, would result in a decrease of strength and flexibility.

The determination of extractable nitrogenous materials may be misleading, especially in the case of indian-tanned leathers. It has been shown previously [1] that the pH of the leather is reflected in the results obtained in this accelerated-aging test. A limit of the R_2O_3 content in the Federal specification appears to be undesirable, since it has been shown that the aging resistance of combination alum- and vegetable-tanned leathers increases with the aluminum oxide content. The significance of a limit on the ash content is also open to question. From these observations and the results of this work, it appears that measurements of such physical properties as strength, stretch, and flexibility, together with an accelerated-aging test, may be expected to give more valuable information about the performance characteristics of lace leathers than the measurements required by present Federal specification.

IV. REFERENCES

[1] J. Research NBS **25,** 149 (1940) RP1319; J. Am. Leather Chem. Assn. **35,** 632 (1940).
[2] J. Am. Leather Chem. Assn. **26,** 545 (1931).
[3] J. Am. Leather Chem. Assn. **35,** 440 (1940).
[4] J. Am. Leather Chem. Assn. **29,** 489 (1940).

WASHINGTON, May 12, 1942.

U. S. Department of Commerce National Bureau of Standards

RESEARCH PAPER RP1484

Part of Journal of Research of the National Bureau of Standards, Volume 29, July 1942

EFFECT OF MODERATE COLD-ROLLING ON THE HARDNESS OF THE SURFACE LAYER OF 0.34-PERCENT-CARBON STEEL PLATES

By Harry K. Herschman

ABSTRACT

The influence of moderate cold-rolling on the surface indentation hardness of 0.34-percent-carbon steel plate initially surface-finished by three different methods was investigated. Variations of the hardness of the surface layers extending to different depths below the surface of the specimens were determined by applying different loads on a Knoop indenter. Indentation hardness tests also were made with the Rockwell Superficial hardness machine. The results obtained with the Knoop indenter showed significantly lower hardness numbers for the superficial layer of the steel after the lighter degrees of rolling, the magnitude of change apparently being influenced by the mode of initial finishing. Hardness decreases were not revealed by tests made with the Rockwell Superficial machine nor in any case in which the penetration of the Knoop indenter exceeded about 0.0003 inch.

CONTENTS

	Page
I. Introduction	57
II. Material	58
III. Method of test	59
1. Rolling treatments	59
2. Indentation hardness tests	59
IV. Results and discussion	60
V. Summary	66
VI. References	66

I. INTRODUCTION

In cooperation with the Bureau of Engraving and Printing, the National Bureau of Standards is studying the effect of different surface finishes on the engraving and transferring properties of 0.34-percent-carbon steel plates. A previous paper [1][1] on the initial phase of this study described results of surface indentation hardness tests made with an elongated pyramidal-diamond (Knoop) indenter [2] on specimens having different metallographic structures and finished under different grinding conditions. Exploratory experiments with these specimens indicated that burnishing the surface by cold-rolling was accompanied by a decrease in hardness of the superficial layer. This appears to be in accord with recent work of Goss and Brenner [3], who presented hardness (monotron test) data showing a hardness reversal during continued cold-rolling of 0.74-percent-carbon (sorbitized) steel. However, similar experiments by these investigators with this steel in the pearlitic condition showed only progressive hardening. A behavior similar to that of sorbitic steel, reported by Goss and Brenner, has been found also in copper, by Atkin [4] and others [5, 6]. Thomp-

[1] Figures in brackets indicate the literature references at the end of this paper.

son [7], who observed no indication of hardness reversals during the progressive cold-rolling of either monocrystalline or polycrystalline copper, briefly summarized a number of suggestions offered by other concurring investigators to account for the apparent anomalous behavior of copper. However, these suggestions apparently did not take into consideration the differences in the properties of the metal immediately adjacent to the surface compared with the metal more remote from the surface as a possible factor influencing hardness tests involving shallow indentations. That such a layer, which possesses distinctive characteristics, exists has been borne out by considerable research since Beilby [8] first postulated the formation of an amorphous layer on metals subjected to polishing and other means of cold-working. Because of the distinctive characteristics of the metal near the surface that has been cold-worked, it is reasonable to assume that the results of the hardness tests will be influenced by the depth of penetration of the indenting tool.

The structure of the surface layer of 18–8 stainless steel has been shown by Wulff [9] to be affected to different degrees by different surface-finishing procedures. This is in accord with the results of Chalmers [10], who found by optical-reflectivity means, significantly different surface-hardness values for annealed copper polished with different abrasives. These results suggest that the initial surface finish of a metal may influence the magnitude of the hardness changes in its surface layer caused by light cold-rolling.

This paper summarizes the results of indentation hardness tests made with the Knoop indenter [2] penetrating to progressively increasing depths beneath the surface of specimens initially finished by different methods and then cold-rolled to different degrees. These results are supplemented by the results of hardness tests made on the same specimens with the Rockwell Superficial hardness tester.

II. MATERIAL

The steel investigated was representative of that used for rotary-press printing plates by the Bureau of Engraving and Printing, with respect to both composition and microstructure. The significant constituents, other than iron, determined by chemical analysis were as follows:

Constituent	Percentage
Carbon	0. 34
Manganese	. 48
Phosphorus	. 04
Sulfur	. 04
Silicon	. 20

These plates are hot-rolled and then annealed, and in this condition the metal at, and in, the immediate vicinity of the surfaces usually is nearly free of carbon. In preparing the plates for engraving and transferring, the decarburized layer is completely removed from the side used for transfer purposes by grinding. However, this precaution is not required in finishing the other side of the plates. The

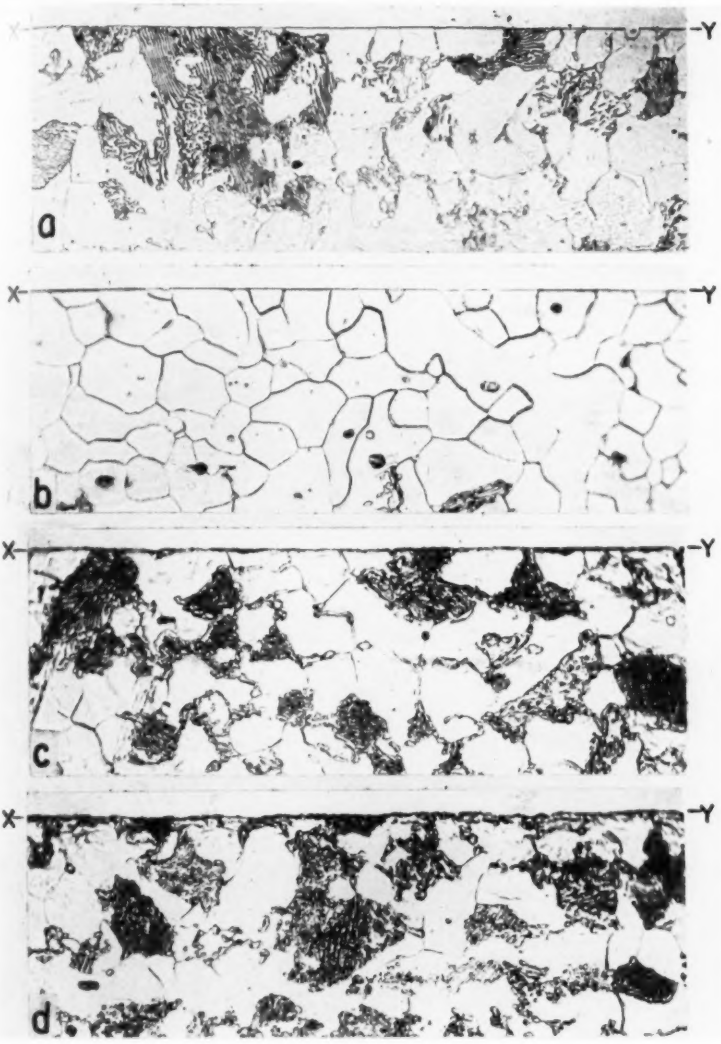

FIGURE 1.—*Characteristic structure of specimens of annealed 0.34-percent-carbon steel as initially surface-finished by different methods, observed in each case in a section perpendicular to the surface under consideration, the trace of which is indicated by line xy.*

a, Surface layer adjacent to transferring surface of plate finished by metallographic polishing. *b*, Decarburized to a depth of 0.01 to 0.02 inch. Surface finished by metallographic polishing. This is characteristic of the surface layer of the underside of transfer intaglio printing plates. *c*, Surface layer adjacent to transferring surface of plate, finished by buffing. *d*, Surface layer adjacent to transferring surface of plate, finished by grinding.

The surfaces (indicated by trace *xy*) of the polished specimens (*a* and *b*) were smooth as compared with those of the specimens buffed and ground, respectively (*c* and *d*). *a*, *c*, and *d* show the microstructural inhomogeneities of the metal adjacent to the test surface (trace *xy*) of the specimens. All the specimens were etched in 1-percent nital. Magnification, ×500.

typical microstructures of the metal near the surface on the two sides of a transfer plate are shown in figure 1 (*a* and *b*, respectively).

The parent test bars used in this study were cut from a single plate of steel to the dimensions 4½ by 1 by ¼ inch thick. Each of these test bars prior to cold-rolling was surface-finished by one of three different methods, as follows:

1. Wet-grinding with a soft alundum abrasive wheel, No. 46 grain, vitrified bond; maximum depth of roughing cuts 0.0005 inch, finishing cut 0.0001 inch.
2. Surface-grinding [2] with a soft wheel and then buffed on a segmented leather "knee" wheel charged with chromic oxide.
3. Wet-grinding as in 1 above, two stages on the tin-lead laps, first with No. 302 abrasive and then with No. 303½ abrasive, and final polishing on velvet charged with a paste of optical rouge in water.

The surface of the plate studied in most cases corresponded to the side of the plate which was free of the decarburized layer. However, metallographic examination frequently has revealed large areas of free ferrite at the transfer surfaces of plates, attributable to various causes. In order to study the effect of rolling on this type of structure, the decarburized side of a series of specimens was polished by method 3, as described above.

III. METHOD OF TEST

1. ROLLING TREATMENTS

All the cold-rolling was done on a two-high rolling mill, power-driven, equipped with hardened steel rolls having a diameter of 5 inches. The specimens were reduced approximately 0.0005 in. in thickness for each pass.

A specimen three-fourths of an inch long was cut from each test bar, as initially surface-finished, and used for hardness tests of the steel in the prerolled condition. The remainder of each bar (about 3¾ by 1 by ¼ inch thick) was cold-rolled to 1-percent reduction in thickness. A coupon approximately 1¼ inch in length was then cut from each bar and reserved for hardness tests. This procedure of rolling and sampling was repeated for nominal reductions of 2 and 4 percent.

2. INDENTATION HARDNESS TESTS

Hardness tests were made with both the Knoop indenter, used with the apparatus described in a previous publication [2], and the Rockwell Superficial hardness tester. The usefulness of the elongated pyramidal-diamond (Knoop) indenter for determining hardness gradients in the surface layer of steel was discussed in the above-mentioned publication [2]. Since preliminary tests suggested that the hardness gradient might be confined to a thin layer immediately below the surface, correspondingly shallow indentations were required to reveal significant changes in hardness in this layer. The smallest load which could be used on the indenter with accuracy, for the apparatus employed, was 50 grams.

Indentation tests with 50-, 100-, 200-, 500-, 1,000-, and 2,000-gram loads on the indenter were made on the finished surface of each speci-

[2] Representative of the finishing treatment applied by the manufacturer of transfer plate used for the present study.

men. The time of contact of the indenter with the specimen in making a test was 20 seconds. All indentations were made so that the long axis was nearly parallel to the direction of rolling and to the scratch marks on the specimens formed during the initial surface-finishing.

IV. RESULTS AND DISCUSSION

The results of the Knoop indentation tests, determined with different loads on the indenter for each of the specimens before and after rolling, are listed in table 1. These data, graphically presented in figures 2 to 5, show the average hardness changes with each load, which occurred during the progressive stage of rolling. In this manner, the effect of rolling on the hardness of layers differing in thickness can be shown. The curves (*A*, *B*, and *C*, figs. 2 to 5) show in most cases that the hardness numbers determined with the 50-, 100-, and 200-gram loads on the specimens after cold-rolling to 1- and 2-percent reductions were significantly less than they were prior to rolling. However, these same curves in general show a progressive increase

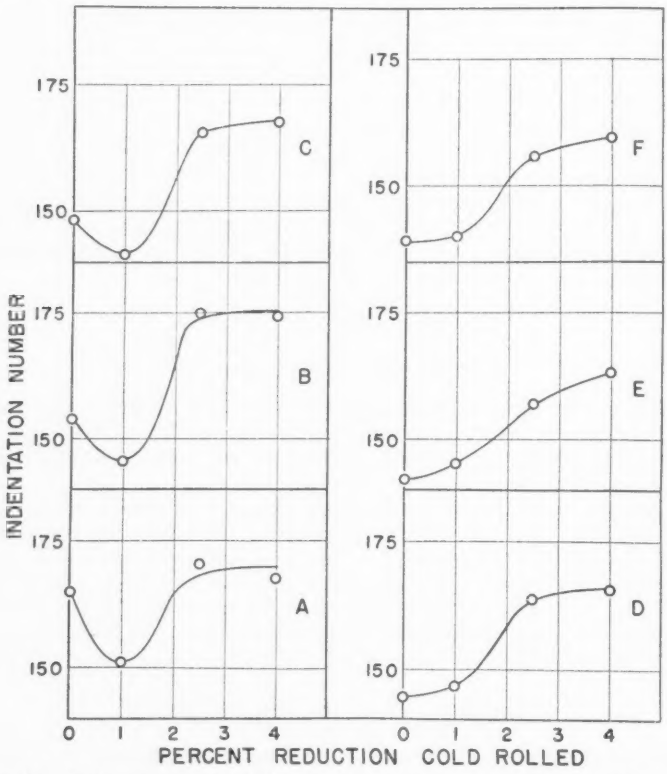

FIGURE 2.—*Influence of cold-rolling on the surface indentation hardness values (Knoop indenter) of annealed 0.34-percent-carbon steel, initially finished by metallographic polishing.*

The loads on the indenter (in grams) for the respective curves were as follows: *A*, 50; *B*, 100; *C*, 200; *D*, 500; *E*, 1,000; *F*, 2,000.

in hardness for reductions greater than 2 percent. This indicates that there was a decrease in hardness during the initial stages of cold-rolling, followed by an increase on further rolling for layers penetrated by the indenter with loads of 50, 100, and 200 grams.

The Knoop hardness numbers obtained with the relatively heavy loads (2,000, 1,000, and in some cases 500 grams, curves *D*, *E*, and *F*,

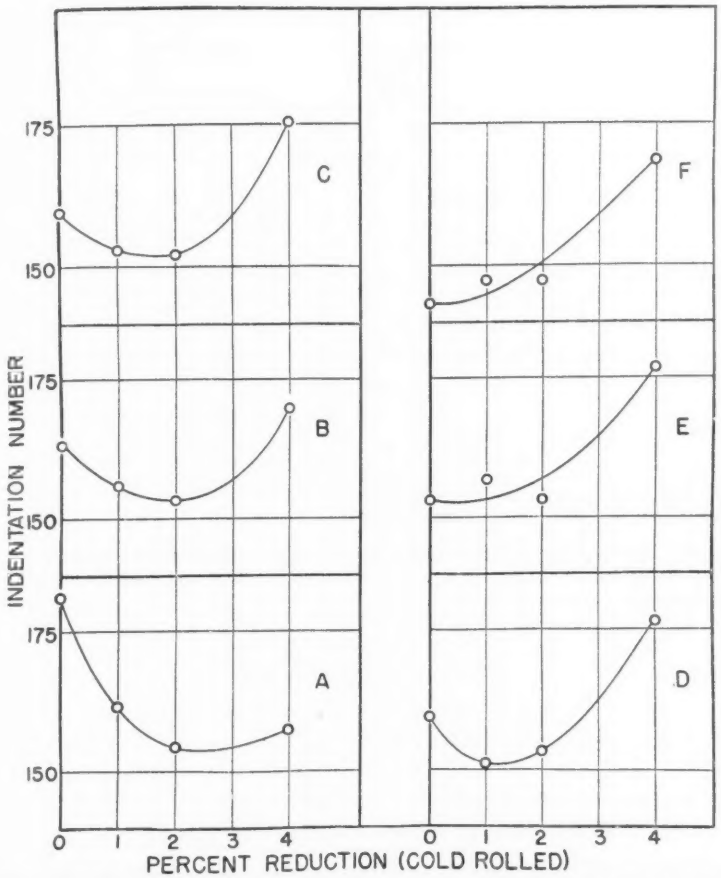

FIGURE 3.—*Influence of cold-rolling on the surface indentation hardness values (Knoop indenter) of annealed 0.34-percent-carbon steel, initially finished by metallographic polishing.*

The test specimens in this case had a decarburized surface layer 0.01 to 0.02 inch in depth. The loads on the indenter (in grams) for the respective curves were as follows: *A*, 50; *B*, 100; *C*, 200; *D*, 500; *E*, 1,000; *F*, 2,000.

figs. 2 to 5) show no indication of hardness decreases at any of the stages of cold-rolling. These results are in accord with those obtained on the same specimens with the Rockwell Superficial tester (15-kilogram load, 1/16-inch steel ball; fig. 6). These data indicate that the indentation numbers obtained under these conditions of test were

not appreciably influenced by the hardness of the outermost portion of the surface layer (penetrated with the 50-, 100-, and 200-gram loads).

TABLE 1.—*Average indentation hardness (Knoop and Rockwell Superficial) numbers of 0.34-percent-carbon steel specimens (1) as initially surface-finished and (2) after moderate cold-rolling to different degrees*

Initial surface finish	Reduction by cold-rolling	Indentation hardness number						
		Knoop indenter[a]						Rockwell Superficial 15T[b]
		Test Load, grams						
		50	100	200	500	1,000	2,000	
	%							
Metallographic polish (no decarburized layer at surface)	0	164	154	148	144	142	139	83
	1	151	145	142	147	145	140	85
	2.5	170	175	166	164	157	156	86
	4	168	174	168	166	163	159	87
Metallographic polish (decarburized surface layer)	0	181	163	159	160	153	143	85
	1	162	156	153	151	157	147	85
	2	154	153	152	153	153	147	85
	4	158	170	175	176	177	168	86
Buffed	0	203	183	176	153	152	149	83
	1	180	180	166	162	158	153	85
	2	182	180	176	170	165	160	85
	4	200	200	181	176	173	166	86
Ground	0	230	227	214	188	168	160	83
	1	226	221	209	184	175	163	85
	2	220	212	200	184	177	167	86
	4	228	220	205	191	183	171	87

[a] Each value is the average of 25 to 60 determinations.
[b] Each value is the average of 10 to 15 determinations.

TABLE 2.—*Relationship of indenting load to depth of penetration below the surface of annealed 0.34-percent-carbon steel plate in the moderately rolled and prerolled conditions*

Load	Approximate average depth of penetration of the indenter, upper and lower limits[a]
Grams	*In units of 10^{-3} inch*
50	7 to 9
100	10 to 13
200	15 to 18
500	25 to 29
1,000	36 to 41
2,000	53 to 58

[a] These values are the limiting computed depths of indentations obtained on specimens initially surface-finished by three different methods (grinding, buffing, and metallographic polishing) and on companion specimens reduced in thickness 1, 2, and 4 percent by cold-rolling.

The depth of the indentations which indicated "softening" of the surface metal during cold-rolling can be calculated, since the depth of the Knoop indentation is linearly related to the length of its long axis (ratio 1:30). The average values for the limiting depth of penetration for the specimens tested, before and after rolling, are listed with the corresponding test load in table 2. A correlation of these values with the Knoop hardness data (table 1) for each load condition suggests that the depth of the metal which significantly decreased in hardness (penetrated with 50, 100, 200, and in some cases 500 grams) during cold-rolling was less than 0.0003 inch.

Although the trends of the results (Knoop tests) were the same for the surfaces investigated, it is noteworthy that the hardness decreases appear more pronounced for the polished specimens than for those which were buffed and ground. An apparent cause for this difference is suggested by the difference of the microstructures of the surface layer of the specimens (fig. 1), which show evidence of cold work (darkened edge) for the buffed and ground specimens but not for the polished ones. The work of Wulff [9] suggests that the layer of dis-

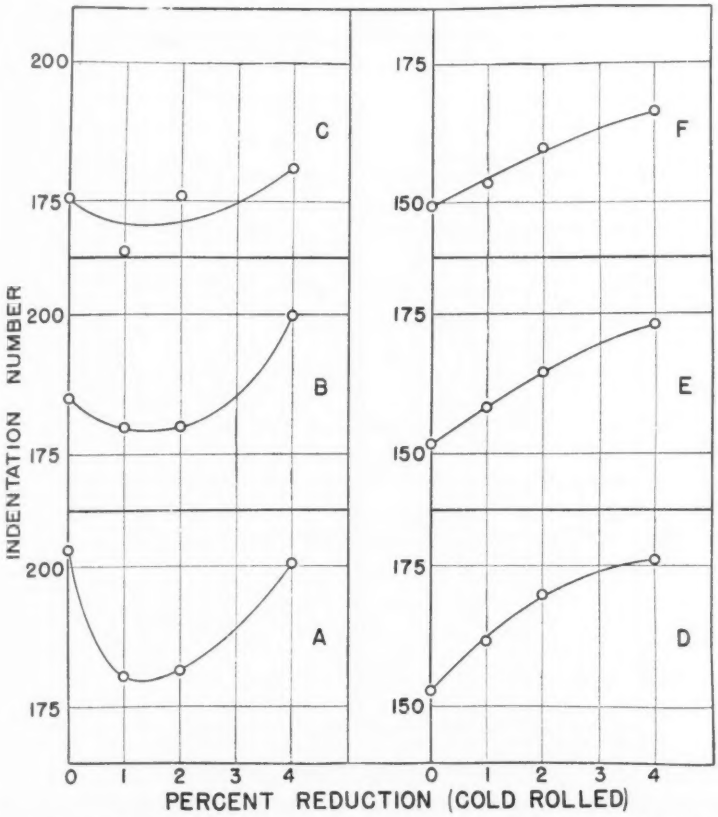

FIGURE 4.—*Influence of cold-rolling on the surface indentation hardness values (Knoop indenter) of annealed 0.34-percent-carbon steel, initially finished by buffing.*

The loads on the indenter (in grams) for the respective curves were as follows: *A*, 50; *B*, 100; *C*, 200; *D*, 500; *E*, 1,000; *F*, 2,000.

turbed metal due to metallographic polishing is very thin (less than 0.00003 inch). However, Thomassen and McCutcheon [11] have shown that the disturbance produced in metal during the preparation of specimens preliminary to polishing (see surfacing treatment No. 3) is not completely removed by a single polishing treatment such as used in the present study. This condition, although not detectable in the micrographs (fig. 1, *a* and *b*), probably is sufficient to obscure variations expected from very thin layers of disturbed metal developed

by polishing only. Therefore, the distinctive microstructural features of the surface layer of the specimens finished by different means, disclosed in figure 1, may not be conclusive as an explanation for the hardness differences noted. Another factor which may have had a bearing on these results is the geometric characteristics of the surface, which differed for the specimens finished by the different methods. (See profiles, fig. 1.) The significance of this factor with respect to

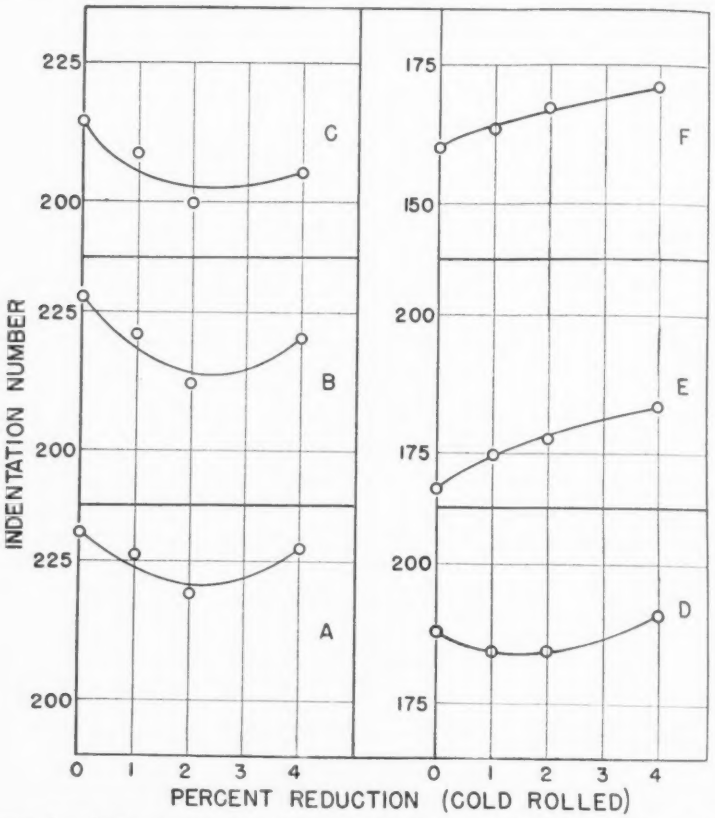

FIGURE 5.—*Influence of cold-rolling on the surface indentation hardness values (Knoop indenter) of annealed 0.34-percent-carbon steel, initially finished by grinding.*

The loads on the indenter (in grams) for the respective curves were as follows: *A*, 50; *B*, 100; *C*, 200; *D*, 500; *E*, 1,000; *F*, 2,000.

its influence on the depth of penetration of the Knoop indenter has been discussed in a previous publication [1].

The present investigation has not advanced sufficiently to warrant an explanation of the underlying cause of the reversals observed. However, the work of Wood [12] and McAdam and Mebs [13] may be significant in this connection. Wood demonstrated that continuous rolling of metals, particularly of copper, causes an increase in diameter of their X-ray diffraction rings to a maximum, following which there is a diminution to a minimum, the two processes alternating on further

cold-working. He concluded that the progressive expansion of the lattice accompanying cold work was indicative of cumulative internal stress and that the contraction was associated with the relief of such stress. McAdam and Mebs have shown in certain cases evidence of the relief of internal stress in severely cold-worked steel after the application of tensile stresses producing slight plastic extensions (0.001- to 0.003-percent permanent set). The results cited suggest

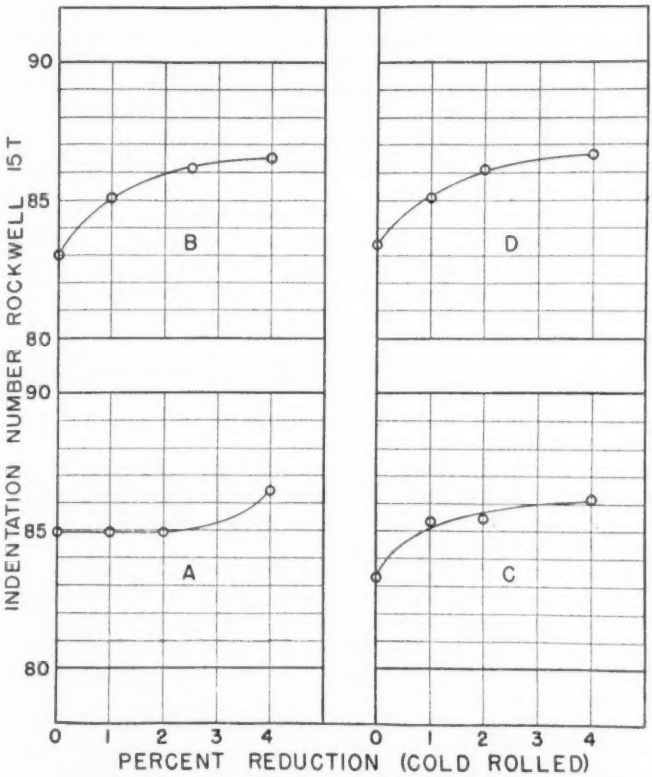

FIGURE 6.—*Influence of cold-rolling on the surface indentation hardness values of the test specimens described in the lengends of figures 2 to 5, as determined with the Rockwell Superficial hardness tester, 1/16-inch ball indenter, 15-kilogram load.*

The initial surface finishes for the respective curves were as follows: *A*, polished (surface layer decarburized); *B*, polished; *C*, buffed; *D*, ground.

the possibility of stress relief induced by the cold-rolling treatments as a significant factor in causing the hardness reversals observed. This presupposes that the surface layer was internally stressed during the polishing, buffing, or grinding treatment. It appears reasonable to assume that such was the case, since it is well known that the surface layer of a metal during mechanical finishing is severely stressed to accomplish the plastic flowing and removing of surface metal characteristic of these treatments.

The possible annealing effect on the surface layer by the heat generated during rolling should be considered in any theory advanced

to explain the fundamental cause of the results obtained. However, this does not propose that such factor is independent of the suggested stress-relief effects which may be a manifestation of annealing reactions. A wholly satisfactory explanation of the phenomenon observed will require further study.

V. SUMMARY

1. A study was made to determine the influence of cold-rolling on the hardness properties of the surface layer of annealed 0.34-percent-carbon steel plate, initially surface-finished by three different methods —grinding, buffing, and metallographic polishing. The test surface of the specimens used for most of the work was essentially free of surface decarburization. However, the metal adjacent to the corresponding surface of one series of specimens tested was decarburized to a depth of 0.01 to 0.02 inch.

2. Hardness tests were made on the specimens before and after rolling, with an elongated pyramidal-diamond (Knoop) indenter under loads of 50, 100, 200, 500, 1,000 and 2,000 grams, respectively. Hardness tests also were made on the same specimens with the Rockwell Superficial hardness tester, by using a 15-kilogram load on a $\frac{1}{16}$-inch steel-ball indenter.

3. The experimental data show that the Knoop hardness number of the surface layer of the steel, distinguished from the underlying metal, was lower after cold-rolling reductions of 1 and 2 percent than it was prior to rolling.

4. Within the limitations of the tests, the results suggested that the most significant hardness decreases which accompanied the lighter degrees of rolling (1- and 2-percent reductions) occurred in a layer less than 0.0003 inch in thickness.

5. The results obtained with the Rockwell Superficial tester in no case revealed a lower indentation hardness for the specimens after cold-rolling than was obtained prior to rolling. In this respect the results obtained with the Knoop indenter under loads of 1,000 grams (1 kilogram) and 2,000 grams (2 kilograms), respectively, were comparable.

6. The test data suggest that the indentation hardness of the surface layer of the steel in the prerolled and rolled conditions was influenced by the nature of the initial surface-finishing treatment.

VI. REFERENCES

[1] H. K. Herschman and F. Knoop, *Influence of grinding treatments on the surface hardness of intaglio printing plates of 0.33-percent carbon steel,* J. Research NBS **26,** 261 (1941) RP1374.

[2] F. Knoop, C. Peters, and W. Emerson, *A sensitive pyramidal diamond tool for indentation measurements,* J. Research NBS **23,** 39 (1939) RP1220.

[3] N. P. Goss and W. Brenner, The Effect of Microstructure upon the Work Hardening Characteristics of 0.74 Percent Carbon Strip Steel, Am. Soc. Metals Preprint No. 6, presented at Metal Congress, Philadelphia, Pa. (October 1941).

[4] W. E. Atkin, *The effect of progressive rolling upon some physical properties of commercially pure copper,* J. Inst. Met. **23,** 381 (1920).

5 H. S. Rawdon and W. H. Mutchler, *Effect of severe cold working on scratch and Brinell hardness,* Trans. Am. Inst. Mining Met. Engrs. **70,** 342 (1924).

[6] F. Körber and H. Hoff, *Ueber die festigkeitseigenschaften und den Reisswinkel kaltgewaltzen Metalle*, Mitt. K. W. Inst. Eisenforschung **10,** 175 (1928).
[7] J. G. Thompson, *Effect of cold rolling on the indentation hardness of copper*, J. Research NBS **13,** 745 (1934) RP742.
[8] G. Beilby, Aggregation of Flow of Solids (The Macmillan Co., 60 Fifth Avenue, New York, N. Y., 1921).
[9] J. Wulff, *The metallurgy of surface finish*, Proc. Special Summer Conference on Friction and Surface Finish, Mass. Inst. Technology, p. 13 (June 5, 6, and 7, 1940); also, *Surface finish and structure*, Trans. Am. Inst. Mining Met. Engrs. (Iron and Steel Div.) **145,** 295 (1941).
[10] B. Chalmers, *Surface hardness of metals*, J. Inst. Met. (London) **57,** 295 (1941).
[11] L. Thomassen and D. M. McCutcheon, *X-ray determination of depth of cold working by machining*, Mech. Eng. **56,** 155, 306 (1934).
[12] W. A. Wood, *The lower limiting crystal size of internal strain in some cold worked metals*, Proc. Roy. Soc. (London) [A] **172,** 231 (1939).
[13] D. J. McAdam, Jr. and R. W. Mebs, *Tensile elastic properties of nickel, copper, open-hearth iron, and typical steels*, J. Research NBS **28,** 311 (1942) RP1459.

Washington, April 7, 1942.

U. S. DEPARTMENT OF COMMERCE NATIONAL BUREAU OF STANDARDS

RESEARCH PAPER RP1485

Part of Journal of Research of the National Bureau of Standards, Volume 29, July 1942

NOTE ON FLEXURAL FATIGUE OF TEXTILES

By Herbert F. Schiefer and Paul M. Boyland

ABSTRACT

Results are given which indicate that the ability of a textile fabric to withstand repeated flexing depends upon the structure of the fabric, the position and structure of the yarn in the fabric, and the kind of fiber from which the fabric is made.

CONTENTS

	Page
I. Introduction	69
II. Testing procedure	69
III. Results	69

I. INTRODUCTION

Textile fabrics are complex structures composed of many fibers arranged in more or less definite patterns according to the distribution of the fibers in the yarns and of the yarns in the fabric. The ability of a fabric to withstand repeated flexing depends not only on the properties of the fibers but also on the structure of the yarn and of the fabric. This dependence was brought out in some experiments on the folding endurance of certain fabrics, the results of which are discussed briefly in this note.

II. TESTING PROCEDURE

Specimens of a fabric were ravelled to 15 mm. in width. Some of these specimens were tested for breaking strength and elongation. The remaining specimens were flexed in an M.I.T. folding tester [1] under a tension of 1.5 kg. The specimens were folded through 135°, alternately toward one face and then toward the other at the rate of 200 double folds per minute. The nominal radius of curvature of the edges of the jaws is 0.38 mm. The flexing tests were discontinued after a certain predetermined number of double folds, and the flexed specimens were then tested for breaking strength and elongation. The percentage decreases in breaking strength and in elongation of the flexed specimens, based upon the original breaking strength and elongation, were computed. Some of the flexed specimens were photographed before they were tested for strength to show the position of the failures of the fibers and of the yarns in relation to the fabric structure. For this purpose the specimen was folded through 180° and placed between two microscope glass slides with the edge of the folded specimen coinciding with the line of folding in the flexing test.

III. RESULTS

Repeatedly flexed specimens are shown in figures 1 and 2. It is clear from these photographs that the fibers which have failed occur

[1] L. W. Snyder and F. T. Carson, A study of the M.I.T. paper folding tester, Paper Trade J. 96, TS276 (June 1, 1933).

in alternate yarns. The positions of the failures of fibers in alternate yarns are attributable to the fabric structure and can be explained with the schematic drawings of a fabric in figure 3. The top view of the fabric is given at *a*. Sectional views through *BB* and *CC*, respectively, are represented by *b* and *c; b′* and *c′* represent these same sections when the fabric is folded upon itself, *B* to *B* and *C* to *C* with the upper surface inside; *b″* and *c″* represent the sections when the fabric is folded with the lower surface inside. It can be seen from these figures that the radius of curvature of the yarns designated *B* is very much larger than in *b′* than in *b″*. The opposite is true for the yarns designated *C*. The bending stress due to folding a given yarn will increase with the increase in the curvature of the fold. The maximum stress of the *B* yarns is obtained when the fabric is folded as in b″, and the maximum stress of the *C* yarns is obtained when the fabric is folded as in *c′*. If these foldings are repeated, as in flexural-fatigue tests, it is apparent that the *B* yarns will begin to fail (rupture) at *x*, and the *C* yarns will begin to fail at *y*. The *x* failures will occur in alternate yarns on one side of the fabric, and *y* failures will occur in the other set of alternate yarns on the other side. This is what is shown in figures 1 and 2, and the position of the failures of the fibers in the alternate yarns of the fabrics is entirely attributable to the differences in stress and strain which arise from the fabric structure. Specimen *A* of figure 1, which was inserted in the folding tester at a slight angle, is of special interest. It shows that the failures of the warp yarns change from one set of alternate yarns to the other set at the position marked *P*. This position corresponds to the place where the bending of the warp yarns over one filling yarn changes to bending over an adjacent filling yarn.

It is also clear in the photographs in figures 1 and 2 that some of the fibers have been broken by repeated folding. The percentage decrease in breaking strength and in elongation due to folding is given in table 1. It is seen to depend upon the number of double folds and upon the kind of fiber. The large percentage decrease for the fabrics made from acetate rayon, fortisan, and silk compared to no decrease for the fabrics made from viscose rayon, nylon, and cotton is outstanding. This difference cannot be attributed to a change in weave or fabric structure. It is more likely that structural differences of the yarns and of the fibers in a yarn account for this large difference.

The short cotton fibers in a yarn are freer to move relative to one another when the fabric is flexed. Hence the fibers would be strained less when the yarn is bent to a given radius of curvature. This would result in an increase in folding endurance of cotton fabrics.

As the freedom of movement of the fibers in a yarn relative to each other is restricted the yarn approaches the properties of a homogeneous beam and the extreme fiber strains for bending to a radius R increases from the value r_1/R, where r_1 is the radius of the fiber, to r_2/R, where r_2 is the radius of the yarn. The extreme fiber stresses would increase correspondingly. Similarly, restriction of the movement of the yarns in a fabric relative to each other would increase the extreme fiber stresses corresponding to a given curvature of the fold. The extreme fiber strain for bending a fabric would approach the value of r_3/R, where r_3 is one-half the thickness of the fabric.

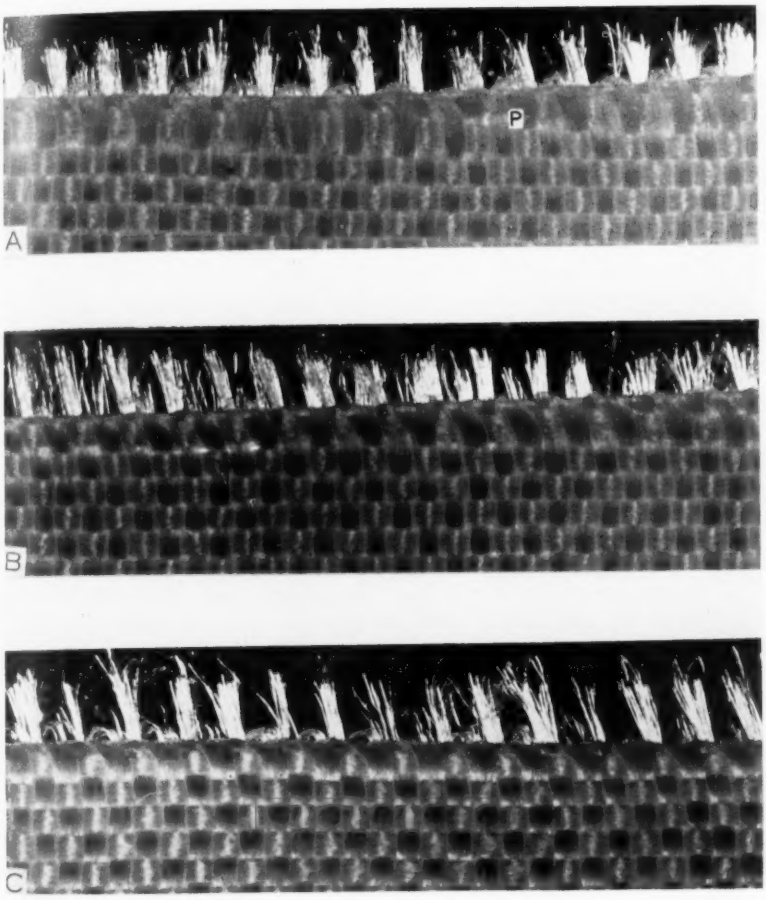

FIGURE 1.—*Test specimens showing that the failures of fibers caused by flexural fatigue occur in alternate yarns.*

A, Fortisan, warp, 10,000 double folds; B, Fortisan, warp, 8,000 double folds; C, Fortisan, filling, 5,000 double folds. Magnification ×14.

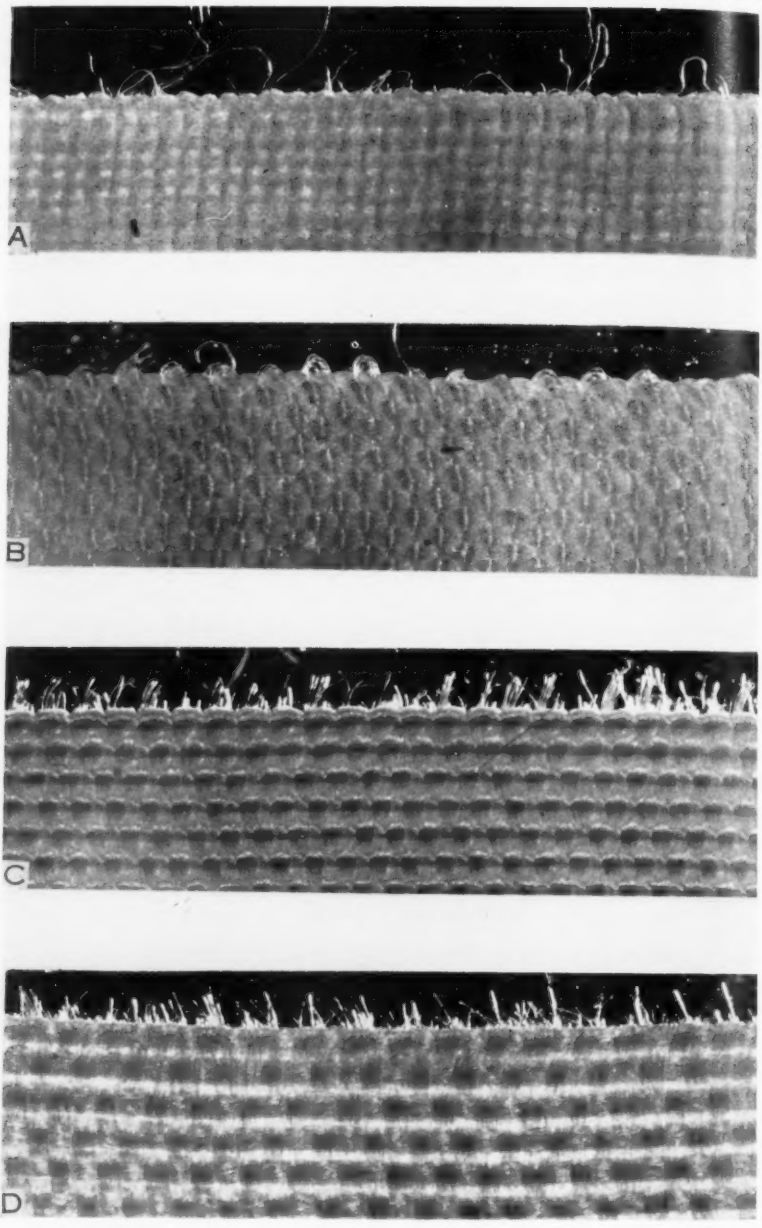

FIGURE 2.—*Test specimens showing that the failures of fibers caused by flexural fatigue occur in alternate yarns.*

A, cotton, filling, 10,000 double folds; B, viscose rayon, filling, 10,000 double folds; C, acetate rayon, warp, 1,500 double folds; D, silk, filling, 10,000 double folds. Magnification ×14.

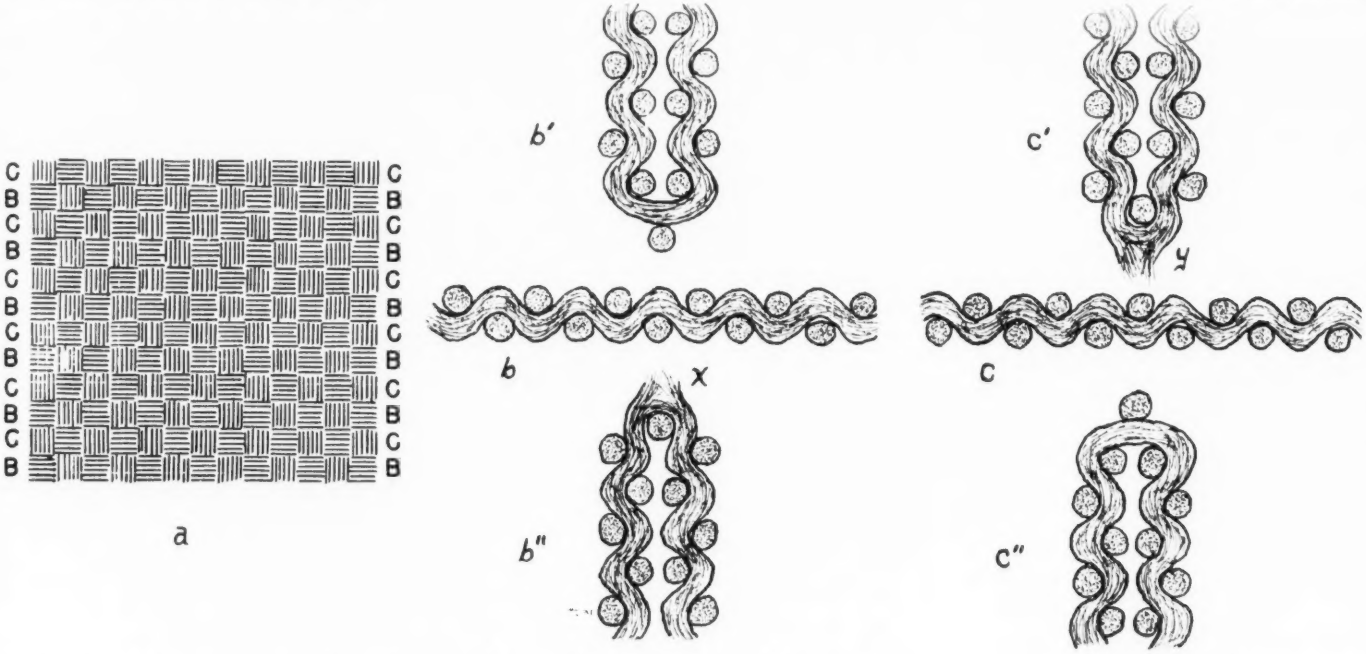
C B C B C B

TABLE 1.—*Decrease in the breaking strength and elongation of fabrics by repeated folding*

Material	Number of double folds	Decrease in—	
		Breaking strength	Elongation
		Percent	*Percent*
Rayon, acetate	1,000	13	31
	1,500	38	55
	1,700	56	59
	2,000	100	100
Fortisan:			
Warp	1,000	25	14
	5,000	58	43
	8,000	63	57
	10,000	68	57
Filling	1,000	0	0
	10,000	35	30
Silk:			
Warp	5,000	27	46
	10,000	46	54
Filling	5,000	27	36
	10,000	55	64
Rayon, viscose	10,000	0	0
Nylon:			
Warp	10,000	0	0
Filling	10,000	0	0
Cotton:			
Warp	10,000	0	0
	50,000	0	0
Filling	10,000	0	0
Fortisan:			
Warp	2,000	47	(a)
	10,000	70	(a)
Filling	2,000	25	(a)
	10,000	54	(a)
Fortisan, rubber-coated:			
Warp	2,000	45	(a)
	10,000	72	(a)
Filling	2,000	38	(a)
	10,000	71	(a)
Fortisan, neoprene-coated:			
Warp	2,000	85	(a)
	3,000	100	(a)
Filling	2,000	50	(a)
	5,000	62	(a)

[a] Elongation was not measured.

It follows that restriction of movement of fibers and of yarns in a fabric should decrease the folding endurance. This effect is shown by the data in table 1 for the rubber and neoprene coatings on a fortisan fabric. The particular neoprene coating greatly increased the stiffness of the fabric, and hence restricted the movement of the fibers and yarns during folding very much more than the rubber coating. The effect of the greater restriction of the movement of the fibers and yarns by the neoprene coating on the folding endurance is clearly indicated.

Similarly, differences in the freedom of movement of the structural units within fibers, which may result from chemical or mechanical treatment of the fibers, would affect the folding endurance of the fibers and also of the yarns and fabrics made from them.

Textile materials are frequently folded to a degree for which the computed value of r/R, the extreme fiber strain, exceeds 0.25. For this value of r/R, which corresponds to an elongation of 25 percent, the elastic limit of some textile fibers is exceeded and permanent deformation or creasing results.

WASHINGTON, May 8, 1942.

U. S. DEPARTMENT OF COMMERCE NATIONAL BUREAU OF STANDARDS

RESEARCH PAPER RP1486

Part of Journal of Research of the National Bureau of Standards, Volume 29, July 1942

ELASTICITY OF WOOL AS RELATED TO ITS CHEMICAL STRUCTURE

By Milton Harris, Louis R. Mizell, and Lyman Fourt [1]

ABSTRACT

Wool protein, like other fibrous proteins, is composed of long, flexible molecular chains. This flexibility appears to be the basis of the "long-range" elasticity of wool fibers. The wool fiber is distinguished from other textile fibers by the presence of covalent disulfide cross-links between these main chains. Rupture of these links by chemical means decreases the strength of the fiber without necessarily affecting the elastic recovery. Rebuilding the covalent linkages largely restores the original properties of the fiber.

Wool appears to be analogous to rubber in several respects. Thus the stress-strain, solubility, and swelling characteristics are greatly influenced by the extent of cross-linking in the two materials.

CONTENTS

	Page
I. Introduction	73
II. Molecular structure of wool	74
III. Experimental procedures	77
1. Preparation of chemically modified wools	77
2. Determination of elasticity	77
IV. Elastic behavior of wool and chemically modified wools	78
V. Analogy between wool and rubber	81
VI. Conclusion	84
VII. References	85

I. INTRODUCTION

The earlier efforts of those engaged in research on textile fibers, and more especially the regenerated or synthetic fibers, were principally devoted to increasing their strengths. It is a matter of history that the first regenerated fibers were so weak, especially in the wet state, that they were considered by many to be a passing fad. The progress that has been made in the interim is well known; the strengths of many of these fibers have been increased to the point where they exceed the demands of many of the purposes for which they are now used.

This progress has resulted from numerous investigations, and in this connection, the early observations by Scherrer [1] [2] and by Herzog and Jancke [2] on ramie, and later by Meyer and Mark [3], Astbury and his collaborators [4], and others, that the fibers show a predominant, preferred orientation, in which the molecules are alined more or less parallel to the axis of the fiber, were extremely helpful. The results of these investigations lead to the concept that fibrous materials, in spite of their lack of homogeneity and their high mole-

[1] Research Associates at the National Bureau of Standards, representing the Textile Foundation.
[2] Figures in brackets indicate the literature references at the end of this paper.

cular weights, are not necessarily amorphous but show a definite crystallizing tendency, in that portions of the fiber apparently consist of compact bundles of long-chain molecules in a parallel arrangement. On the basis of this concept, it has been possible to explain many facts concerning the structure and strength of high-polymers in general and of the fibers in particular. For example, for a given fiber it has been frequently shown that the strength is directly related to the degree of orientation; that is, the more highly oriented the crystallites of the fiber the higher the strength. While it is recognized that other factors, such as molecular chain length and the nature of the intermolecular forces, also have a profound influence on the strength of fibers, it can be shown that in a general way the strengths of entirely different classes of fibers are comparable on the same basis. The data in table 1 illustrate this point.

TABLE 1.—*Comparison of different classes of fibers*

Fiber	Relative degree of "crystallinity"	Breaking strength
		lb./in.[2]
Flax	Very high	Up to 156,000
Ramie	do	129,000 to 135,000
Nylon	High	72,500 to 100,000
Cotton	Medium	40,000 to 111,000
Rayons [1]	Low to high	22,000 to 110,000
Silk	Medium	46,000 to 74,000
Wool	Low	17,000 to 25,000

[1] Value depends on degree to which the rayon is oriented during manufacture.

Having achieved considerable success with respect to the production of fibers of high strength, many investigators have shifted their attention to the problem of trying to improve other mechanical properties of fibers. It appears that part of this trend has arisen from attempts to obtain fibers having "wool-like" qualities or properties. In view of this, it is pertinent to inquire into some of the properties which make wool different from other textile fibers. From the industrial point of view, the principal difference is found in the long-range elasticity of wool fibers; that is, their ability to recover from deformations of magnitudes considerably greater than those permitted by other types of fibers. The concept of orientation was effectively utilized in increasing the strength of the fiber, but, unfortunately, orientation is not directly correlated with long-range elasticity and, accordingly, the understanding of this unique mechanical property of wool must be sought in some other feature of its molecular structure. It is the purpose of this paper to examine certain aspects of the molecular structure from the point of view of their relations to long-range elasticity as well as to strength.

II. MOLECULAR STRUCTURE OF WOOL

Wool is composed principally of protein substance and, accordingly, it appears appropriate at this time to consider the factors which may influence the mechanical properties of fibrous proteins in general and wool in particular.

Proteins are poly-condensation products in which the different amino acids are linked together to form the polypeptide chain, shown in the following scheme:

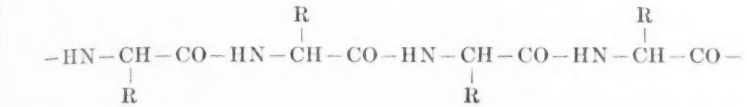

The mechanical properties of such chains can be considered, in general, to depend on the following four factors.

1. They exhibit great flexibility. This enables the protein molecule to assume a great number of possible configurations which could be either of the folded or spiral type. The importance of this molecular flexibility was first recognized by Astbury and Woods, who in their earlier work on wool [5] preferred a rather specific type of fold for the molecules of the fiber in the unstretched state, which they referred to as the α-keratin configuration. The long-range extensibility of wool was ascribed to the opening of these folds into the more nearly straight chain configuration known as the β-keratin form. The original α-keratin configuration has been shown to be untenable by Neurath [6], and a new type of fold has now been proposed by Astbury and Bell [7]. Such structures have been suggested on the basis of the X-ray data, and should accordingly be found principally in the "crystalline" regions of the fiber. Since, as also is indicated by the X-ray diffraction patterns, these regions account for only a relatively small proportion of the total wool fiber, it appears that one may assume a more or less random type of folding in the "amorphous" regions which make up the bulk of the fiber. That a variety of configurations can exist is readily demonstrable by the construction of molecular scale models of polypeptide chains [8]. In considering the mechanical properties of wool, it seems therefore that more attention should be directed to the less organized regions of the fiber than has heretofore been done. It would be expected, for example, that the extension process might manifest itself to a greater extent in the amorphous rather than in the crystalline regions, and that the increase in crystallinity obtained on stretching a fiber may result from orientation of the unoriented regions as well as from changes in the already oriented portions of the fiber.

2. They possess a large number of the highly polar peptide linkages which can give rise to inter- and intra-molecular hydrogen bonding. While these bonds contribute much toward increasing the strength of the fiber, such close spacings of these groups along the molecular chain would be detrimental to other desirable fiber properties, were it not for another factor discussed in the following section. Carothers and Hill [9] have demonstrated that a preponderance of polar groups in synthetic materials renders linear polymers nonflexible and brittle.

3. They contain relatively large side chains (R groups in the scheme of the polypeptide chain) which prevent close packing of the protein molecules and thus decrease the extent to which hydrogen bonding can occur. In wool, nearly all of the constituent amino acids are of the type having large side chains, as shown by the data in table 2. From these data it can be estimated that close to 50 percent

of the weight of wool is in the side chains. Close packing of molecular chains composed of such amino acids would indeed be difficult and intermolecular hydrogen bonding would be minimized. It would accordingly be expected that wool fibers would exhibit relatively low tensile strengths, an expectation which is borne out by experiment (table 1). It should be pointed out, however, that wool fibers would exhibit even lower tensile strengths were it not for the presence of covalent cross-links (discussed in the following section) between the molecular chains.

TABLE 2.—*Amino-acid composition of wool*

Amino acid	Present in wool	Reference	Grams of residue per 100 grams of wool	Grams of side-chain per 100 grams of wool
	Percent		*Grams*	*Grams*
Glycine	6.5	[30]	4.94	0.09
Alanine	4.4	[31, 32]	3.52	.74
Serine	9.41	[33]	7.80	2.76
Proline	6.75	[31]	5.69	2.46
Valine	4.72	[31]	3.99	1.73
Threonine	6.76	[33]	5.74	2.59
Cystine/2	[a] 12.72	[34]	10.83	4.89
Leucine isomers	11.3	[31]	9.75	4.92
Aspartic acid	7.27	[35]	6.28	3.22
Lysine	3.3	[38]	2.89	1.63
Glutamic acid	15.27	[35]	13.40	7.58
Methionine	0.71	[31]	0.62	0.36
Histidine	.7	[30]	.62	.37
Hydroxylysine	.21	[36]	.19	.11
Phenylalanine	3.75	[31]	3.34	2.07
Arginine	10.4	[37]	9.33	5.97
Tyrosine	5.8	[39]	5.23	3.43
Tryptophane	.7	[30]	.64	.45
Total	110.67		94.80	45.37
Ammonia N	1.18	[40]	−.30	−.30
Total, corrected for ammonia N			94.50	45.07

[a] Based on 3.55 percent total sulfur, subtracting methionine sulfur.

4. They exhibit association forces other than those contributed by hydrogen bonds. These may arise from various sources, but in the present discussion only those contributed by the amino acid cystine, which is found in unusually large amount in wool and other mammalian hair fibers, will be considered. Cystine, as first suggested by Astbury and Street [10], is responsible for a considerable amount of covalent cross-linking in the fiber. More recently, new chemical evidence [11] has been offered which supports the original conclusion of Astbury and Street. Wool may thus be considered a network of polypeptide chains linked together by the disulfide groups of the amino acid, cystine. Such a concept suggests that the role of cystine in wool must be an important one, and indeed it has been shown that many of the chemical, physical, and biological properties of wool protein [12] are dependent on the presence of these cross-links. The importance of these cross-links becomes even more apparent in the subsequent discussion in this paper concerning the experimental alteration or rupture of these links.

III. EXPERIMENTAL PROCEDURES

1. PREPARATION OF CHEMICALLY MODIFIED WOOLS

The wool fibers used in the present study were a portion of a lot used in previous investigations in this laboratory and had been subjected to no chemical or mechanical treatment other than successive extraction with alcohol and ether followed by washing with water at 40° C [13].

The preparation of chemically modified wools in which the mode of linkage of the sulfur has been altered, without visibly affecting the fiber structure, has previously been described in detail [11]. The methods involve the reduction of wool with thioglycolic acid solution, followed by treatment of the reduced product with an alkyl halide. The reactions appear to affect only the disulfide groups of the cystine in wool and may be represented by the following equations:

$$W-S-S-W+2HS-CH_2-COOH \longrightarrow 2W-SH+(S-CH_2-COOH)_2 \quad (1)$$

$$W-SH+RX \longrightarrow W-SR+HX \quad (2)$$

$$2W-SH+(CH_2)nX_2 \longrightarrow W-S-(CH_2)n-S-W+2HX, \quad (3)$$

where W represents the portions of the wool connected by the disulfide groups, R represents an alkyl group, and X, a halogen atom. Reactions 1 and 2 result in a permanent rupture of covalent cross linkages. Reactions 1 and 3 result in the formation of new cross-links in which the sulfur atoms of the cystine are connected by short hydrocarbon chains.

2. DETERMINATION OF ELASTICITY

Measurements of the elastic properties were made on individual fibers by a modification of the method described earlier [13]. In this method the 30-percent index is the energy required to stretch a fiber to 30-percent elongation after a treatment, divided by the similar energy requirement prior to the treatment. This index is based on Speakman's demonstration that wool fibers can be elongated 30 percent without permanent deformation or weakening [14], if the duration of the strain is short. In the former investigations from this laboratory, however, the stress-strain characteristics of fibers were determined only during the extension process. In the present work, this procedure was modified so that measurements of the behavior of the fiber during its retraction could also be obtained.

The interpretation of these experiments involves four considerations, of which the first is the fraction of the original covalent bonds which has been altered. This may be inferred from the change in the percentage of cystine, which was determined by Sullivan's method [15] as used in this laboratory [16]. The cystine content of the untreated wool was 12 percent, and in the modified wools varied downward to 1 percent or less. The second consideration is the resistance to extension, which can be conveniently referred to as strength. The third is the completeness of recovery in the unloading, or retraction, part of the stress-strain cycle. The fourth is the time function, which involves both the rate of change of stress and the effect of internal structure on viscosity. Experiments are now in progress to analyze these kinetic relations more directly.

IV. ELASTIC BEHAVIOR OF WOOL AND CHEMICALLY MODIFIED WOOLS

Figure 1 shows the behavior of a typical wool fiber during two successive stress-strain determinations. The fiber was allowed to relax for approximately 24 hours between the first and second extensions. It is noteworthy that the entire stress-strain cycle is reproducible. This fact makes it possible to compare the stress-strain characteristics of a particular fiber in retraction as well as in extension, before and after a modification of its chemical structure.

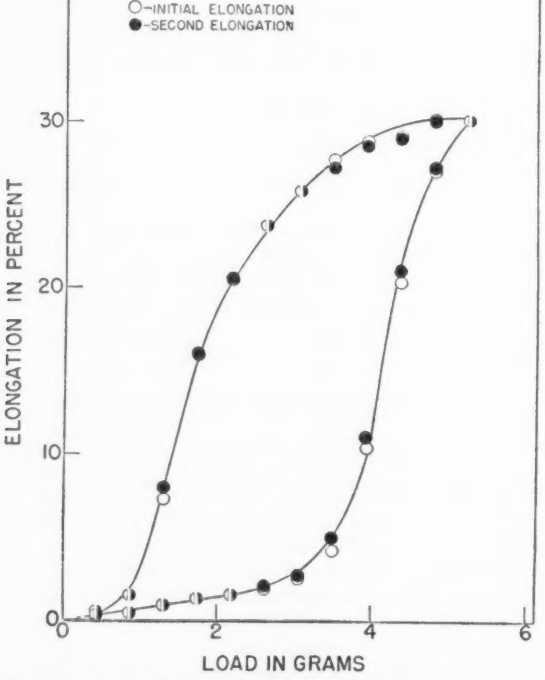

FIGURE 1.—*Typical untreated wool fiber during two stress-strain cycles, separated by 24 hours.*

30-percent index=0.99.

When the cross-linkages have been permanently ruptured by the reduction process, followed by alkylation of the sulfhydryl groups with an alkyl monohalide of low molecular weight, such as methyl iodide or ethyl bromide, the resistance to extension is greatly altered, as shown in figure 2. Much less energy is required to elongate the fiber after the cross-links have been split, the 30-percent index dropping to the low value of 0.26. In this material the S-shaped curve, characteristic of the original wool fiber and of other highly elastic materials, is not observed in extensions to only 30 percent, but can be demonstrated in experiments involving higher extensions. The whole scale of the relations of stress to strain has been shifted toward

greater extensions for smaller forces. It should be added that the recovery from 30-percent extension to the original length is complete and rapid.

If, after reduction, the cross-links are largely rebuilt by reoxidation of the sulfhydryl groups to the disulfide form, the wool recovers to a large extent its original properties, as shown in figure 3. The small discrepancy may arise either from the possibility that reoxidation has not been complete or that a few SH groups had reacted, during the reoxidation, with sulfhydryl groups other than those with which they were combined in the original fiber.

Alkylation of the reduced wool with an alkyl dihalide, such as methylene bromide or trimethylene bromide, results in the re-forma-

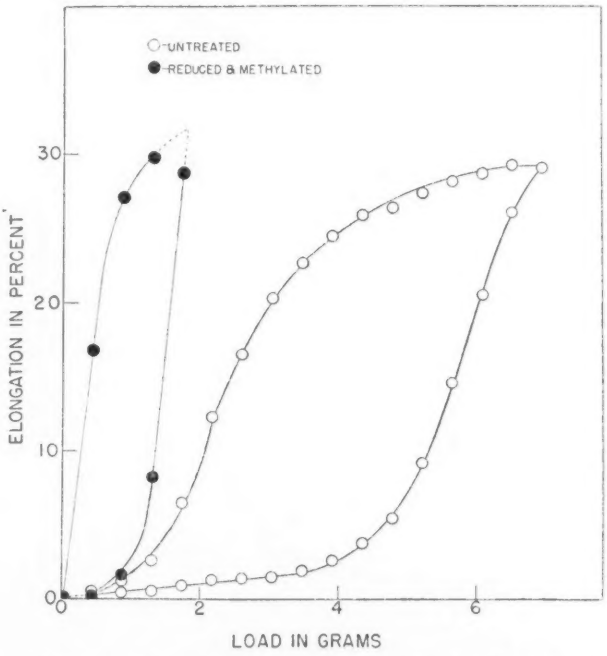

FIGURE 2.—*Effect on the stress-strain cycle of opening 5/6ths of the cross-linkages by reduction and alkylation with methyl iodide.*

30-percent index=0.26.

tion of cross-linkages, but in this case, the disulfide linkage has been replaced by a *bis*-thioether linkage of the type $-S(CH_2)_nS-$. While the position of the stress-strain curve for the fiber after such treatment has been slightly shifted (fig. 4) from that of the original fiber, the shape of the curve and the recovery are very similar to those of the original fiber. A slight shift in the position of the curve is to be expected, since, obviously, the lengths of the cross-linkages have been increased and one would expect a slightly greater ease of extension of the fiber.

Figure 5 shows the behavior of wool after reduction followed by alkylation with a large alkyl monohalide, benzyl chloride. Although

in this case the covalent cross-linkages have been ruptured, the behavior of the fiber is very different from that of one in which covalent linkages have been ruptured by reduction followed by alkylation with small alkyl monohalides such as methyl iodide or ethyl bromide. As will be noted, the benzylated wool shows a considerably greater resistance to extension than the methylated wool (compare fig. 2). After sufficient load has been applied, the extension curve rises steeply

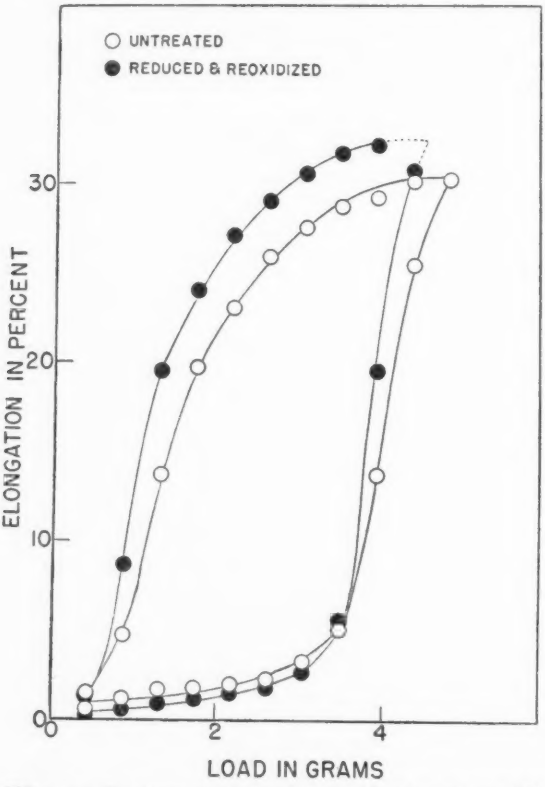

FIGURE 3.—*Effect on the stress-strain cycle of reduction of one-half of the cross-linkages, followed by rebuilding by oxidation with oxygen.*

30-percent index=0.96.

with respect to the load axis. The relations with respect to time cannot be presented completely in this type of experiment, but it can be stated that the rate of flow is less than that of methylated wool. On removal of the load there appears to be a great resistance to the contraction of the fiber to its original length. Whereas in the other experiments presented here the elastic recovery was rapid and nearly complete within 1 minute after the removal of the last unit of load, in this experiment with benzylated wool retraction required 3 hours to reach an equal degree of completeness. This is indicated by the dotted line in figure 5. The behavior is such as to suggest that while covalent cross-linkages have been broken, some interaction between

the polypeptide chains still exists. It may be that benzyl groups on adjacent sulfur atoms exhibit mutual interaction of a van der Waals type, or that there is an attraction between benzyl groups and a portion of a neighboring polypeptide chain. At the point of maximum extension the benzyl groups appear to form new interactions which resist the tendency of the fiber to return to its original length. An alternative explanation could be that the large volume of the benzyl group increases the energy of activation required for flow [17]. A

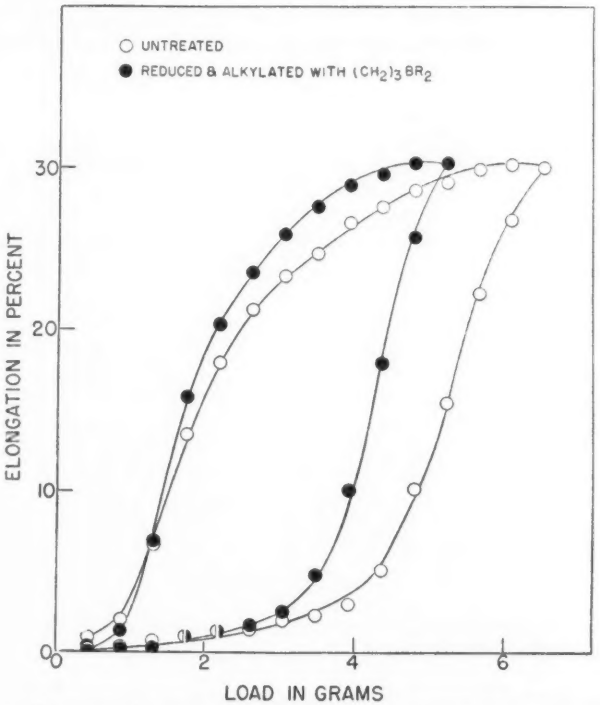

FIGURE 4.—*Effect on the stress-strain cycle of rebuilding of 5/6ths of the cross-linkages as bis-thioethers by reduction and alkylation with trimethylene bromide.*

30-percent index=0.82.

quantitative investigation of the effects of both the size of the substituent and the temperature upon the flow is necessary for a more detailed explanation of these phenomena.

V. ANALOGY BETWEEN WOOL AND RUBBER

The results of the present investigation suggest that in many ways wool is quite analogous to rubber, and indeed in some respects may serve as a useful model for explaining certain properties of the latter.

It appears that the long-range extensibilities of both rubber and wool depend on the fact that both have configurations which can be straightened out during the stretching process [18]. Both wool and

rubber are largely amorphous in the unstretched state although in this state the former appears to contain a somewhat higher proportion of a crystalline phase. As indicated by X-ray studies [19, 4], the amount of this phase is greatly increased during the process of stretching.

Probably the most interesting analogy, however, is found in comparing the properties of raw and vulcanized rubber with those of wool, before and after the rupture of its disulfide groups.[3] While it is

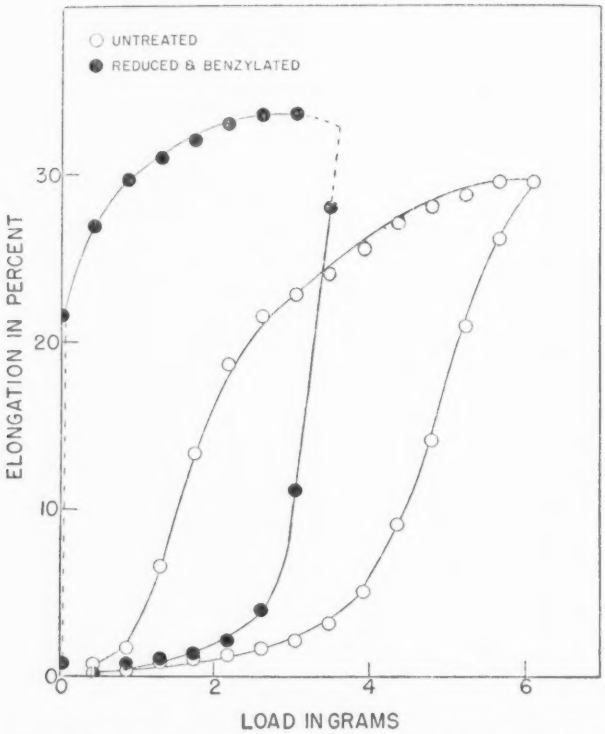

FIGURE 5.—*Effect on the stress-strain cycle of opening of 5/6ths of the cross-linkages by reduction and alkylation with benzyl chloride.*

30-percent index=0.65. The dotted line along the ordinate axis indicates a slow completion of the cycle by contraction at low stress.

generally assumed that vulcanization of rubber involves a cross-linking process [21, 18], it appears that proof of the chemical structure of the cross-links is lacking. On the other hand, it now seems well established that in wool the disulfide groups of the amino acid cystine do form cross-links between molecular chains. Thus the difference in behavior of wools before and after rupturing these cross-links serves as a useful model for rubber, and indeed, as is seen in the following discussion, lends considerable support to the hypothesis of cross-linking in vulcanized rubber.

A consideration of the chemistry of the wool fiber during the course of its production brings forth some additional points relative to this

[3] Astbury and Dickinson have suggested that keratin is a "vulcanized" protein [20].

discussion. A growing wool fiber consists of a root and a shaft, the former being the living region situated beneath the surface of the skin, whereas the latter is the nonliving portion extending above the surface. Examination of the root portion reveals that it is principally a gelatinous protein mass containing a relatively large amount of sulfhydryl groups [22]. In other words, it would appear that in the synthesis of wool, cysteine rather than cystine is synthesized into the polypeptide chains. The material in the root of the hair is in some ways comparable to rubber latex. When the hair cells die, oxidation presumably takes place, since the sulfhydryl groups are completely converted to disulfide groups. At this stage, the soft, plastic material of the root becomes the tough, elastic wool fiber. This, in a sense, can be considered to be analogous to the vulcanization process.

The solubility and swelling properties of both wool and rubber serve to emphasize the similarity in the physical structures of these two materials. Untreated wool fibers swell appreciably in a variety of aqueous solutions but are definitely insoluble in the usual protein solvents. Rupture of the disulfide cross-links yields a product which is readily soluble, for example in alkaline solutions, but the original insolubility is restored after re-formation of these links [11]. Similarly, it can be shown that whereas unvulcanized rubber is soluble in a variety of organic solvents, vulcanization renders the material insoluble in the same solvents. With unvulcanized rubber, it is possible to form a clear solution of the rubber in a solvent, but the vulcanized rubber appears only to swell and form a gel-like structure [23].

Since, in the absence of imposed strain, neither material exists in the fully extended form, there can be little close packing and accordingly there will be relatively few points of interaction as compared with highly oriented materials such as the cellulose, silk, or nylon fibers. As would be expected, the tensile strengths, or, more generally, the resistance to further extension, of such normally unoriented materials is always low. Within the range from zero strength to these low maxima, however, resistance to extension is sensitively related to the frequency and intensity of molecular interactions. This is readily demonstrated by the stress-strain behavior of unvulcanized rubber, or of wool in which practically all of the disulfide cross-linkages have been ruptured. However, when rubber is vulcanized or the cross-links are introduced into reduced wool, similar changes in the mechanical properties of both materials are observed, as shown in figures 2 and 6. It is seen that with cross-linking the materials become stronger, and their moduli of elasticity become higher. In addition, they show lower extensibilities at break. Modified wool fibers in which most of the cross-linkages have been ruptured may be extended more than 100 percent when stretched in water, whereas untreated wool fibers can be extended only about 50 to 60 percent before breaking. A representative sample of unvulcanized rubber had an elongation of 1,200 percent at break whereas after vulcanization the elongation at break of a similar sample was only 700 percent [25].

There is, however, one principal difference between the two types of molecules. Rubber is practically entirely hydrocarbon and accordingly exhibits only low-order molecular cohesion or interactions whereas wool contains a large proportion of highly polar groups ca-

pable of forming relatively strong molecular interactions. For this reason, the sensitivity of rubber to temperature is not shared by dry wool. On the other hand, the mechanical properties of the latter are greatly affected by moisture, which swells the protein and presumably decreases intermolecular cohesion. Thus it is found that the influence of heat on the mechanical behavior of rubber is very similar to the influence of moisture on the behavior of wool.

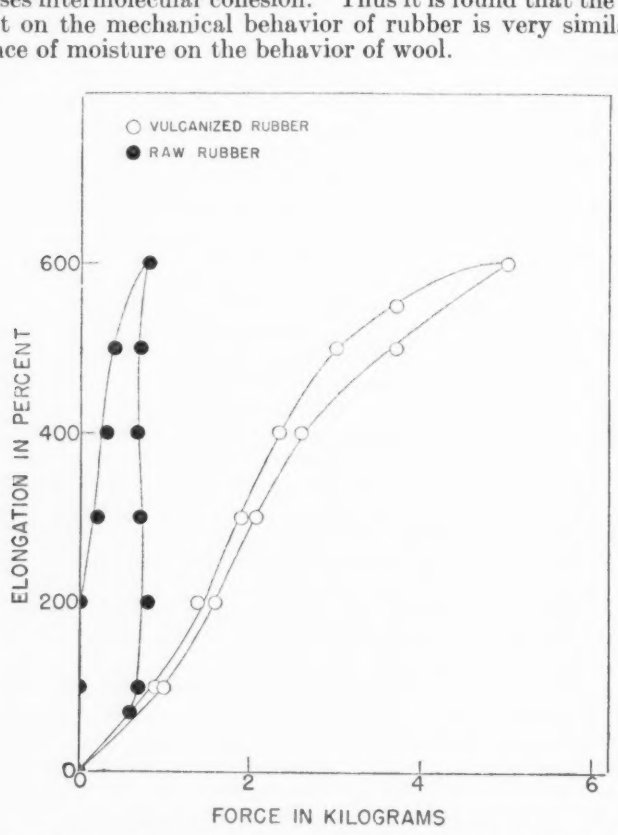

FIGURE 6.—*Stress-strain cycles of a sample of rubber before and after vulcanization*

Data from Hock and Bostroem [24].

VI. CONCLUSION

These experiments and comparisons lead to a better understanding of the molecular basis of the elastic properties of wool. The long-range elastic characteristics are not dependent on the presence of crosslinks, but probably result from the ability of flexible chain molecules to contract from the less probable stretched state to a more random form. Meyer [26] and Mark [27] have reviewed the evidence for this view of the origin of long-range elasticity. The function of cross-links is to strengthen the materials and suppress plastic flow. The introduction of a higher proportion of cross-links would decrease the flexibility and reduce the range of elasticity, as illustrated by the properties of highly vulcanized rubber (ebonite). This analysis of the mechanical properties of these systems leads to the conclusion that a

textile fiber having desirable long-range elastic characteristics must consist of flexible chains reinforced with a proper balance of cross-links.[4]

The influence of covalent chemical cross-linking on the properties of wool, rubber, and other high-polymer systems is now receiving considerable attention. As far as the authors are aware, wool is not only the first substance in which covalent cross-linking has been established, but also is the only one in which the cross-links can be quantitatively ruptured and rebuilt at will. It may thus serve as an excellent model for many other high-polymeric systems.

VII. REFERENCES

[1] P. Scherrer, Göttinger Nachr. **1918,** 98.
[2] R. O. Herzog and W. Jancke, Z. Kaiser Wilhelm Ges. (1921); Z. physik. Chem. [A] **139,** 235 (1920).
[3] K. H. Meyer, and H. Mark, Ber. deut. Chem. Ges. **61,** 1932 (1928).
[4] W. T. Astbury and H. J. Woods, Nature **126,** 913 (1930).
[5] W. T. Astbury and H. J. Woods, Phil. Trans. Roy. Soc. (London) [A] **232,** 333 (1933).
[6] H. Neurath, J. Phys. Chem. **44,** 296 (1940).
[7] W. T. Astbury and F. O. Bell, Nature **147,** 696 (1941).
[8] H. S. Taylor, Proc. Am. Philos. Soc. **85,** 1 (1941).
[9] W. H. Carothers and J. W. Hill, J. Am. Chem. Soc. **54,** 1579 (1932).
[10] W. T. Astbury and A. Street, Phil. Trans. Roy. Soc. (London) [A] **230,** 333 (1931).
[11] W. I. Patterson, W. B. Geiger, L. R. Mizell, and M. Harris, J. Research NBS **27,** 89 (1941) RP1405; Am. Dyestuff Rptr. **30,** No. 17, 425–430; Textile Research **11,** 379 (1941).
[12] W. B. Geiger, W. I. Patterson, L. R. Mizell, and M. Harris, J. Research NBS **27,** 459 (1941) RP1433; Am. Dyestuff Rptr. **30,** No. 24, 659 (1941). M. Harris, Textile Research **12,** 19 (1941).
[13] A. M. Sookne and M. Harris, J. Research NBS **19,** 535 (1937) RP1043; Am. Dyestuff Rptr. **26,** No. 22, 659–669 (1937).
[14] J. B. Speakman, Proc. Roy. Soc. (London) [B] **103,** 377 (1928).
[15] M. X. Sullivan, Public Health Reports 86 (1930).
[16] M. Harris and A. L. Smith, J. Research NBS **18,** 623 (1937) RP998; Am. Dyestuff Rptr. **26,** No. 15, 413–415 (1937).
[17] W. Kauzman and H. Eyring, J. Am. Chem. Soc. **62,** 3113 (1940).
[18] R. Houwink, Elasticity, Plasticity, and Structure of Matter, Cambridge University Press (1937).
[19] J. R. Katz, Naturwissenschaften **13,** 411 (1925).
[20] W. T. Astbury and S. Dickinson, Nature **135,** 95 (1935).
[21] I. Williams, Theories and Phenomena of Vulcanization, in C. C. Davis and J. T. Blake's The Chemistry and Technology of Rubber, p. 237 (Reinhold Publishing Corp., New York, N. Y. 1937).
[22] C. W. Hock, R. C. Ramsay, and M. Harris, J. Research NBS **27,** 181 (1941) RP1412; Am. Dyestuff Rptr. **30,** No. 18, 449–456 (1941); Textile Research **11,** 415–428 (1941).
[23] W. F. Busse, p. 181 in C. C. Davis and J. T. Blake's The Chemistry and Technology of Rubber (Reinhold Publishing Corp. New York, N. Y., 1937).
[24] L. Hock and S. Bostroem, Kautschuk **2,** 132 (1926).

[4] In this connection, it is interesting to note that the absence of any appreciable amount of covalent cross-linkings undoubtedly accounts to a large extent for the low tensile strengths, especially in the wet state, of regenerated protein fibers made from casein, soybean protein, etc. Silk fibers, on the other hand, which apparently do not contain any covalent cross-linking exhibit very high tensile strengths. Examination of their chemical constitutions reveals that nearly two-thirds of the amino acid content is accounted for by glycine and alanine, compounds which have only hydrogen and methyl groups as side chains [28]. From the available analytical figures it is found that only 36 percent of the weight of silk is in the side chains, in contrast to 48 percent for wool and 54 percent for casein. It follows that while in wool the chain weight is to the side chain weight as 1 to 1, in silk this ratio is nearly 2 to 1. Polypeptide chains of silk may thus be considered to be significantly more bare than those of wool, making possible a considerable amount of close packing and interchain hydrogen bonding, which would account for the high observed strengths. Comparison of the X-ray diagrams of silk and of wool [29] shows a much higher "degree of crystallization" in the silk.

[25] P. Rosbaud and E. Schmid, Z. tech. Physik **9,** 98 (1928); G. S. Whitby and M. Katz, Ind. Eng. Chem. **25,** 1204, 1338 (1933) cited from: L. A. Wood, NBS Circular C427 (1940).
[26] K. H. Meyer, Chem. Rev. **25,** 137 (1939).
[27] H. Mark, Chem. Rev. **25,** 121 (1939).
[28] M. Bergmann, and C. Neimann, J. Biol. Chem. **115,** 77 (1936); J. Biol. Chem. **118,** 301 (1937).
[29] W. T. Astbury, Fundamentals of Fiber Structure (Oxford Press, London, 1933).
[30] R. J. Block, J. Biol. Chem. **128,** 181 (1939).
[31] A. J. P. Martin and R. L. M. Synge, Biochem. J. **35,** 91 (1941).
[32] E. Abderhalden and A. Voitinovici, Z. physiol. Chem. **52,** 348 (1907).
[33] A. J. P. Martin and R. L. M. Synge, Biochem. J. **35,** 294 (1941).
[34] J. McCallum, unpublished data in this laboratory.
[35] J. B. Speakman and F. Townend, Nature **139,** 411 (1937).
[36] D. D. van Slyke, A. Hiller, and D. A. MacFayden, J. Biol. Chem. **141,** 681 (1941).
[37] H. B. Vickery, J. Biol. Chem. **132,** 325 (1940).
[38] H. A. Rutherford, M. Harris, and A. L. Smith, J. Research NBS **19,** 467 (1937) RP1038.
[39] H. A. Rutherford and M. Harris, cited from J. Steinhardt and M. Harris, J. Research NBS **24,** 335 (1940) RP1286.
[40] J. Steinhardt, unpublished data in this laboratory.

WASHINGTON, February 2, 1942.

U. S. DEPARTMENT OF COMMERCE NATIONAL BUREAU OF STANDARDS

RESEARCH PAPER RP1487

Part of Journal of Research of the National Bureau of Standards, Volume 29, July 1942

SPECIFIC HEAT OF THE SYNTHETIC RUBBER HYCAR O.R. FROM 15° TO 340° K

By Norman Bekkedahl and Russell B. Scott

ABSTRACT

Measurements of specific heat were made on a sample of Hycar O.R. synthetic rubber from 15° to 340° K by means of an adiabatic vacuum-type calorimeter. The experimental values of the specific heat between 15° and 22° K were well represented by the Debye specific-heat equation, using a $\beta\nu$ value of 80, and accordingly the values below 15° K were calculated with this equation. At about 250° K the material has a transition of the second order, the specific heat increasing by about 40 percent to a value of 1.84 Int. joules·gram^{-1}·degree^{-1} just above the transition. From 250° to 340° K the specific heat-temperature curve is nearly linear, and the values can be calculated to within 0.2 percent from the formula $C_p = 0.00283T + 1.126$, in Int. joules·gram^{-1}·degree^{-1}. At 298.16° K (25°C) the specific heat is 1.971 Int. joules·gram^{-1}·degree^{-1} (0.4712 calories·gram^{-1}degree^{-1}). The increase in entropy resulting from heating from 0° to 298.16° K was calculated to be 1.743 $\pm$0.002 Int. joules·gram^{-1}·degree^{-1} (0.4167 $\pm$0.0005 calories·gram^{-1}·degree^{-1}).

CONTENTS

		Page
I.	Introduction	87
II.	Sample	88
III.	Specific heat	89
IV.	Thermal history	92
V.	Entropy	93
VI.	Summary and discussion	93
VII.	References	95

I. INTRODUCTION

The determination of the specific heat of Hycar O.R. (oil-resistant) synthetic rubber is a continuation of a program started some years ago at the National Bureau of Standards, the object of which is to furnish thermodynamic data on various types of rubber, both natural and synthetic, and the monomers from which they are polymerized. Such data have been obtained for unvulcanized natural rubber [4] [1] and its monomer, isoprene [5], and the equilibrium relationship between the two has been studied [2]. In the present paper, specific heat measurements on synthetic rubber Hycar O.R. are described, and the increase in entropy from absolute zero to 25° C is calculated.

It has been found very useful in previous work to correlate thermal measurements with volume measurements. Anomalies in the enthalpy-

[1] Figures in brackets indicate the literature references at the end of this paper.

temperature relation or its derivative are found to be associated with similar changes in the volume-temperature relation or its derivative. Measurements of the volume-temperature relation by means of a dilatometer, therefore, furnish a relatively simple method of determining the location of transitions and a guide for thermal measurements.

Volumetric work on several samples of synthetic rubber has shown that they, as well as natural rubber, may undergo transitions [16]. Two types of transition are found. In first-order transitions, the fundamental properties, such as enthalpy, undergo large changes in a rather narrow temperature interval. Crystallization and fusion are first-order transitions. In second-order transitions, the derivatives of the fundamental properties, rather than the properties themselves, undergo the large changes. The changes therefore manifest themselves in the expansivity and in the specific heat, which are the derivatives of the fundamental quantities, volume and enthalpy.

Natural rubber has been shown, both by thermal measurements [4] and dilatometric measurements [3, 17] to exhibit both a first-order and a second-order transition. Many of the synthetic rubbers, however, unlike natural rubber, show no evidence of crystallization or fusion. Since the crystallization of a rubber-like substance may make the thermal investigation very complicated and time-consuming [6], it was thought advisable to make thermal measurements first on a synthetic rubber which does not crystallize. Volume measurements [16] with a mercury-filled dilatometer have failed to show any evidence of crystallization or fusion in Hycar O.R., and it was selected for the first thermal studies. The volume measurements showed a second-order transition at 250° K.

II. SAMPLE

Hycar O.R., for samples of which we are indebted to the Hycar Chemical Co. of Akron, Ohio, is an oil-resistant synthetic rubber which has been on the market since early in 1941. Its chemical composition has not yet been disclosed by the manufacturer, but it is reported to be a butadiene co-polymer, and to contain about 2 percent of phenyl-beta-naphthylamine as a stabilizer [1]. Some of the physical properties of the compounded Hycar are given by Garvey, Juve, and Sauser [8].

The density of a sample of unvulcanized Hycar O.R. was found to be 0.999 gram per cubic centimeter at 25° C. An analysis of the material showed that it contained the following:

	%
Carbon	80. 1
Hydrogen	9. 3
Nitrogen	10. 2
Ash	0. 1
Total	99. 7

Since practically the whole weight of the material, within experimental error, was accounted for in this manner, analytical determinations for other elements were not made. The carbon and the hydrogen were

determined by the usual combustion technique and the nitrogen by the Kjeldahl method.

Both the high nitrogen content and the oil-resistant properties of the polymer would lead to the conclusion that the co-monomer used with the butadiene might be acrylonitrile. Since information is lacking as to the possible presence of other ingredients, and in view of the known ease of hydrolysis of nitriles, conclusions drawn from these figures as to the exact ratio of butadiene to acrylonitrile may be misleading.

The sample used for the specific-heat measurements was cut into small pieces averaging about 5 to 10 cubic millimeters in volume. These small pieces were placed in the sample container of the calorimeter and kept under vacuum for several days to remove moisture and air. The container was then filled with helium at atmospheric pressure and 25° C and sealed with solder. The weight of the dried sample was 30.030 grams.

III. SPECIFIC HEAT

The calorimeter used for the measurements of specific heat was of the adiabatic vacuum-type described by Southard and Brickwedde [15]. It was similar to the apparatus previously used to determine the specific heat of rubber [4] and of isoprene [5], with some alterations intended to increase the convenience and facility of the measurements.

The results of all the measurements of specific heat are given, in chronological order, in table 1. The temperatures given in the table are the mean between the beginning and end temperatures for each heating. The values of C_p were obtained from the equation given by Osborne, Stimson, Sligh, and Cragoe [11]:

$$[C_p]_{T_m}=\frac{\Delta Q}{\Delta T}-\left[\frac{\partial^2 C_p}{\partial T^2}\right]_{T_m}\frac{(\Delta T)^2}{24},$$

where ΔQ is the heat added per gram of sample, ΔT is the temperature rise, and T_m is the mean temperature of the heating. However, the second term of the right-hand member of this equation was not significant except at temperatures between 238° and 251° K, in which region the second derivative of the specific heat with respect to temperature was large. At its maximum the last term in the equation amounted to about 2 percent of the total. The temperature rise during a heating period was usually from 5 to 10 degrees, although this interval was considerably increased in a few instances where the specific heat-temperature curve was nearly linear, so that a larger temperature interval could be used without causing appreciable error. The rates of heating were varied from about 0.5° to 1.0° per minute. No consistent differences were observed between the data obtained from long heating intervals and those from short intervals, nor between the data obtained from rapid heating and those from slow heating.

TABLE 1.—*Specific heat values (observed)*

Run No.	T_m	C_p	Run No.	T_m	C_p
	°K	j/g·°C[a]		°K	j/g·°C[a]
I	89.80	0.5545	VI	213.79	1.1221
	96.00	.5965		223.42	1.1688
	101.99	.6250		230.76	1.2068
	107.84	.6527		235.84	1.2388
	113.58	.6782		240.88	1.2708
	119.21	.7070		245.80	1.3317
	129.13	.7505		250.19	1.6996
				254.47	1.8482
II	92.95	.5817		258.52	1.8583
	104.84	.6382			
	116.16	.6929	VII	15.18	0.0728
	127.06	.7437		19.51	.1046
	137.65	.7914		23.72	.1383
	148.01	.8353		28.65	.1777
	158.19	.8806		33.35	.2193
	168.21	.9257		39.78	.2661
	178.08	.9683		47.68	.3215
	187.82	1.0113		55.08	.3695
	197.45	1.0527		61.98	.4094
	206.98	1.0969		65.62	.4321
	216.39	1.1400		68.88	.4543
				76.51	.4942
III	201.45	1.0670		84.26	.5364
	210.92	1.1117		91.57	.5746
	220.27	1.1553		98.59	.6065
	229.49	1.2024			
	238.58	1.2565	VIII	18.55	.0982
	247.26	1.4161		25.36	.1522
	255.08	1.8471		32.03	.2074
	262.37	1.8698		38.57	.2588
	269.67	1.8903		42.66	.2865
				45.76	.3075
IV	260.65	1.8621		55.11	.3690
	268.65	1.8841		65.05	.4305
	276.64	1.9126		74.43	.4810
	283.35	1.9304		84.46	.5368
	290.06	1.9478		95.13	.5907
	296.78	1.9675			
	303.51	1.9861	IX	283.92	1.9262
				303.28	1.9740
V	207.24	1.0932		312.46	2.0042
	228.42	1.1967		322.53	2.0406
	237.71	1.2495		333.52	2.0669
			X	310.85	2.0009

[a] Int. joules·gram^{-1}·degree^{-1}.

The specific-heat data given in table 1 are plotted in figure 1. The broken line at the lowest temperatures is calculated from the Debye equation [10, 14] for specific heats, with a value of 80 for the parameter $\beta\mu$. This value was selected because it was found to give the best agreement with the three lowest experimental points.

The data from table 1 were also used to prepare a large graph in which C_p/T values were plotted as a function of the temperature. Since in the temperature range 18° to 340° K the values of C_p/T lie between 0.0052 and 0.0073 Int. joule·gram^{-1}·degree^{-2}, it was not difficult to plot the values on a scale sufficiently large to do justice to the accuracy of the data. From the best smooth curve drawn through the plotted values of C_p/T, values of C_p were obtained at integral temperatures and are presented in table 2.

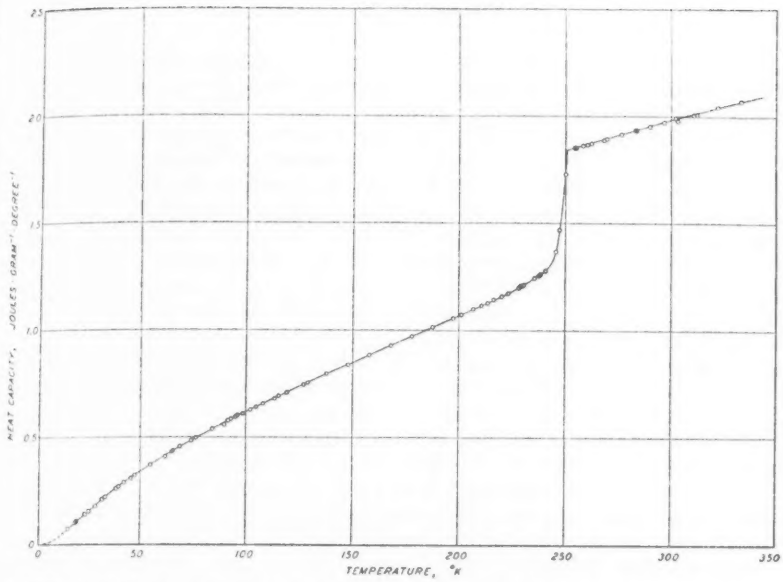

FIGURE 1.—*Relation between the heat capacity of Hycar O.R. and temperature.*
The dotted part of the curve is calculated from the Debye equation.

TABLE 2.—*Specific heat values (from graph)*

T	C_p	T	C_p	T	C_p
°K	j/g·°C[a]	°K	j/g·°C[a]	°K	j/g·°C[a]
0	[b] 0.000	125	0.733	246	1.358
5	[b] .004	130	.756	247	1.402
10	[b] .030	135	.778	248	1.466
15	.071	140	.800	249	1.562
20	.108	145	.823	250	1.678
25	.149	150	.845	251	1.838
30	.191	155	.867	255	1.849
35	.232	160	.890	260	1.863
40	.268	165	.912	265	1.878
45	.303	170	.934	270	1.892
50	.336	175	.955	275	1.905
55	.369	180	.977	280	1.919
60	.400	185	.998	285	1.933
65	.429	190	1.020	290	1.946
70	.458	195	1.041	295	1.960
75	.486	200	1.063	298.16	1.969
80	.514	205	1.085	300	1.973
85	.540	210	1.107	305	1.986
90	.566	215	1.130	310	2.000
95	.591	220	1.154	315	2.013
100	.615	225	1.179	320	2.028
105	.639	230	1.205	325	2.042
110	.663	235	1.233	330	2.055
115	.687	240	1.265	335	2.071
120	.710	245	1.329	340	2.087

[a] Int. joules·gram^{-1}·degree^{-1}.
[b] Calculated from the Debye equation.

IV. THERMAL HISTORY

The temperature changes of the sample during the specific-heat measurements will be given in some detail, since it is possible that the results of this investigation may depend somewhat on the thermal history of the material. The first run was made after the sample had cooled quickly from room temperature to that of liquid air, about 85° K. Seven individual heatings in this run brought the temperature to 136° K. The sample was then cooled quickly again to 85° K and the second run was made, ending at 221° K. Next the sample was cooled by carbon dioxide snow to about 195° K. In the third run the temperature was raised to 273° K. At about 251° K (mean temperature of heating 247.26° K), the end of the sixth heating of this run, the temperature drifted downward at an initial rate of about a thousandth of a degree per minute under the usual adiabatic conditions. The drift continued for about 2 hours before it became inappreciable. At temperatures more than about 10 degrees above or below the second-order transition, the temperature became constant within a period of about 8 minutes after the completion of a heating.

Overnight the temperature was allowed to rise to 287° K. From this temperature the specimen was cooled to 257° K, and during the fourth run the temperature was raised to 307° K. The specimen was cooled quickly again to 196° K for the fifth run. At about 246° K, the temperature at the end of the fourth heating of the run, a downward drift of temperature again took place. Before the temperature became constant, more heat was added until the temperature was 250° K.

The temperature was then allowed to decrease slowly by discontinuing the heating of the thermal shields around the sample container. The temperature fall was at the average rate of about 2.4° per hour. At 209° K the sixth run was started. Downward drifts of temperature were again observed at the ends of the fifth, sixth, and seventh heatings of this run, although only the normal time was required for equilibrium in all the other heatings. The approximate times required for a constant temperature to be reached after each of the three heatings just mentioned were 0.5 hour at 243° K, 1.5 hours at 248° K, and 1 hour at 252° K. From 260° K where the run ended, the temperature was reduced slowly, reaching about 241° K in 16 hours. When subjected to adiabatic conditions after this treatment, the sample was found to drift upward slowly in temperature. The initial upward drift was about the same as the previous downward drifts, about a thousandth of a degree per minute. After about 2 hours no further change in temperature could be observed. The specimen was next heated to 254° K, and a downward drift of temperature was again observed.

The specimen was then allowed to come to room temperature and remained at that temperature for several days. The temperature was next quickly lowered to 12.5° K, and the seventh run brought it up to 102° K. An immediate cooling brought the temperature to 21° K in preparation for the eighth run. After this run the specimen was warmed to 217.5° K and a 50-minute heating, to be discussed in more detail later, raised the temperature to 270.2° K. After the sample had remained at room temperature overnight, the ninth run

was made from 299° to 339° K. The tenth run included only one heating, which was from 299° to 323° K.

The 50-minute heating of the specimen from 217.5° to 270.2° K, mentioned in the previous paragraph, required 2.4 percent less heat than that indicated by the curve of figure 1. The third and sixth runs, upon which the section of the curve near the transition is based, differed from each other by only 0.21 percent over the range mentioned. If this 2.4-percent discrepancy is real and not due to experimental error, it is probably connected with the time effect near the transition. The long drift in temperature before equilibrium near the transition should cause no error, since adiabatic conditions were maintained.

V. ENTROPY

The entropy increase of Hycar O.R. from 0° to 20° K was calculated from the Debye equation, using a $\beta\nu$ of 80. The value so obtained was

$$S_{20}-S_0=0.056 \text{ Int. joule}\cdot\text{gram}^{-1}\cdot\text{degree}^{-1}.$$

The entropy change from 20° to 298.16° K was obtained from graphical integration of the curve C_p/T against T, and gave

$$S_{298.16}-S_{20}=1.687 \text{ Int. joules}\cdot\text{gram}^{-1}\cdot\text{degree}^{-1}.$$

This value was also checked within experimental error by the integration of the C_p versus log T curve. The increase in entropy resulting from heating from the absolute zero of temperature to 25° C is calculated to be

$$S_{298.16}-S_0=1.743\pm0.002 \text{ Int. joules}\cdot\text{gram}^{-1}\cdot\text{degree}^{-1}.$$

(or 0.4167 ± 0.0005 calorie$\cdot$gram$^{-1}\cdot$degree^{-1}).[2] This value, with its probable error of 0.002, refers to the particular sample used under the conditions described.

VI. SUMMARY AND DISCUSSION

The specific-heat curve of figure 1 shows a transition of the second order at about 250° K. During this transition the specific heat increases abruptly by about 40 percent without the evolution or absorption of any heat. The transition first makes itself evident at about 225° K, where the specific-heat curve begins to deviate from the almost-linear increase which it has shown for over 100° below this temperature. Above 225° K the specific heat increases at an accelerated rate through the region of the transition. About half the change of specific heat seems to occur between 249° and 251° K. The curve is drawn with a discontinuous slope at 251° K, since the results from several heatings which were begun just above 251° K showed no evidence of the transition, the points determined from them falling exactly on the linear curve.

A similar second-order transition is found in natural rubber at about 200° K, as has already been mentioned. Second-order transitions at widely different temperatures are found in many other substances of high molecular weight, such as styrene polymers [12], isobutene polymers [7], and methyl rubber [13]. Of the materials which have been studied, all which have rubber-like properties have been found to have a second-order transition, and it is only above this transition temperature that such rubber-like properties have been observed. It

[2] 1 calorie=4.1833 Int. joules.

seems likely that at temperatures below that of the transition no substance exhibits the extensibility and elasticity associated with natural rubber at normal temperatures.

The occurrence of a second-order transition of this type has been explained as resulting from a very slow approach to the equilibrium state at temperatures below the transition. On this view the location of the transition depends on the rate of temperature change; and at temperatures more than a few degrees below the transition, the times required for equilibrium are beyond the range of accessibility. Consequently at these temperatures one deals with a substance in an unstable state. Jenckel [9] studied the second-order transition in selenium at 30° C by volume measurements. He extended the measurements over the long periods of time which were necessary to reach equilibrium. Thus he was able to measure the rate of approach to equilibrium over a range of about 7° below the temperature at which the second-order transition occurs when the cooling is at the rate of more than a few tenths of a degree per minute. The drifts in temperature under adiabatic conditions, as described under the section on thermal history, may quite likely be explained on the basis of the slow approach to equilibrium. However, this point will not be discussed further, since it was not considered advisable at this time to make a detailed calorimetric study of the phenomenon.

Crystallization, a transition of the first order, is well known in natural rubber. In Hycar O.R., however, no evidence of it was found at any temperature. The failure of the atoms in this case to become part of an ordered crystalline structure is probably connected with the attachment of the nitrile groups to the main chain of the carbon atoms. Perhaps it is because of the size of the nitrile group, or perhaps it is because of the randomness of its position of attachment.

The specific-heat curve from 250° to 340° K is almost linear, so that the values of the specific heat for any temperature in this range may be calculated to within 0.2 percent by means of the formula

$$C_p = 0.00283\ T + 1.126,$$

in which C_p is in Int. joules·gram^{-1}·degree^{-1} and T is the absolute temperature. The value at 298.16° K (25° C) is 1.971 Int. joules·gram^{-1}·degree^{-1} (0.4712 calorie·gram^{-1}·degree^{-1}). This value is only slightly higher than that for natural rubber hydrocarbon, which is given as 1.880 Int. joules·gram^{-1}·degree^{-1} [4].

The increase in entropy resulting from heating from the absolute zero of temperature to 298.16° K was found to be 1.743 Int. joules·gram^{-1}·degree^{-1} for the Hycar, as compared with 1.881 for the natural rubber hydrocarbon.

Since the Hycar O.R. was not in a crystalline state, it cannot be assumed without further evidence that the entropy at the absolute zero of temperature has a value of zero. However, since no significant difference in entropy could be found in the previously mentioned comparison of the amorphous and crystalline states of the natural rubber, it is possible that the same may be the case for the synthetic material.

VII. REFERENCES

[1] Anonymous, *Properties, processing, and compounding of Hycar O.R. synthetic rubber*, Rubber Age (N. Y.) **48,** 315 (1941).
[2] N. Bekkedahl, *Application of thermodynamics to the chemistry of rubber*, Proc. Rubber Tech. Conference, London, 1938, p. 223. Reprinted in Rubber Chem. T[illegible] **12,** 150 (1939).
[3] N. Bekkeda[illegible], *Forms of rubber as indicated by temperature-volume relationship*, J. Research NBS **13,** 411 (1934) RP717. Reprinted in Rubber Chem. Tech. **8,** 5 (1935).
[4] N. Bekkedahl and H. Matheson, *Heat capacity, entropy, and free energy of rubber hydrocarbon*, J. Research NBS **15,** 503 (1934) RP844. Reprinted in Rubber Chem. Tech. **9,** 264 (1936).
[5] N. Bekkedahl and L. A. Wood, *Entropy of isoprene from heat capacity measurements*, J. Research NBS **19,** 551 (1937) RP1044.
[6] N. Bekkedahl and L. A. Wood, *Influence of the temperature of crystallization on the melting of crystalline rubber*, J. Chem. Phys. **9,** 193 (1941). Reprinted in Rubber Chem. Tech. **14,** 544 (1941).
[7] J. D. Ferry and G. S. Parks, *Studies in glass. XIII. Glass formation by a hydrocarbon polymer*, J. Chem. Phys. **4,** 70 (1936).
[8] B. S. Garvey, Jr., A. E. Juve, and D. E. Sauser, *Hycar O. R. Properties of typical compounds*, Ind. Eng. Chem., Ind. Ed. **33,** 602 (1941). Reprinted in Rubber Chem. Tech. **14,** 728 (1941).
[9] E. Jenckel, *The cooling process in glasses and artificial resins*, Z. Electrochem. **43,** 796 (1937).
[10] W. Nernst, The New Heat Theorem, p. 247 (Methuen & Co., Ltd., London, 1926).
[11] N. S. Osborne, H. F. Stimson, T. S. Sligh, and C. S. Cragoe, *Specific heat of superheated ammonia vapor*, BS Sci. Pap. **20,** 65 (1925) S501.
[12] W. Patnode and W. J. Scheiber, *Density, thermal expansion, vapor pressure, and refractive index of styrene; density and thermal expansion of polystyrene*, J. Am. Chem. Soc. **61,** 3449 (1939).
[13] M. Ruhemann and F. Simon, *Knowledge of the physical properties of rubber*, Z. physik. Chem. [A] **138,** 1 (1928).
[14] F. Simon, *The determination of free energy*, Handbuch der Physik **10,** p. 367.
[15] J. C. Southard and F. G. Brickwedde, *Low temperature specific heats. I. An improved calorimeter for use from 14 to 300 °K. The heat capacity and entropy of naphthaline*, J. Am. Chem. Soc. **55,** 4378 (1933).
[16] L. A. Wood and N. Bekkedahl, (work not yet published).
[17] L. A. Wood, N. Bekkedahl, and C. G. Peters, *Application of the interferometer to the measurements of dimensional changes in rubber*, J. Research BNS **23,** 571 (1939) AP1253. Reprinted in Rubber Chem. Tech. **13,** 290 (1940).

WASHINGTON, May 22, 1942.

463607—42——7

U. S. DEPARTMENT OF COMMERCE NATIONAL BUREAU OF STANDARDS

RESEARCH PAPER RP1488

Part of Journal of Research of the National Bureau of Standards, Volume 29, July 1942

EQUATION OF MOTION FOR THE STEADY MEAN FLOW OF WATER IN OPEN CHANNELS

By Garbis H. Keulegan

ABSTRACT

There is disagreement in the literature regarding the use of the Coriolis and the Boussinesq velocity-distribution coefficients in the open-channel flow equation. It is shown in this paper that the use of either coefficient is correct, provided the terms representing the effects of resistance are properly interpreted. The methods of deriving the two forms of the flow equation are given in detail, and it is shown that in the form of equation containing the Boussinesq coefficient, the friction coefficient is related directly to the wall friction. In the form of equation containing the Coriolis coefficient, the friction coefficient is related to the rate of energy loss in the water. This has a direct bearing on the correct use of Manning's "n" in the equation of flow in open channels.

CONTENTS

		Page
I.	Introduction	97
II.	Purpose of paper	98
III.	Reynolds equations of turbulent motion	98
IV.	Energy principle in turbulent flow	99
V.	Momentum equations for a stream tube	104
VI.	Pressure law in gradually varied flow	105
VII.	The two equations of open-channel flow	106
VIII.	The coefficients of loss and friction in the varied flow equations	109
IX.	Selecting the more useful form of the equation of motion for an open channel	110
X.	References	110

I. INTRODUCTION

The equation of motion of steady mean flow in open channels is the equation which describes, for the permanent regime of flow, the relation between the depth of water, the variation of this depth with distance along the bed of the channel, the mean velocity in a section, the variation of this velocity with distance, the slope of the bed, and the coefficient of resistance. The physical significance of the coefficient of resistance is determined by the manner in which the equation is derived. Essentially there are two methods of derivation, one of which involves the application of the energy equation, the other of a momentum equation, both of which result from the general hydrodynamic equations of motion. In addition to the quantities mentioned, the equation of motion contains a coefficient resulting from the velocity distribution in a section. The meaning of the latter, like that of the coefficient of resistance, depends on the way in which the equation is derived.

The results obtained by the two methods differ slightly. It seems that the significance of this difference and its bearing on the meaning of the coefficient of resistance are not generally recognized. Conse-

quently, for investigations in the field of open-channel flow, the reasons for selecting one relation in preference to the other do not appear to be clearly understood today. Preference for one or the other relation depends, obviously, on the concept of the coefficient of friction which is adopted. It will be shown later in this paper that if the equation of motion is derived by the energy method, the concept underlying the friction coefficient in that equation is that of energy dissipation in the fluid per unit length of channel. On the other hand, if the momentum method is used, the concept of the friction coefficient is based on the frictional force exerted on the fluid by the walls of the channel.

II. PURPOSE OF PAPER

The purpose of this paper is to show the difference between the equation of steady mean flow in an open channel when derived by the energy method and the corresponding equation derived by the momentum method, and to explain the significance of this difference. Finally, it will be shown that the equation based on momentum considerations is the convenient one to use in discussing steady mean flow in open channels. Since the historical aspects of the problem have recently been discussed adequately by Bakhmeteff [1][1], they will not be given here.

III. REYNOLDS EQUATIONS OF TURBULENT MOTION

Before proceeding with the method of energy or momentum, it is necessary to adopt a system of dynamical equations of motion applicable to a liquid medium at the point (x, y, z). The selection of these dynamical equations depends on whether the stresses due to relative motions are essentially viscous, or essentially apparent (turbulent), or in part viscous and in part apparent. Since the matter to be studied relates to turbulent flow in open channels, we may assume that in these channels the turbulent core occupies the whole cross section when the solid surfaces are covered with asperities; and the very small area of the laminar sublayer may be disregarded when the solid surfaces are smooth. We assume that the apparent stresses predominate everywhere in this core and that, therefore, no sensible error is introduced when the viscous stresses are neglected. The restrictions involved in these assumptions are not important for the general argument that will be followed in this paper. Neglecting the viscous stresses and denoting the temporal mean velocities in the directions of x, y, and z by u, v, and w, respectively, the dynamical equations of motion to be adopted are of the form, assuming the liquid to be incompressible [2],

$$\left.\begin{aligned}
\rho\frac{du}{dt} &= -\frac{\partial p}{\partial x} - \rho\frac{\partial \Omega}{\partial x} + \frac{\partial R_{xx}}{\partial x} + \frac{\partial R_{yx}}{\partial y} + \frac{\partial R_{zx}}{\partial z},\\
\rho\frac{dv}{dt} &= -\frac{\partial p}{\partial y} - \rho\frac{\partial \Omega}{\partial y} + \frac{\partial R_{xy}}{\partial x} + \frac{\partial R_{yy}}{\partial y} + \frac{\partial R_{zy}}{\partial z},\\
\rho\frac{dw}{dt} &= -\frac{\partial p}{\partial z} - \rho\frac{\partial \Omega}{\partial z} + \frac{\partial R_{xz}}{\partial x} + \frac{\partial R_{yz}}{\partial y} + \frac{\partial R_{zz}}{\partial z},
\end{aligned}\right\} \quad (1)$$

[1] Figures in brackets indicate literature references at the end of this paper. Additional unnumbered references are given but not cited in the text.

where Ω denotes the potential energy per unit mass at the point (x, y, z), due to gravitational force; ρ the density of the liquid; p the temporal average of the pressure, and R the apparent, or Reynolds, stresses. In terms of the velocity fluctuations, u', v', w', these latter stresses are given by

$$\left.\begin{aligned} R_{xx} &= -\rho\overline{u'u'}, & R_{xy} &= R_{yx} = -\rho\overline{u'v'}, \\ R_{yy} &= -\rho\overline{v'v'}, & R_{zz} &= R_{xz} = -\rho\overline{u'w'} \\ R_{zz} &= -\rho\overline{w'w'}, & R_{yz} &= R_{zy} = -\rho\overline{v'w'}. \end{aligned}\right\} \tag{2}$$

Since the flow is permanent, the operator d/dt is

$$\frac{d}{dt} = u\frac{\partial}{\partial x} + v\frac{\partial}{\partial y} + w\frac{\partial}{\partial z}. \tag{3}$$

The effect of introducing the Reynolds stresses in the above equations is to give the mean temporal velocities, u, v, w, the character of velocities in stream-line flow. But the question then arises as to what we mean by a stream line or a fluid filament in turbulent flow. We shall define a fluid filament as a line for which the average directions of the instantaneous velocities at all points of the line are tangential to the line, or rather as a tubular surface composed of such lines and having a normal section of infinitely small dimensions. Stream lines are fixed in space, but, owing to turbulence, a particle of fluid initially on a stream line does not always remain on this line. However, if a surface made up of fluid filaments is selected, then the temporal average of the flow across this surface vanishes. For such a surface, if u_0, v_0, and w_0 are the velocity components of the mean motion at a point on the surface, and l, m, and n are the direction cosines of a normal drawn to the surface,

$$lu_0 + mv_0 + nw_0 = 0. \tag{4}$$

In turbulent flow the mean temporal velocities are subject to the compressibility condition, and this fact is denoted by the equation of continuity,

$$\partial u/\partial x + \partial v/\partial y + \partial w/\partial z = 0, \tag{5}$$

which will be used frequently in this paper.

IV. ENERGY PRINCIPLE IN TURBULENT FLOW

If we multiply the three dynamical equations, eq 1, by u, v, w, respectively, use eq 3, and add, we obtain, in view of the condition of compressibility, eq 5,

$$\begin{aligned} \frac{\rho}{2}\left[\frac{\partial}{\partial x}(uq^2) + \frac{\partial}{\partial y}(vq^2) + \frac{\partial}{\partial z}(wq^2)\right] &= -\rho\left[\frac{\partial}{\partial x}(u\Omega) + \frac{\partial}{\partial y}(v\Omega) + \frac{\partial}{\partial z}(w\Omega)\right] \\ &-\left[\frac{\partial}{\partial x}(up) + \frac{\partial}{\partial y}(vp) + \frac{\partial}{\partial z}(wp)\right] + \frac{\partial}{\partial x}(uR_{xx} + vR_{xy} + wR_{xz}) \\ &+ \frac{\partial}{\partial y}(uR_{yx} + vR_{yy} + wR_{yz}) + \frac{\partial}{\partial z}(uR_{zx} + vR_{zy} + wR_{zz}) - \Psi, \end{aligned} \tag{6}$$

where q is the absolute velocity,

$$q^2=u^2+v^2+w^2, \tag{7}$$

and Ψ is the turbulent dissipation function:

$$\Psi=R_{xx}\frac{\partial u}{\partial x}+R_{yy}\frac{\partial v}{\partial y}+R_{zz}\frac{\partial w}{\partial z}+R_{xy}\left(\frac{\partial u}{\partial y}+\frac{\partial v}{\partial x}\right)+R_{xz}\left(\frac{\partial u}{\partial z}+\frac{\partial w}{\partial x}\right)$$
$$+R_{yz}\left(\frac{\partial v}{\partial z}+\frac{\partial w}{\partial y}\right). \tag{8}$$

The physical meaning of eq 6 can be explained in a concise manner, if we multiply the two sides of eq 6 by $dxdydz$, perform the integration for a volume V, such as shown in figure 1, and consider the result.

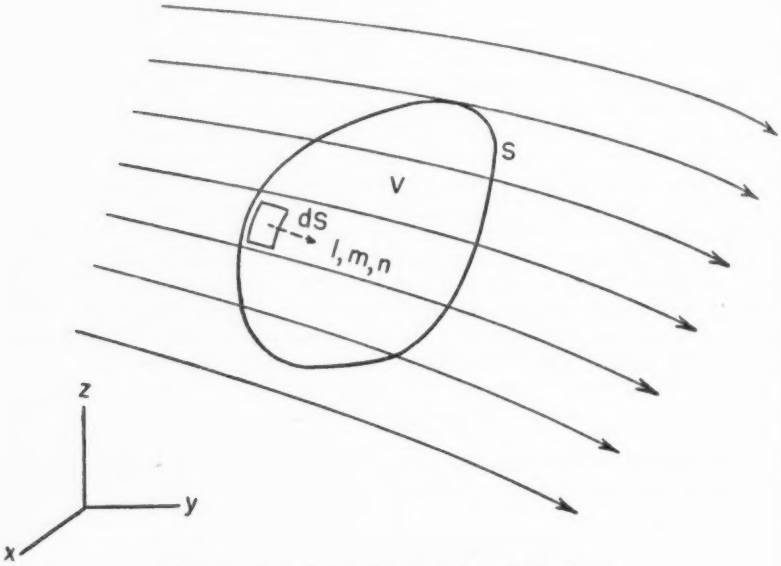

FIGURE 1.—*A closed surface in a field of flow.*

To facilitate the required integration use may be made of Green's theorem in three dimensions (also referred to as Gauss' theorem or the divergence theorem),

$$\int_V\left(\frac{\partial X}{\partial x}+\frac{\partial Y}{\partial y}+\frac{\partial Z}{\partial z}\right)dV=-\int_S(lX+mY+nZ)dS, \tag{9}$$

where X, Y, Z are any three functions, finite, single valued, and differentiable at all points of the connected region V completely bounded by one or more closed surfaces, S. The quantities l, m, n are the direction cosines of the normal drawn inwards. An element of volume is denoted by dV, and an element of surface by dS. The volume

integral is taken throughout the region of V and the surface integral on the boundaries S. Effecting the integration, we find

$$\int_S \left(p+\frac{\rho}{2}q^2+\rho\Omega\right)(lu+mv+nw)dS=$$

$$\int_s (uR_{hx}+vR_{hy}+wR_{hz})dS+\int_v \Psi dV, \tag{10}$$

where

$$\left.\begin{aligned} R_{hx}&=lR_{xx}+mR_{yx}+nR_{zx}\\ R_{hy}&=lR_{xy}+mR_{yy}+nR_{zy}\\ R_{hz}&=lR_{xz}+mR_{yz}+nR_{zz}\end{aligned}\right\} \tag{11}$$

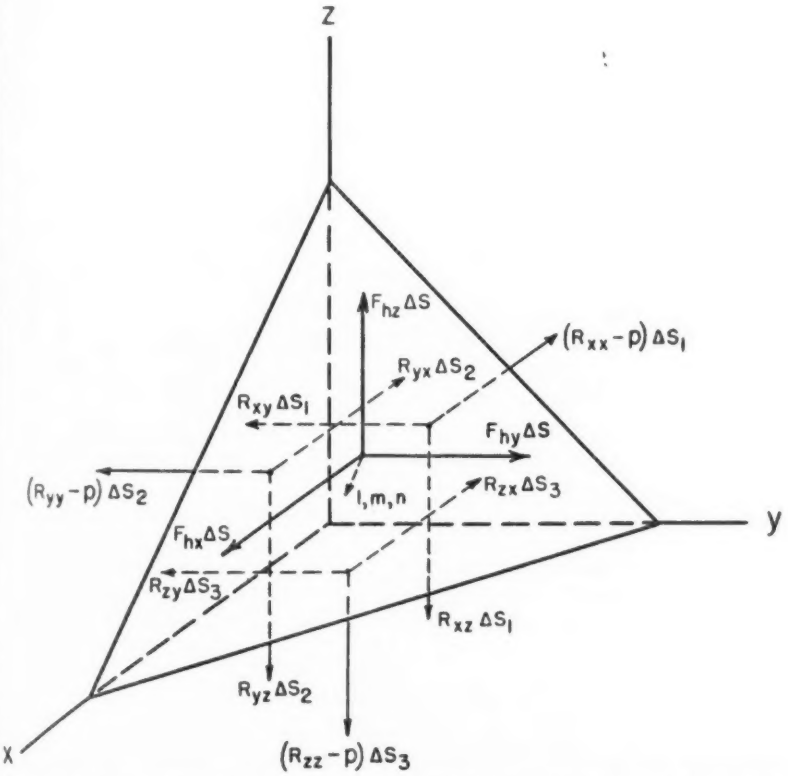

FIGURE 2.—*Boundary stresses expressed in terms of Reynolds stresses by means of tetrahedron.*

To give physical significance to R_{hx}, R_{hy}, and R_{hz}, consider the force FdS which the liquid outside of S exerts on dS, dS being on the boundary of V. See figure 2. The components of FdS in the three directions of x, y, z are $F_{hx}dS$, $F_{hy}dS$, $F_{hz}ds$, respectively. Using Cauchy's theorem of the tetrahedron, we find, in view of eq 11, the expressions

$$\left.\begin{aligned} -F_{hx}&=R_{hx}-lp,\\ -F_{hy}&=R_{hy}-mp,\\ -F_{hz}&=R_{hz}-np. \end{aligned}\right\} \tag{12}$$

Hence R_{hx}, R_{hy}, R_{hz} are the boundary stresses on the liquid outside of V with the pressures removed. They are the boundary stresses due to turbulence.

To interpret the relation in eq 10 consider figure 3. In this figure, S and S' represent the envelopes of the same body of liquid at the times t and $t+\Delta t$, respectively, in the sense of stream-line flow. Denote the volume of liquid within the surface S by V_1+V_0; that

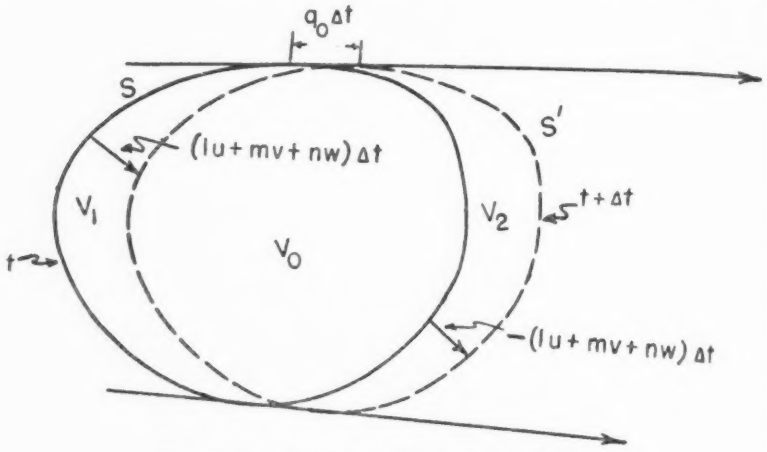

FIGURE 3.—*Motion of a limited body of liquid.*

within S' by V_2+V_0. Denote the kinetic and the potential energies of the liquid having the volume V_1 by K_1 and P_1, respectively. The corresponding quantities for V_0 are K_0 and P_0; for V_2 they are K_2 and P_2. Obviously, the increase of the kinetic energy of the liquid in S as S moves into its new position is $K_0+K_2-(K_0+K_1)$ or K_2-K_1. Now

$$K_2-K_1=\frac{\rho}{2}\int_{V_2}q^2dV-\frac{\rho}{2}\int_{V_1}q^2dV.$$

Since $lu+mv+nw$ is the velocity of mean motion along the direction of the normal drawn inwards,

$$\text{for } V_1\text{: } dV=(lu+mv+nw)dS\Delta t,$$
$$\text{for } V_2\text{: } dV=-(lu+mv+nw)dS\Delta t,$$

and hence

$$K_2-K_1=-\Delta t\frac{\rho}{2}\int_S q^2(lu+mv+nw)dS.$$

It can be shown in a similar manner that the increase of potential energy is

$$P_2 - P_1 = -\Delta t \rho \int_S \Omega(lu+mv+nw)dS.$$

On the other hand, the work done by the pressure, p, on the liquid in S at time t during the subsequent interval Δt is

$$W = \Delta t \int_S p(lu+mv+nw)dS.$$

Accordingly, the terms on the left-hand side of eq 10 give the excess of the work done on the liquid by pressure in that portion of the liquid bounded by the surface S over the variation of the kinetic and potential energies of the same liquid, all per unit time. The kinetic energy of the liquid in this case is the energy of mean motion. The right-hand member gives the dissipation in the body of water inside of the surface S due to the Reynolds stresses and the work done by these stresses on the liquid outside of S. In other words, the equation states:

$$W = E + L_1 + L_2,$$

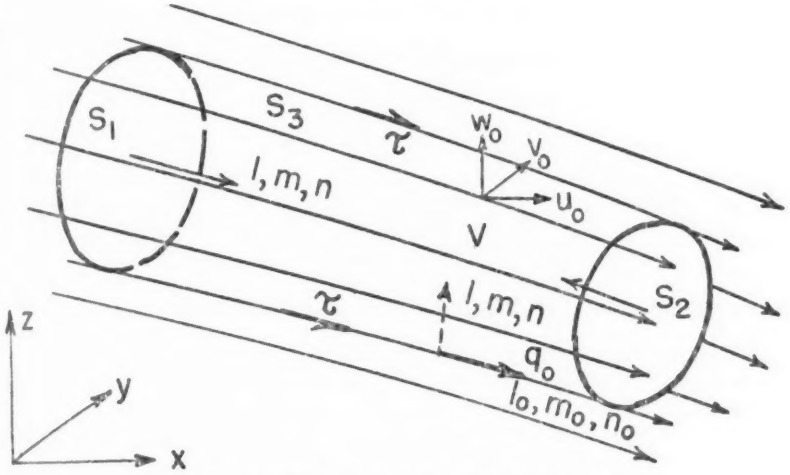

FIGURE 4.—*Segment of a tube of fluid filaments.*

where W is the work done on the fluid in S by the external hydrostatic pressure, E is the increase in energy, L_1 is the work done by the fluid inside of S against turbulent boundary stresses, and L_2 is the energy dissipated.

Obviously eq 10 is the energy equation for steady mean motion. The consideration of the equation becomes more fruitful if we select for the volume V the region bounded by a tube of fluid filaments and two planes, the planes forming the two ends of the tube. See figure 4. Let S_3 represent the surface formed by the outer fluid filaments; S_1 the surface at the end of the tube through which the liquid is entering; and S_2 the surface at the other end of the tube, through which the liquid is leaving. There is no flow across the bounding surface; that is, the mean motion across it is zero; hence the mean motion at S_3 is tangen-

tial. Let q_0 denote the absolute velocity of flow at this surface and let u_0, v_0, w_0 be its components. Denote the direction cosines of q_0 by l_0, m_0, n_0.

Hence

$$u_0=q_0l_0,\ v_0=q_0m_0,\ w_0=q_0n_0; \tag{13}$$

and, in view of eq 4,

$$ll_0+mm_0+nn_0=0. \tag{14}$$

Next, consider the surface force $+FdS$ exerted on dS, an element of S_3, by the liquid outside the tube, and denote its component in the direction of q_0 by τdS. Then

$$\tau=l_0F_{hx}+m_0F_{hy}+n_0F_{hz}.$$

From eq 12 and 14

$$-\tau=l_0R_{hx}+m_0R_{hy}+n_0R_{hz}.$$

From eq 13

$$-q_0\tau=u_0R_{hx}+v_0R_{hy}+w_0R_{hz}. \tag{15}$$

Using the latter relation, eq 10 becomes

$$\int_{s_1}(p+\rho\Omega+\rho q^2/2)(lu+mv+nw)dS+\rho\int_{s_2}(p+\rho\Omega+\rho q^2/2)(lu+mv+nw)dS=$$
$$\int_{s_1}(uR_{hx}+vR_{hy}+wR_{hz})dS+\int_{s_2}(uR_{hx}+vR_{hy}+wR_{hz})dS-\int_{s_3}\tau q_0dS+\int_V\Psi dV, \tag{16}$$

where V represents the volume of the tube bounded by the surfaces S_1, S_2, and S_3. This is the energy equation of mean flow for a filament tube of finite cross section.

V. MOMENTUM EQUATIONS FOR A STREAM TUBE

For an incompressible liquid, the first of the three dynamical equations in eq 1 may be written, using the condition of compressibility, eq 5, as

$$\rho\left[\frac{\partial}{\partial x}(u^2)+\frac{\partial}{\partial y}(uv)+\frac{\partial}{\partial z}(uw)\right]=\frac{\partial\Pi_x}{\partial x}+\frac{\partial R_{yx}}{\partial y}+\frac{\partial R_{zx}}{\partial z}, \tag{17}$$

where

$$\Pi_x=-p-\rho\Omega+R_{xx}. \tag{18}$$

Multiplying the two members of this by $dxdydz$ or dV, integrating through the space V of the tube in figure 4, and again using Green's theorem with inward-drawn normal, we obtain, after changing the signs:

$$\rho\int_{s_1}u(lu+mv+nw)dS+\int_{s_2}u(lu+mv+nw)dS=\int_{s_1}(l\Pi_x+mR_{yx}+nR_{zx})dS$$
$$+\int_{s_2}(l\Pi_x+mR_{yx}+nR_{zx})dS+\int_{s_3}(l\Pi_x+mR_{yx}+nR_{zx})dS. \tag{19}$$

The integral on the left over S_3 vanishes, since, by eq 13 and 14,

$$l_0u_0+m_0v_0+n_0w_0=0.$$

This is the momentum equation for the flow through the tube with reference to the x-direction, which states that the time rate of change of the momentum equals the x-component of the forces acting. The equation suggests that, to evaluate the difference of momenta of the liquid entering through S_1 and leaving through S_2, it is necessary to know the values of the pressure, the Reynolds stresses, and the potential in respect to the gravitational force at the bounding surfaces, and the direction cosines of the normals to these surfaces. The momentum equations corresponding to the y and z directions may be derived in a similar manner. A simpler method would be to obtain them from eq 19 by applying the cyclic permutations $u \rightarrow v \rightarrow w$, $x \rightarrow y \rightarrow z$, and $l \rightarrow m \rightarrow n$.

VI. PRESSURE LAW IN GRADUALLY VARIED FLOW

The application of the energy and momentum equations to open-channel flow will give practical results only when some definite restrictions are imposed on the form of channel and on the variation of the depth of water. Otherwise, too many quantities difficult to evaluate numerically will appear in the results.

Taking the x-axis in the bed of the channel, the positive branch being in the direction of flow, the y-axis horizontal, positive z-axis directed upwards, the equation of the surface forming the channel may be given by

$$z_1 = f(x_1, y_1),$$

where x_1, y_1, z_1, are the coordinates of a point on the channel boundary. Denote the direction cosines of the inward-drawn normal to this surface by l_1, m_1, n_1. The restriction of the channel form to be assumed is that l_1 and $H\partial l_1/\partial x$, where H is depth of water, are small quantities, the squares of these being negligible with respect to unity. We take as the depth of water the z-coordinate of the free surface. The restriction of the depth of water to be assumed is that, H being a function of x only, Hd^2H/dx^2 and the square of dH/dx are negligible with respect to unity. In Boussinesq's language, the flow is "gradually varied". These restrictions isolate the localities where the slope of the bed or the cross section of the channel changes abruptly. They isolate also the places where hydraulic jumps or bends of the watercourse occur.

The restrictions made in the above have the following kinematical and dynamical consequences. The squares, v^2 and w^2, are negligible with respect to u^2, and hence $q^2 = u^2$. The derivatives of the ratios w/u and v/u with respect to x are negligible in comparison with the derivatives of these ratios with respect to y and z. Then the accelerations in the directions of y and z are negligible; that is, the left-hand terms in the second and the third equations in eq 1 may be discarded [3].

In addition to the above, it becomes necessary to make certain assumptions in regard to the Reynolds stresses. First, the velocity fluctuations are such that

$$\overline{u'u'} = \overline{v'v'} = \overline{w'w'};$$

that is, $R_{xx} = R_{yy} = R_{zz}$, and thus $\Pi_x = \Pi_y = \Pi_z = \Pi$.

Second, u being the predominant component, the correlation between the fluctuations v' and w' and the derivatives of this correlation with respect to y and z are negligible in comparison with the correlation between u',v' and v',w' and the corresponding derivatives. That is, the derivatives of R_{xy} with respect to y and z may be neglected. Third, since the flow is gradually varied, the x-derivatives of R_{xy} and R_{xz} may be ignored.

With these assumptions in mind, the second and the third equations in eq 1 reduce to

$$\frac{\partial p}{\partial y}+\rho\frac{\partial \Omega}{\partial y}-\frac{\partial R_{yy}}{\partial y}=0, \tag{20}$$

and

$$\frac{\partial p}{\partial z}+\rho\frac{\partial \Omega}{\partial z}-\frac{\partial R_{zz}}{\partial z}=0. \tag{21}$$

Take the horizontal plane passing through the point $P(0,0,0)$ as the surface of reference for the potential energy. Denote the bed inclination, that is, the angle between the x-axis and this plane by i. Then

$$\rho\Omega=\rho gz-ixg\rho; \tag{22}$$

assuming that i is small. The general solution of eq 21 is

$$p+\rho gz-ixg\rho-R_{zz}=f(x,y),$$

where f is an arbitrary function. At the free surface, that is, at $z+H$, the pressure is atmospheric, so that $p=p_a$. Obviously, the fluctuations w' vanish at the free surface, or $R_{zz}=0$ at $z=H$. Hence

$$p_a+\rho gH-\rho ixg=f(x,y).$$

Subtracting, we have

$$p=\rho g(H-z)+R_{zz}+p_a,$$

or, since $R_{xx}=R_{zz}=R_{yy}$,

$$p=\rho g(H-z)+R_{xx}+p_a, \tag{23}$$

which relation satisfies eq 20 also. This is the law of pressures in gradually varied flow. Differentiating eq 18, and using eq 22 and 23, we obtain

$$-\frac{\partial \Pi}{\partial x}=\rho g\frac{dH}{dx}-\rho gi. \tag{24}$$

VII. THE TWO EQUATIONS OF OPEN-CHANNEL FLOW

Let us first consider the energy method. We regard the portion of water in the channel between the planes $x=x_1$ and $x=x_2$ as the filament tube for which the energy relation of eq 16 is to be evaluated. See figure 5. The sections A_1 at x_1 and A_2 at x_2 are identified with S_1 and S_2, respectively. The free surface and the wetted surface between the sections at x_1 and x_2 constitute the surface S_3. Accordingly, q_0 is the velocity of water at the free surface or in the plane of the peaks of the asperities of the solid boundary, or the velocity at the face of the laminar sublayer if the bounding surface is smooth. At the section A_1, $l=1$,

$m=0, n=0$. At A_2, $l=-1, m=0$, and $n=0$. At the surface S_3, $l=l_1$, $m=m_1$, and $n=n_1$. It must be remembered that l_1 is small. The energy relation for the flow in channel from eq 16 is thus, using eq 11:

$$\int_{A_1}\left(\frac{\rho u^2}{2}+\rho\Omega+p-R_{xx}\right)udA-\int_{A_2}\left(\frac{u^2}{2}+\rho\Omega+p-R_{xx}\right)udA=$$

$$\int_{A_1}(vR_{xy}+wR_{xz})dA-\int_{A_2}(vR_{xy}+wR_{xz})dA-\int_{S_3}\tau q_0 dS+\int_V \Psi dV. \quad (25)$$

Since we have assumed that $R_{xx}=R_{yy}=R_{zz}$ and that the liquid is incompressible, the dissipation function Ψ as given in eq 8 now takes on the form

$$\Psi=R_{xy}\left(\frac{\partial u}{\partial y}+\frac{\partial v}{\partial x}\right)+R_{xz}\left(\frac{\partial u}{\partial z}+\frac{\partial w}{\partial x}\right)+R_{yz}\left(\frac{\partial v}{\partial z}+\frac{\partial w}{\partial y}\right). \quad (26)$$

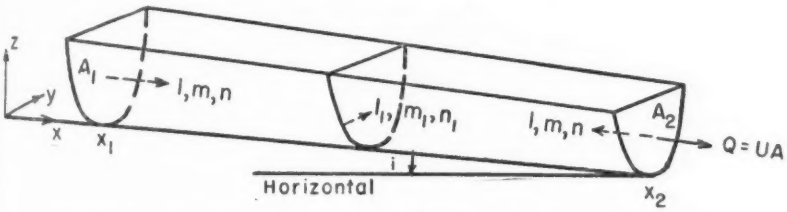

FIGURE 5.—*Segment of a tube of fluid filaments in gradually varied flow.*

Since we are dealing with gradually varied flow, the value of the product τq_0 in terms of the Reynolds stresses and the wall velocities takes on a simpler form. The general value of this product is, from eq 15 and 11,

$$-\tau q_0=u_0(l_1R_{xx}+m_1R_{yx}+n_1R_{zx})+v_0(l_1R_{xy}+m_1R_{yy}+n_1R_{zy})+ w_0(l_1R_{xz}+m_1R_{yz}+n_1R_{zz}).$$

Using eq 4 and remembering that $R_{xx}=R_{yy}=R_{zz}$, this simplifies to

$$-\tau q_0=(u_0m_1+v_0l_1)R_{yx}+(u_0n_1+w_0l_1)R_{zx}+(v_0n_1+w_0m_1)R_{yz}.$$

Since the flow is gradually varied, v_0l_1 is negligible in comparison with u_0m_1, and w_0l_1 in comparison with u_0n_1, and thus we have

$$-\tau q_0=u_0m_1R_{yx}+u_0n_1R_{zx}+(v_0n_1+w_0m_1)R_{yz}. \quad (27)$$

We wish to obtain the channel equation in its differential form. To do this we select $x_1=x$ and $x_2=x+dx$. We suppose that the Reynolds stresses vanish at the free surface, and remember that $dV=Adx$, $n_1dS=dy_1dx_1$ and $m_1dS=-dz_1dx_1$, since we shall evaluate the line integrals counterclockwise in the yz-plane.
Then eq 25 becomes

$$-\frac{d}{dx}\int_A(\rho u^2/2+\rho\Omega+p-R_{xx})udA=-\frac{d}{dx}\int_A(vR_{xy}+wR_{xz})dA-$$

$$\oint_{P_W}u_0(R_{yx}dz_1-R_{zx}dy_1)+\oint_{P_W}Ryz(v_0dy_1-w_0dz_1)+\int_A\Psi dA, \quad (28)$$

where A is the cross section at x, P_W is the wetted perimeter, and dz_1 and dy_1 are the projections of an arc ds of the wetted perimeter.

Next we express the left-hand terms of the last equation in terms of a quantity which is measurable when the channel is prismatic and the flow is uniform. The measurable quantity that will be used is

$$\oint_{P_W} R_{yx}dz_1 - R_{zx}dy_1 = -\tau_0 P_W, \tag{29}$$

where τ_0 in the case of uniform flow in an open channel is the magnitude of the average shear on the wall per unit length of channel and is a positive quantity. Denote the hydraulic radius by R, so that

$$RP_W = A.$$

Denote the average velocity in the direction of x by U and the discharge by Q: then

$$Q = UA = \int_A u dA. \tag{30}$$

Introduce the dimensionless coefficients, N_1 and N_2, such that

$$\int_A (vR_{xy} + wR_{zx})dA = -N_1\tau_0 UA = -N_1\tau_0 Q, \tag{31}$$

and

$$\oint_{P_W} u_0(R_{yx}dz_1 - R_{zx}dy_1) - \oint_{P_W} R_{yx}(v_0 dy_1 - w_0 dz_1) - \int_A \Psi dA = -N_2\tau_0 Q/R. \tag{32}$$

In addition to these we introduce also the well-known dimensionless coefficient α of Coriolis; which is defined by

$$\int_A u^3 dA = \alpha U^3 A = \alpha U^2 Q. \tag{33}$$

In view of eq 24, 30, 31, 32, and 33, eq 28 now may be given in the form

$$g\frac{dH}{dx} + \alpha U\frac{dU}{dx} = gi - \frac{d}{dx}(N_1\tau_0/\rho) - N_2\tau_0/\rho R, \tag{34}$$

which is the equation of motion of steady flow in open channels, as derived by the energy method.

Consider secondly the momentum method. Working with the same fluid tube as in the above we have, from eq 19, after transforming the Π terms back into a volume integral, the relation,

$$\int_{A_1} \rho u^2 dA - \int_{A_2} \rho u^2 dA = -\int_V \frac{\partial \Pi}{\partial x} dV + \int_{S_3} (m_1 R_{yx} + n_1 R_{zx})dS.$$

The differential relation derived from this, by putting $x_1 = x$ and $x_2 = x + dx$, $dV = Adx$, $n_1 dS = dy_1 dx_1$, $m_1 dS = -dz_1 dx_1$, reduces to

$$-\frac{d}{dx}\int_A u^2 dA = -\int_A \frac{\partial \Pi}{\partial x} dA + \oint_{P_W} (R_{zx}dy_1 - R_{yx}dz_1). \tag{35}$$

Now introduce the Boussinesq coefficient η by means of the relation

$$(1+\eta)U^2 A = \int_A u^2 dA,$$

or

$$(1+\eta)UQ=\int_A u^2dA. \tag{36}$$

Differentiating both sides of this equation by x and assuming that η changes slowly with x, we have

$$\frac{d}{dx}\int_A u^2dA=(1+\eta)Q\frac{dU}{dx}. \tag{37}$$

In view of eq 18, 22, 24, and 37, eq 35, after dividing by ρA, reduces to

$$g\frac{dH}{dx}+(1+\eta)U\frac{dU}{dx}=gi-\tau_0/\rho R, \tag{38}$$

which is the equation of motion of steady flow in open channels, as derived by the momentum method.

VIII. THE COEFFICIENT OF LOSS AND FRICTION IN THE VARIED-FLOW EQUATIONS

The two equations of motion, eq 34 and 38, of varied flow in open channels given above, are in conformity with theory. Examining these two equations, it must be emphasized that the equation derived from the general energy equation, that is, eq 34, contains N_1 and N_2 in addition to τ_0. All three of these quantities are unknown even if we suppose that H, U, and α are known as functions of x, through observation. Since by the mere observation of H, U, and α, the quantities τ_0, N_1, and N_2 can not be determined, the terms involving these unknowns may be represented as a single term. That is, we put

$$R\frac{d}{dx}(N_1\tau_0)+N_2\tau_0=+\lambda_e\cdot\frac{1}{2}\rho U^2, \tag{39}$$

and then eq 34 takes the form

$$g\frac{dH}{dx}+\alpha U\frac{dU}{dx}=gi-\lambda_e\frac{U^2}{2R}, \tag{40}$$

where λ_e is a dimensionless coefficient arising solely from the fact that there is dissipation of energy in the flow. The quantity

$$\lambda_e\frac{U^2}{2R}\cdot\rho Q,$$

where Q is the constant discharge in the open-channel flow, represents the rate of loss of energy in the channel per unit length of channel. This interpretation follows from the fact that the results were derived from the general energy equation. Accordingly, we must look upon λ_e as a coefficient of energy loss.

On the other hand, the equation derived from the general momentum equation, that is, eq 38, contains the single unknown, τ_0. If we write

$$\tau_0=\lambda\rho\frac{U^2}{2}, \tag{41}$$

eq 38 takes on the form

$$g\frac{dH}{dx}+(1+\eta)U\frac{dU}{dx}=gi-\lambda\frac{U^2}{2R}. \tag{42}$$

Since τ_0 is the frictional force of the channel per unit length, the coefficient λ represents the coefficient of friction.

IX. SELECTING THE MORE USEFUL FORM OF THE EQUATION OF MOTION FOR AN OPEN CHANNEL

If the equations above given were equally advantageous, a selection between the two would be meaningless. But this is not the case. Of the coefficients, λ_ϵ and λ, the second being directly associated with the friction exerted by the walls of channel is the less affected by changes in dU/dx. This is obvious when we consider the equation which expresses the coefficients in terms of the shear. Judging solely on this basis, the universal use of eq 42 as the equation of motion for varied flow in open channels would naturally be favored.

In this connection an error that is often made in the use of the equations above discussed should be pointed out. Frequently, eq 40 is employed to determine Manning's "n" for open channels. Since Manning's "n" relates to the magnitude of the frictional force in channels, obviously the correct equation to use is eq 42, the relation between n and λ being

$$n=1.486R^{1/6}(\lambda/2g)^{1/2}, \tag{43}$$

where R and g are measured in English units; that is, in feet and in seconds.

The following general remarks regarding the role of the energy and the momentum equations in hydrodynamics may be made in passing. In the present problem we are concerned solely with the relation between wall resistance and mean flow in the channel, and hence no advantage is achieved by the simultaneous use of the energy and momentum equations. The reason for this is that the law of velocity distribution in open channels, when the flow is turbulent, is not susceptible of theoretical determination. Experience establishes the relation between the local velocities and the shear at the wall. This being the case, one of these equations is sufficient, as explained above. But if the problem considered is one in streamline flow, and if solutions are attempted by approximate methods, then the simultaneous use of the energy and momentum equations results in improving the approximations of the solutions obtained.

In solving the problems of boundary layer on a plate and at the entrance section of a pipe, for example, it is necessary first to establish the law of velocity distribution. It has been customary to use the momentum relation to obtain the approximate form of this distribution. If, in addition, the energy relation is used, a better approximation results.

The author expresses his appreciation to George W. Patterson and Herbert N. Eaton for valuable criticism and review of the paper.

X. REFERENCES

[1] B. A. Bakhmeteff, *Coriolis and the energy principle in hydraulics*, Applied Mechanics, Theodore von Kármán Anniversary Volume, p. 59 (1941).

[2] Hunter Rouse, Fluid Mechanics for Hydraulic Engineers, p. 179 (McGraw-Hill Book Co., New York, N. Y., 1938).

[3] J. Boussinesq, *Essai sur la théorie des eaux courantes*, Mém. divers Savants Acad. Sci. **32**, 56 (1891).

ADDITIONAL REFERENCES

G. G. Coriolis. *Sur l'établissement de la formule qui donne la figure des remous, et sur la correction qu'on doit y introduire pour tenir compte des différences de vitesse dans les divers points d'une même section d'un courant.* Annales des Ponts et Chaussées, 1st semester (1836) (series 1, vol. 11).

Vauthier, *Note sur la correction que M. l'ingénieur en chef Coriolis propose de faire subir à la formule du mouvement permanent des eaux courantes, pour tenir compte des differences de vitesse des molecules fluides, aux divers points d'une même section transversale du courant.* Annales des Ponts et Chaussées, 2d semester (1836) (series 1, vol. 12).

A. J. C. B. de Saint-Venant, *Des divers manières de poser les equations du mouvement varié des eaux courantes.* Annales des Ponts et Chaussées, 1st semester (1887) (series 6, vol. 13).

WASHINGTON, May 15, 1942.